Multiparticle Production in Strong Interactions

Fredrik Söderberg

Department of Theoretical Physics
Lund University, Sweden

Thesis for the degree of Doctor of Philosophy

Thesis Advisors: Bo Andersson and Gösta Gustafson

Faculty Opponent: Tamás Csörgő

To be presented, with the permission of the Faculty of Natural Sciences of Lund University, for public criticism in Lecture Hall F of the Department of Theoretical Physics on Friday, May 9th, 2003, at 10.30 a.m.

To Ann

This thesis is based on the following publications:

I B. Andersson and F. Söderberg,
The Diagonalisation of the Lund Fragmentation Model I
European Physical Journal **C16**, 303–310 (2000).

II B. Andersson, S. Mohanty and F. Söderberg,
The Lund Fragmentation Process for a Multi-gluon String According to the Area Law
European Physical Journal **C21**, 631–647 (2001).

III B. Andersson, S. Mohanty and F. Söderberg,
The λ-Measure and the Generalised Dipoles in the Lund Model
Nuclear Physics **B646**, 102–126 (2002).

IV S. Mohanty and F. Söderberg,
Coherence Chains and Bose-Einstein Correlations in the Lund Model
LU TP 03-08.

Contents

Introduction **1**
The Atom Model 2
Matter Particles 3
Quantum Chromo Dynamics 5
The Lund Model 7
The Lund Dipole Cascade Model 8
The Lund String Fragmentation Model 9
The Bose-Einstein Effect in the Lund Model 12
The Papers 15
Acknowledgments 17

1 The Diagonalisation of the Lund Fragmentation Model I **19**

2 The Lund Fragmentation Process for a Multi-gluon String According to the Area Law **39**

3 The λ-Measure and the Generalised Dipoles in the Lund Model **81**

4 Coherence Chains and Bose-Einstein Correlations in the Lund Model **113**

Introduction

"The time has come," the Walrus said,
"To talk of many things:
Of shoes–and ships–and sealing-wax–
Of cabbages–and kings–
And why the sea is boiling hot–
And whether pigs have wings"
–Lewis Carroll,
Through the Looking-Glass and
What Alice Found There.

This thesis is based upon four papers, written between 1999 and 2003, on the subject of multiparticle production in strong interactions. This branch of physics is dedicated to the understanding of the fundamental building blocks of matter—the elementary particles. The language of science is mathematics, and as a consequence it is a real challenge to explain the models that we build to a reader who is not used to think in mathematical terms.

In order to introduce non-physicists to the world of particle physics, the first part of this introduction contains an overview of the modern model describing the elementary particles—the Standard Model. I have tried to avoid writing equations in this first part. It is impossible to cover all the details in this brief introduction. However, the interested reader can find a list of references that I find useful if one wants to learn more about this fascinating subject.

The second part, describing the specific model that the papers are based upon, is of a more technical character and it is aimed at students with a basic knowledge of high-energy physics.

A reader working in the field of multiparticle dynamics can go directly to the third part of the introduction, where the papers are summarised, or maybe even directly to the papers listed in chronological order after this introduction.

Part I: The Atom Model

The principle that matter contains small building blocks that cannot be divided any further can be traced back to the ancient Greeks [1]. For a long time, matter was proposed to consist of indivisible particles called atoms.

The concept of the atom explains a lot of experimental findings and it is an important model of physics. However, experiments have indicated that the atom has an inner structure. In 1909, Ernest Rutherford suggested an experiment where high energy α-particles were used as projectiles on atoms in the form of a thin gold foil [2]. From large deflections in the path of the projectile, Rutherford drew the conclusion that the atom contains a tiny nucleus and that the electric charge of the atoms was concentrated to the nucleus and to electrons going around the nucleus.

The development of the experiments made it possible to resolve the tiny structure of the nuclei, and the existence of protons and neutrons inside the nucleus was established. The size of the atom is $\sim 10^{-10}$ m and the size of the nucleus is only $\sim 10^{-15}$ m. It is believed that the electrons are point-like objects without an inner structure.

The electron has a negative charge and the proton has a positive charge, while the neutron is electrically neutral. Therefore, there will be an electromagnetic interaction (attractive force) between the electrons and the nucleus in the atom. Since the protons have positive charge, there should be a repelling force between them. Consequently, there must be something else responsible for the fact that the nucleus is a bound object, i.e. there must exist an attractive force between the protons stronger than electromagnetism. This is the strong force of nature.

In 1968, an experiment was performed at the Stanford accelerator with electron-proton scattering; the experiment indicated a possibility of scattering on smaller constituents inside the proton—the quarks [3]. This means that the proton and the neutron have an inner structure. The quarks have electromagnetic charge but also a "new" type of charge called colour charge[1]. Just as electrically charged electrons and nuclei combine to make neutral atoms, the quarks combine to make colour neutral particles called hadrons (protons, neutrons, pions, etc).

Experiments with protons have shown, in addition to the fact that they seem to contain quarks, that a lot of the proton momentum is carried by something that is electromagnetically neutral —the gluons[2]. Consequently, in the modern picture the proton is assumed to be a very complicated thing, contain-

[1] Used in this context, the word colour means something very different from the colour that we see with our eyes. We will come back to this issue in the next subsection.

[2] The gluons are related to the strong force and therefore important for the work presented in this thesis. We will come back to them in the next subsection.

ing both quarks and gluons, and we see that the search for the fundamental constituents has taken us down to very small sizes. Physicists still have a tremendous amount of unanswered questions about the fundamental particles. New experiments at very high energies are being performed today, in the hope of finding the answers to these questions. The research in this field is most active. In the next subsection, I will summarise the modern view of particle physics, the so-called Standard Model.

Part I: Matter Particles

In this section, I will describe the fundamental objects of which all matter is composed according to the Standard Model of modern particle physics. A particle is considered to be fundamental if it has no inner structure.

The Standard Model subdivides the materia that our world is made of into two subgroups: quarks and leptons [4]. In the previous subsection, it was mentioned that the protons and the neutrons inside the nucleus of an atom are made of quarks. So far, we have found six types of quarks in nature. We say that the quarks come in six different flavours. They are normally presented as doublets where the top row has electric charge $\frac{2}{3}e$ and the bottom row has electric charge $-\frac{1}{3}e$, where e is the magnitude of the electric charge of the electron [4]. This means that we are left with three doublets and they are usually referred to as families. The six quarks are called: up, down, charm, strange, top and bottom.

	first family	second family	third family
Quarks :	$\begin{pmatrix} \text{u} \\ \text{d} \end{pmatrix}$	$\begin{pmatrix} \text{c} \\ \text{s} \end{pmatrix}$	$\begin{pmatrix} \text{t} \\ \text{b} \end{pmatrix}$

The second subgroup of fundamental particles in the Standard Model, the leptons, can be arranged in a similar way:

	first family	second family	third family
Leptons :	$\begin{pmatrix} \nu_e \\ e \end{pmatrix}$	$\begin{pmatrix} \nu_\mu \\ \mu \end{pmatrix}$	$\begin{pmatrix} \nu_\tau \\ \tau \end{pmatrix}$

The bottom row has electric charge $-e$ and the particles in the top row are electrically neutral. The first family contains the electron which is the particle going around the nucleus in an atom. The other particle in the first family doublet is the electron neutrino. The electron neutrino is involved in the β-decay of the neutron[3]. The second family contains the muon (μ) and the muon

[3] I will come back to the β-decay when I describe the interaction of particles in the Standard Model.

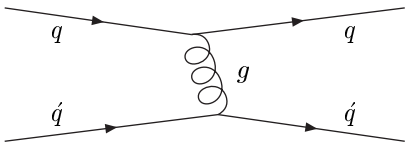

Figure 1: The figure shows a schematic example where two quarks (q and $\acute{q}$) interact by interchanging a gluon (g).

neutrino (ν_μ). The muon shares all the properties of the electron except that it is much heavier. This is also true for the third family containing the tau lepton (τ) and the tau neutrino (ν_τ). All stable matter that we see around us is made up from the quarks and leptons from the first family. All the particles listed above also have a partner with opposite charge (quantum numbers) called an antiparticle. Elementary particles can also interact with each other. The theory describing the interaction is called Quantum Field Theory. In Quantum Field Theory, particles interact with each other by exchanging a new kind of "interaction particles" called gauge bosons. The gluon, mentioned in the previous section, is the gauge boson of the strong force. This means that quarks can interact with each other by interchanging gluons like in the process drawn in Fig. 1. Quarks can also interact by exchanging photons, since they also carry electric charge (the photon is the gauge boson of the electromagnetic force).

Nature, as we know it today, can be described by four kinds of interactions (forces) [4]. They are summarised in Table 1. The first interaction listed in

Interaction	*Affects*	*"Interaction particle" (Gauge boson)*
Gravity	All particles	Graviton?
Electromagnetism	All electrically charged particles	Photon (γ)
Weak interaction	Quarks, leptons, electroweak gauge bosons	$W^{\pm}$,Z^0
Strong interaction	Quarks and Gluons	Gluons (g)

Table 1: The table shows the four kinds of interactions in nature and the corresponding gauge bosons.

this table is gravity. The modern theory for the gravitational force is Einstein's theory of general relativity. Gravity can be neglected in the calculations in this

thesis since it is very weak compared with the other relevant forces. I have marked the gauge boson for gravity with a question mark, since we do not have a quantum theory for gravity. Normally, gravity is not included in the Standard Model.

The electromagnetic interaction is responsible for nearly all chemical processes around us and for electromagnetic waves such as light and radio-waves. The modern theory for the electromagnetic interaction is Quantum Electrodynamics (QED). In QED, electrically charged particles can interact by an exchange of a particle called a photon. QED describes the interaction of light and matter and it is one of the most successful theories of physics [5].

It turns out that electromagnetism can be combined with the weak interaction into the so-called electro-weak force. The weak interaction is responsible for the important β-decay of a nucleus where a neutron decays into a proton plus an electron and an electron neutrino.

The fourth force listed in Table 1 is the strong force. This thesis deals with the modern theory for the strong force, Quantum Chromodynamics (QCD). Besides the electric charge, quarks carry colour charge. Particles that carry colour charge can interact via the strong force in the same way as electrically charged particles can interact via the electromagnetic force. The three possible colour charges are red, green and blue. A very special feature of QCD is that it states that the particles we observe in nature must be colour neutral objects. This means that a single isolated quark cannot exist in nature. However, three quarks with colour charges red, green and blue can combine into a colour neutral object called a baryon[4]. Protons and neutrons are baryons containing the quark combinations (uud) and (udd) respectively (the reader is encouraged to check that the sum of the electric charge of the individual quarks add up to the charge of the proton and the neutron respectively). Another possibility to create a colour neutral object is to combine a quark and an antiquark. In this case, the quark and the antiquark, carrying colour and anticolour respectively, combine into a colour neutral meson. Quantum Chromodynamics is described in more detail in the next subsection.

Part I: Quantum Chromo Dynamics

In the previous subsection, we learned that quarks carry colour charge and that the strong force is mediated by gluons. Quantum Chromodynamics is the model used for the strong force and it has some very special properties. We have seen that scattering experiments are used to probe the behaviour of elementary particles. Physicists collide two beams of particles and observe the final state in order to learn about the interaction and the particles involved.

[4]This justifies the use of the word colour in this context.

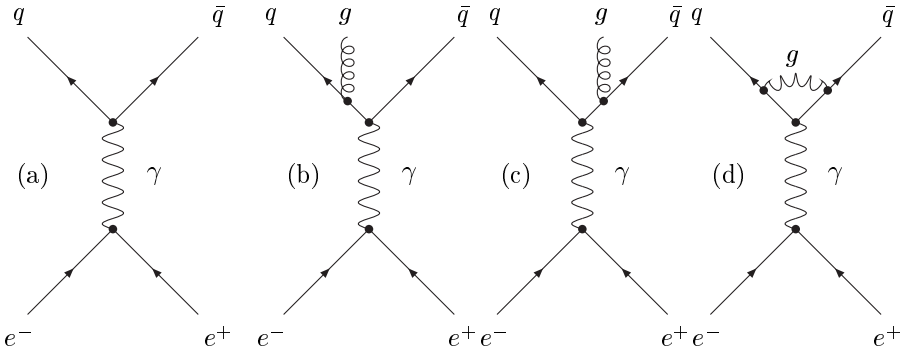

Figure 2: The figure shows diagrams contributing to the process $e^+e^- \rightarrow$ hadrons. Diagram (a) is the lowest order contribution. The diagrams (b),(c) and (d) give corrections of order α_s as explained in the text.

The likelihood of any particular result (final state) can be expressed in terms of a quantity known as the cross section (σ) [6]. This quantity is normally very hard to calculate for a general process in QCD. Perturbation theory is a systematic method to approximate the exact result. The idea is to write the exact result as a sum of an infinite number of terms where the successive terms become smaller and smaller in magnitude. This means that even if we only sum a few terms, we will obtain a good approximation to the exact result. The exact result for the cross section can in this way be written [7]:

$$\sigma = A_1\alpha_s + A_2\alpha_s^2 + \ldots$$

i.e. every term in the sum can be written as a product of two factors. One factor is α_s, the coupling constant of the strong interaction which determines the strength of the interaction. We say that α_s is the expansion parameter in the perturbation series in which the power of α_s determines the order of the contributing term. If α_s is a small number (and if the factors A_j stay limited), then we only need to sum a few terms in the above series for the cross section. This is because every term is suppressed by a factor of α_s compared to the previous term (remember that α_s is assumed to be a small number). The factors labelled A_j can be calculated using a diagrammatic notation called Feynman diagrams after their inventor. The idea is to draw diagrams for all the possible ways in which a given initial state can be transformed into a given final state. Having all the diagrams, there exist rules by which one can translate the diagrams into mathematics. It is beyond the scope of this brief introduction to

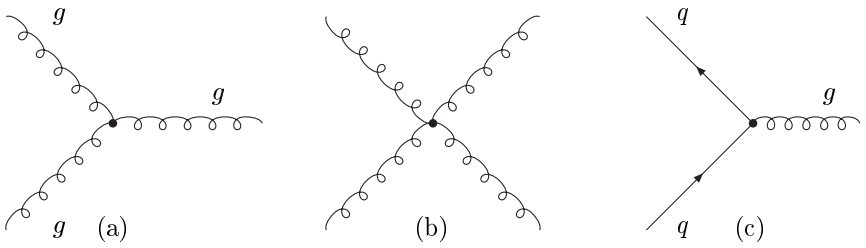

Figure 3: Gluons carry colour charge and therefore they couple to themselves. An example of this is the triple gluon vertex of QCD in fig.(a) and the 4 gluon vertex in fig.(b). Gluons couple to quarks according to the vertex in fig.(c).

explain the details of this procedure.

In this thesis, we mostly deal with the process $e^+e^- \rightarrow$ hadrons. A few feynman diagrams for this process are drawn in Fig. 2.

In this figure, diagram (a) is the lowest order contribution. The diagrams labelled (b),(c) and (d) involve a gluon and therefore they will be higher order contributions. This is because every time we have a vertex with a gluon we have to insert the coupling between the gluon and the quark and this will contribute with a factor of α_s.

A special property of QCD is that the gluons carry colour charge and therefore they can interact with each other like in the diagrams drawn in Fig. 3. This is not the case in QED, since the photons do not carry electric charge.

The key concept in QCD is asymptotic freedom. At short distances, the quarks are weakly coupled to each other. At large distances, the coupling becomes very strong and this implies that free quarks are not observed in nature. Instead, at large distances quarks are confined within hadrons.

Consequently, perturbation theory is only applicable when it comes to short distances. This thesis treats the long distance behaviour of QCD, where perturbation theory is not applicable and where we have to rely on various models instead. One such model is the Lund model described in the next part of this introduction.

Part II: The Lund Model

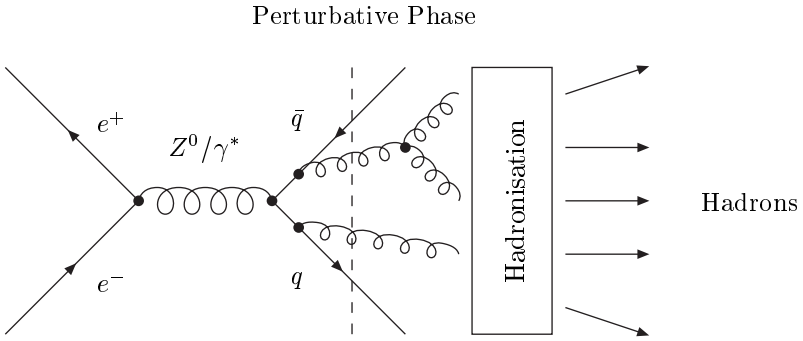

Figure 4: The figure shows a typical e^+e^--annihilation event, and the two different phases involved, as described in the text.

A common factor among the papers in the thesis is multiparticle production, like the e^+e^- collision event drawn in Fig.4. A process of this kind can be described in terms of two phases. The first phase is a short time perturbative phase dominated by large momentum transfers (small distances). Partons are being created during this phase. It is possible to make use of the asymptotic freedom of QCD and perform a perturbative calculation. The second is a long time soft interaction phase (hadronisation phase) where perturbation theory is no longer valid. The energy-momenta of the partons are transformed into hadrons during this second phase. Since perturbation theory is no longer valid, we have to rely on phenomenological models in order to describe this phase. One such model is the Lund model. This thesis is based upon two cornerstones of the Lund model: *the Lund string fragmentation model* [8] and *the Lund dipole cascade model* [9]. Together they describe the process in Fig.4. The Lund dipole cascade model describes the hard phase. In principle, this phase is calculable inside perturbative QCD, but the exact result is only known for a few gluons. The Lund dipole cascade model is a good approximation to the full QCD result. The Lund string fragmentation model describes the soft phase. The two models are described in the following two subsections.

The Lund Dipole Cascade Model

Electric currents in one place can affect other charges far away. This is a fact that we use everyday in tele communication. The physical explanation is that an accelerated charged particle radiates photons. When a charged particle travels through matter it will therefore radiate photons and lose energy, because the electric field of the nuclei in matter will accelerate (and decelerate) the particle. This process is called *bremsstrahlung*. A coloured object can in a similar way emit gluons. Consequently, we expect a great many gluons and photons to be emitted in a typical e^+e^-collision.

In the first part of this introduction, we learned that there is a big difference between QED and QCD. The emitted photons in QED are uncharged, and therefore the original current is not changed after the emission of a photon (if we neglect recoil effects). In QCD, the gluons carry colour charge and after the emission the current contains three colour charges moving in different directions, something which makes the situation much more complicated.

Let us go back to the event drawn in Fig.4 and look at the gluon emission from the $q\bar{q}$-pair. As noted in the previous section, the Lund dipole cascade model is an approximation of the full perturbative QCD result for the parton cascade. The results of perturbative QCD can be formulated in two complementary ways, in terms of quarks and gluons or in terms of colour dipoles [9].

The original $q\bar{q}$-pair can be regarded as a colour dipole when it comes to the emission of the first gluon. After the emission of the first gluon, we are left with two dipoles, one between the quark and the gluon and the other between the gluon and the antiquark. It turns out that, to a very good approximation, they can be treated as two independent dipoles when it comes to the emission of a second gluon [15] and this is an immense simplification.

The Lund dipole cascade model assumes that the process can be generalised to any number of gluons. In the process above this means that a third gluon can be emitted from three independent dipoles. This procedure is a very good description provided that the transverse momentum, $k_\perp$, of the emitted gluon is smaller than the transverse momentum of the previously emitted gluon.

The parton emission process is formulated as an iterative cascade terminated by an infrared cut-off in $k_\perp$. After n dipole emissions, there are $n+1$ dipoles. At the end of the cascade we are left with a chain of dipoles spanned between the quark via all the emitted gluons to the antiquark [9].

This model is implemented in the well-known Monte Carlo program ARIADNE [10]. We have made extensive use of ARIADNE in the work presented in this thesis. We will come back to the Dipole Cascade Model in the third paper, where we discuss some properties of the parton cascades. This ends my very brief introduction to the Dipole Cascade Model. The interested reader is

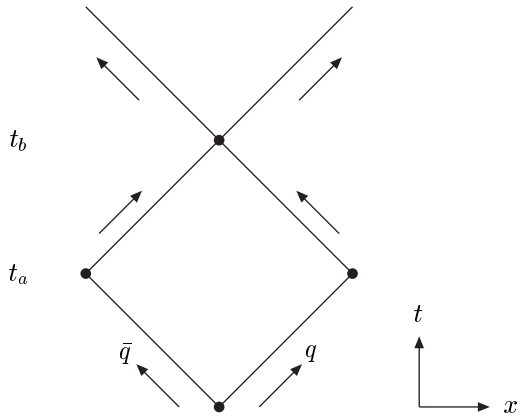

Figure 5: The figure shows a space-time diagram for the periodic motion of a $q\bar{q}$-state in the Lund string model. When moving apart, the quarks stretch the string and therefore they lose energy-momentum. At time t_a they have used up all energy and consequently they will turn and move towards each other again. The time t_b indicates the half period of the motion of the system.

referred to the original presentation [9], where all relevant formulae are presented.

The Lund String Fragmentation Model

Let us once again go back to the process in Fig.4. The process in which the final state hadrons are formed, known as the hadronisation process, is modelled by the Lund string fragmentation model.

In QCD, the potential is linear in the distance (for large distances). The linear potential is the starting point in the Lund string fragmentation model , where the massless relativistic string is used to model the QCD field between coloured constituents [11, 12, 13].

The string has a constant tension, which gives rise to a linear potential. The endpoints of the string are identified as a quark and an antiquark. Let us assume that a quark and an antiquark are produced at a single space-time point (vertex) and that they start to move apart. The quark and the antiquark will stretch the string when they move apart and therefore lose energy-momentum. Because of this they will sooner or later have to reverse their direction of motion and again gain energy-momentum from the string. The motion of a simple string system with a massless quark and antiquark at the endpoints will therefore be the so-called yoyo-motion [11, 12, 13], drawn in Fig.5.

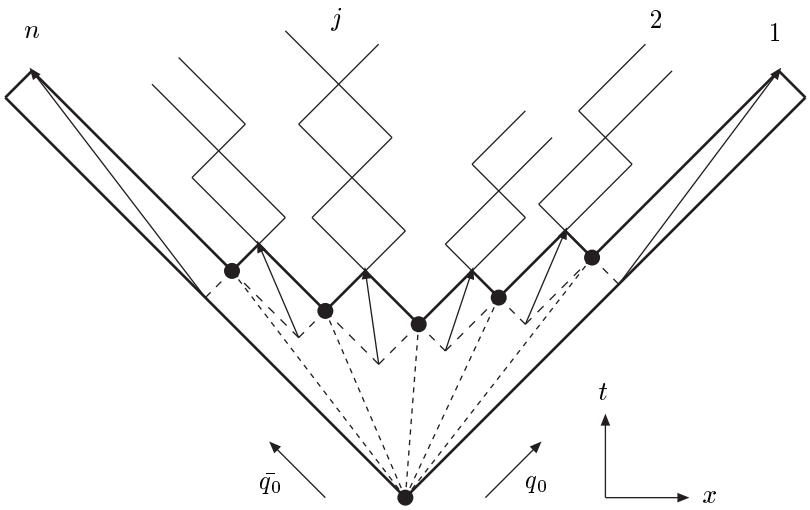

Figure 6: The break-up of a Lund string into hadrons. The solid dots are the vertices where $q\bar{q}$-pairs are being produced. The arrows indicate the hadron momenta. The area enclosed by thick lines is the area in the Lund area law.

The final state hadrons observed in high energy e^+e^--collisions stem from the break-up of the force field. New quark–antiquark pairs are then produced from the field. If the energy is high enough, the string state described above can split into smaller string pieces. A typical Lund string break-up process can be found in Fig.6. A set of new $q\bar{q}$-pairs are produced at certain space-time points, called vertices, and the original string is split into smaller string pieces.

In the Lund model, there is no field between a $q\bar{q}$-pair produced at a single vertex. A string force field is always confining because it has a fixed energy per unit length and the force field vanishes at the end-point charges.

A convenient ordering prescription for the hadrons is rank-ordering. Two hadrons that share the same vertex will be defined to have adjacent rank. If one starts to count from the original quark end, this means that the hadron which contains this quark and an antiquark from a break-up vertex will have rank 1, cf. Fig.6. The probability to produce a set of n hadrons with given

energy-momenta is calculable and it is given by the Lund model area law. The area law states that the probability to produce a set of hadrons with momenta $p_1, p_2, \ldots, p_n$ and total momentum P_{tot} is given by:

$$dP_n(\{p_j\}; P_{tot}) \propto \tag{1}$$
$$\propto \prod_{j=1}^{n} \{N_j d^2 p_j \delta({p_j}^2 - {m_j}^2)\}\, \delta(\sum_{j=1}^{n} p_j - P_{tot}) \exp(-bA)$$

i.e. the phase space times a negative exponential of an area. The area (A) is the area spanned by the string state before it decays, cf. Fig. 6.

The model is suitable for a Monte Carlo implementation, since it can be formulated as an iterative process along one of the lightcones. The break-up process can be described as a set of steps along the positive light-cone momentum, where each hadron takes a fraction z_j of the remaining light-cone momentum, cf. Fig.7.

The probability to produce a hadron with mass m taking a fraction z of the remaining (positive) light-cone momentum is given by $f(z)dz$, where $f(z)$ has the asymptotic form:

$$f(z) \quad = \quad N\frac{1}{z}(1-z)^a exp(-\frac{bm^2}{z}) \tag{2}$$

f is called the Lund symmetric fragmentation function, and it can be derived from Eq.(1). We note that small z values will be exponentially suppressed, while large z values will be power suppressed. The final result is that the vertices typically will be along a hyperbola in space-time in the Lund model. We have only discussed string states without gluons in this introduction. The first paper in this thesis deals with the properties of the hadronisation process in this kind of string states and an alternative formulation of the model is presented. Gluons will complicate the motion of a string tremendously, since they are interpreted as internal excitations of the string in the Lund model [16]. The properties of such gluonic strings are discussed in detail in the second paper of the thesis.

The Bose-Einstein Effect in the Lund Model

The final state particles in an event can be subdivided into bosons and fermions. Bosons obey Bose-Einstein statistics while fermions obey Fermi-Dirac statistics. The Bose-Einstein effect implies an enhanced production of pairs of identical bosons which are close to each other in phase space and it is of a quantum mechanical nature. Pions are examples of bosons that are common in a final state produced in e^+e^--annihilation events. Consequently, we may expect that it is important to consider the Bose-Einstein effect in a fragmentation model.

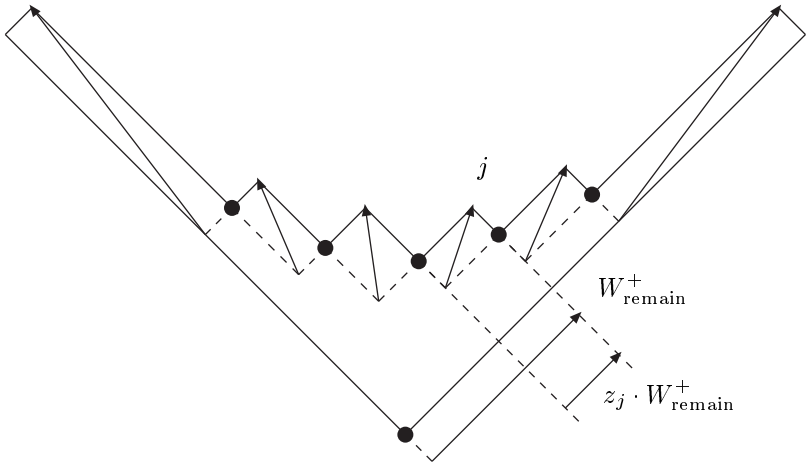

Figure 7: The break-up of a Lund string into hadrons. The figure shows a hadron with rank order j, taking a fraction z_j of the remaining positive lightcone momentum as described in the text.

The Bose-Einstein effect is often described as an enhancement of the two-particle correlation function when the two particles have similar energy-momenta. The two-particle correlation function is defined as:

$$R_2(Q) = \frac{\rho_{2\mathrm{withBE}}}{\rho_{2\mathrm{withoutBE}}}$$

where

$$\rho_2(Q) = \frac{1}{N}\frac{\mathrm{d}n}{\mathrm{d}Q} \tag{3}$$

n is the number of pairs of identical bosons (with energy-momenta p_1 and p_2) and $Q^2 \equiv -(p_1 - p_2)^2$. The quantity $\rho_{2\mathrm{withoutBE}}$ corresponds to an uncorrelated reference sample and it is of course not directly measurable, but there exists sophisticated methods to measure it indirectly.

Since the Bose-Einstein effect is of a quantum mechanical nature, it is absent in the semi-classical Lund string fragmentation model based upon a classical probability concept. In the rest of this subsection, I will explain how the Bose-Einstein effect can be introduced in the Lund string fragmentation model.

The Lund model area law, Eq.(1), can be interpreted as a product of the phasespace and a square of a matrix element [17, 18]:

$$\mathrm{d}P = \mathrm{d}(\mathrm{phasespace}) \times |\mathcal{M}|^2 \tag{4}$$

A form for the matrix element that will reproduce the area law was proposed in [17]:

$$\mathcal{M} \quad = \quad exp\left(i\kappa - \frac{b}{2}\right) A \tag{5}$$

where κ is the string constant (with a phenomenological value of $\simeq 1$ GeV/fm) and b is the parameter in the area law.

In the Lund model, the Bose-Einstein effect stems from the fact that identical final states of hadrons can be obtained where identical bosons are ordered in different ways along the string. We call these different "configurations" and they will give separate contributions to the amplitude for the final state of hadrons. Consequently, in calculating the probability for a final state of hadrons we have to consider all possible permutations of the identical bosons, i.e. we have to find all the configurations. In other words, we should symmetrise the event amplitude ($\mathcal{M}$) [17, 18]:

$$\mathcal{M} = \sum_P \mathcal{M}_P \tag{6}$$

where P stands for all the possible permutations of the identical bosons. Since $\mathcal{M}_P$ depends upon the area and since different permutations (configurations) involves different areas, this will introduce interference effects in the model.

The Monte Carlo programs that we use are however based upon classical probability concepts. This means that a given final state of hadrons that contains identical bosons is produced with the probability:

$$|\mathcal{M}|^2 = \sum_P |\mathcal{M}_P|^2 \tag{7}$$

The interference effect can be introduced in the Monte Carlo by an event weight multiplying every event obtained [5] [18]:

$$w_P \quad = \quad \frac{|\sum_{P'} \mathcal{M}_{P'}|^2}{\sum_{P'} |\mathcal{M}_{P'}|^2} \tag{8}$$

In the fourth paper, we will show how this event-weight can be calculated and we will make use of it to study the Bose-Einstein effect for multijet events.

[5] The event weight is not uniquely defined. Eq.(8) shows the event weight used in the fourth paper of this thesis and it is different from the event weight used in [18].

Part III: The Papers

Paper 1

The basic result for the string break-up process in the Lund model, the area law, states that the probability to produce a given set of n hadrons from the field is given by the phase space times an exponential of the area spanned by the string before it decays. In this paper, we subdivide this area into triangular regions, each described by the two vertex positions involved in producing a hadron. In this approach, it is possible to define a transition operator describing the two vertices and the hadron that is produced in between them. We find that this operator has a discrete set of orthonormal eigenfunctions and a discrete set of eigenvalues. The eigenvalues only depend upon the particle mass whereas the eigenfunctions only depend upon the vertex positions.

The transition operator technique outlined above is an alternative approach that can be used in order to learn more about the basic properties of the Lund fragmentation model.

The material presented in this paper is only valid for string states without gluons. Interpreted as internal excitations of the string [16], gluons will complicate the geometry of the string surface. Formulating a fragmentation process, valid for multigluon strings, that fulfils the area law is a non-trivial task as we will see in the presentation of the next paper.

Paper 2

The world surface of the Lund string is a minimal surface completely determined by its boundary curve. The boundary curve for a Lund string surface is normally called the directrix and it can be constructed by laying out the energy-momenta of the partons in colour order. For multigluon string states, the world surface is a geometrically bent $(1+1)$-dimensional surface embedded in (1+3)-dimensions. Hard gluons will have a major influence upon the geometric shape of the directrix because they will cause the directrix to change its direction at the "gluon corners" in a dramatic way.

We show that the fragmentation process can be formulated as a stochastic process along the directrix provided that we allow local modifications of the directrix in order to pass the above mentioned "gluon corners". We find that the necessary modifications of the directrix in our approach is at most of the order of the hadron mass scale. The directrix is normally obtained using a perturbative QCD cascade and therefore it is only defined down to an infrared cut-off value below which the perturbative calculation breaks down. This makes the local modification of the directrix feasible.

Our model has been implemented in a Monte Carlo fragmentation program called ALFS [19]. PYTHIA [14] handles multigluon strings in a different way.

We end with a comparison between PYTHIA and ALFS and conclude that they give the same inclusive result but that there are differences on an event to event basis.

Paper 3

This paper is devoted to a study of the perturbative QCD parton cascades. We make use of the Lund dipole cascade model (DCM) [9] as it is implemented in the Monte Carlo program ARIADNE [10]. In the DCM, the available phasespace for gluon emission, called ℓ in this paper, can be written as a sum over contributions from individual dipoles $\ell = \sum_j \Delta\ell_j$, where $\Delta\ell_j$ in some sense is the size of a dipole.

We find that ℓ has a strong linear correlation with the average number of gluons emitted. We explain the linear correlation by performing a study of the contributions from the individual dipoles. It turns out that the distribution of sizes of gluon–gluon dipoles, $\Delta\ell$, is insensitive to the cms energy and global event variables. Moreover, we find that there are no correlations between adjacent $\Delta\ell$s in an event. The linear correlation is therefore expected according to the central limit theorem.

More interesting than the linear relationship is the fact that the slopes of the lines, representing the number of gluons per unit phase space, are independent of the cms energy, thrust and even of changes in the ordering variable. As we go to smaller values of the ordering variable, the running coupling should increase the number of emissions per unit phase space. However, it turns out that the phase space variable itself scales to absorb any increase of emissions per unit phase space.

An infrared stable generalisation of the ℓ-measure called the λ-measure, useful in the context of hadronisation, was defined in [20]. We demonstrate that the λ-measure can be written as a sum over individual contributions, $\Delta\lambda$, from more abstract entities that we call Generalised Dipoles in this paper. All the above mentioned properties for the ℓ-measure are reflected in the λ-measure.

An analytical model, based upon a simple gain-loss equation, that qualitatively describes our findings is also presented.

Paper 4

The Bose-Einstein effect between identical bosons is of a quantum mechanical nature. As such, it is not incorporated in the semi-classical Lund model based upon probabilities instead of amplitudes.

An amplitude based approach was presented in [17, 18], introducing the Bose-Einstein effect in the Lund model for string states without gluons. In such circumstances, when identical bosons are present in the final state, it is always possible to find an alternative set of vertices that will lead to the same

final state for a given partonic state. Therefore it is necessary to consider the possible permutations of the identical bosons in the final state. The different permutations will involve different areas and this gives rise to interference effects [18].

In this paper, we propose a model for implementing the Bose-Einstein effect in the Lund model for multigluon strings. The paper is divided into two distinct parts. In the first part, we define a basic concept used in our model—the Coherence Chain.

We subdivide the hadrons in an event into subgroups. All hadrons inside a subgroup have their momenta, up to some maximum allowed fluctuation, in a plane. The process can therefore be thought of as subdividing the full hadronic event into (1+1)-dimensional regions, each with a different orientation. We call such a subgroup a Coherence Chain and we find that the corresponding distributions have some interesting and useful properties. Once the size of the maximum allowed fluctuation is set, the hadron multiplicity distribution from the Coherence Chain is independent of the cms energy and global event variables.

In the second part of the paper, we propose a model for implementing the Bose-Einstein effect based upon the Coherence Chains and their properties. In the proposed model, we only consider permutations of identical particles within a Coherence Chain and this allows an extension of the model presented in [18] to multigluon strings.

Like the model presented in [18], our model is based upon an event weight and therefore it can be incorporated into a probability based Monte Carlo program. Using the Monte Carlo program ALFS, based upon the ideas presented in the second paper, we show that the model based upon the Coherence Chains shows an enhancement of the two particle correlation function for small momentum differences between identical pions. We also study how the correlation function varies with the number of jets for 2, 3 and 4-jet events.

Acknowledgments

First of all, I would like to express my gratitude to my supervisor, the late Prof. Bo Andersson, for his excellent guidance. Bo was always on the move, full of new ideas and eager to share his visions. I consider myself lucky to have known him for three years. He was a great teacher. I would also like to thank my good friend Fredrik Persson. It has been a pleasure sharing the same office with someone who understands the beauty of J.R.R. Tolkien's Middle-earth! Finally, I would like to thank my present supervisor Prof. G. Gustafson for his support and guidance during my final year as a Ph.D. student, when Bo Andersson was no longer with us.

References

[1] *Nordisk familjebok* .38 vols, Stockholm: Nordisk Familjeboks förlag, 1904–1926, vol.2 p.347.

[2] E. Rutherford, Philosophical Magazine (6) 21 (1911) 669-688.

[3] M. Breidenbach *et al.*, *Phys. Rev. Lett.* **23** (1969) 935.

[4] G. Kane, *Modern Elementary Particle Phsycis*, Addison-Wesley Publishing Company, 1993.

[5] Richard P. Feynman, *QED the Strange Theory of Light and Matter*, Princeton University Press, 1985.

[6] M.E. Peskin and D.V. Schroeder, *An Introduction to Quantum Field Theory*, Addison-Wesley, 1995.

[7] Particle Data Group, Review of Particle Physics, *Eur. Phys. J.* **C15** (2000) 1-878.

[8] B. Andersson, G. Gustafson, G. Ingelman and T. Sjöstrand, *Phys. Rep.* **97** (1983) 31.

[9] G. Gustafson, U. Pettersson, *Nucl. Phys.* **B306** (1988) 746.

[10] L. Lönnblad, *Computer Phys. Commun.* **71** (1992) 15.

[11] B. Andersson, G. Gustafson and C. Peterson, *Z. Phys.* **C1** (1979) 105.

[12] B. Andersson, G. Gustafson and B. Söderberg, *Z. Phys.* **C20** (1983) 317.

[13] B. Andersson, *The Lund Model*, Cambridge University Press, 1998.

[14] T. Sjöstrand, P. Edén, C. Friberg, L. Lönnblad, G. Miu, S. Mrenna and E. Norrbin, *Computer Phys. Commun.* **135** (2001) 238.

[15] Ya.I. Azimov et al. *Phys. Lett.* **B147** (1985) 165, Yu.L. Dokshitzer, V.A. Khoze and S.I. Troyan, in A.H. Mueller ed.,*Perturbative QCD*, p.241, World Scientific [27].

[16] B. Andersson and G. Gustafson, *Z. Phys.* **C3** (1980) 223.

[17] B. Andersson and W. Hoffman, *Phys. Lett.* **B169** (1986) 364.

[18] B. Andersson and M. Ringnér, *Nucl. Phys.* **B513** (1998) 627.

[19] S. Mohanty, LU TP 03-09 (2003).

[20] B. Andersson, G. Gustafson and B. Söderberg,
Nucl. Phys. **B264** (1986) 29.

The Diagonalisation of the Lund Fragmentation Model I

Paper I

LU TP 99-32
October 1999

The Diagonalisation of the Lund Fragmentation Model I

Bo Andersson[1]

Fredrik Söderberg[2]

Department of Theoretical Physics, Lund University,
Sölvegatan 14A, S-223 62 Lund, Sweden

Abstract
We will in this note show that it is possible to diagonalise the Lund Fragmentation Model. We show that the basic original result, the Lund Area law, can be factorised into a product of transition operators, each describing the production of a single particle and the two adjacent breakup points (vertex positions) of the string field. The transition operator has a discrete spectrum of (orthonormal) eigenfunctions, describing the vertex positions (which in a dual way corresponds to the momentum transfers between the produced particles) and discrete eigenvalues, which only depend upon the particle produced. The eigenfunctions turn out to be the well-known two-dimensional harmonic oscillator functions and the eigenvalues are the analytic continuations of these functions to time-like values (corresponding to the particle mass). In this way all observables in the model can be expressed in terms of analytical formulas. In this note only the $1+1$-dimensional version of the model is treated but we end with remarks on the extensions to gluonic radiation, transverse momentum generation etc, to be performed in future papers.

[1] bo@thep.lu.se
[2] fredrik@thep.lu.se

1.1 Introduction

The Lund Fragmentation Model is built upon a few very general assumptions: there is a string-like force field between the coloured constituents, there is causality and Lorentz covariance, the production of the particles can be described in terms of a stochastical process and the process will obey a saturation hypothesis. Using semi-classical probability considerations we are then led, [1, 2], to a unique stochastical process for the breakup of the force field into the final state hadrons. In Section 1.2, we will provide a set of necessary formulas to describe the dynamical developments along the surface, spanned by the string field. The major result is that the probability to reach a particular (exclusive) final state is given by the phase space of the state multiplied by a negative exponential of the area spanned before the string decays ("the Lund area-law"). In general the model has been used as it is implemented in the well-known Monte Carlo simulation program JETSET, [3]. This means, on the one hand, that it is possible to take into account a large amount of kinematical complications, in particular from the decay of the primary produced resonances. On the other hand, in order to make the simulation programs time-effective, it is necessary to introduce routines that make the process rather difficult to follow. In particular, it is difficult to disentangle the major dynamical features of the model from the many necessary numerical compromises in the simulation program.

In this note, we will show how to diagonalise the basic stochastical process, i.e. how to define a complete set of eigenfunctions and eigenvalues describing the process on the local level. In this way we can provide analytical formulas for all possible correlations between the observables in the process.

In Section 1.3, we will factorise the Lund area law in a somewhat different way than the ordinary. It is done by defining an operator that describes the transition from one production point to the next in the process. It can be written as an integral operator describing the probability to go from one breakup point along the string field to the next thereby producing a particular hadron. We show how to diagonalise the operator in terms of its eigenfunctions (which in a very neat way corresponds to two-dimensional harmonic oscillator functions) and calculate its eigenvalues, that are closely related to the Lund fragmentation function.

These eigenvalues turn out to be the major building stones in all the model correlations and in Section 1.4, we show a set of properties of the eigenvalues. It turns out that the eigenvalues form a discrete set, and that they correspond to analytical continuations of the harmonic oscillator eigenfunctions from space-like to time-like regions. We show how to use the factorisation properties of the model to provide a set of useful relations for the products of the eigenvalues. We also exhibit the relationship to a field theory in a two-dimensional Euclidian space that will be further pursued in future publications.

We will in this note be satisfied to treat only the simplest case corresponding to the $1+1$-dimensional dynamics of the Lund Model. We will, however, end with an outlook on future work, in particular on the effects of gluon emission and transverse momentum properties of the hadronisation process.

1.2 The Lund Fragmentation Model

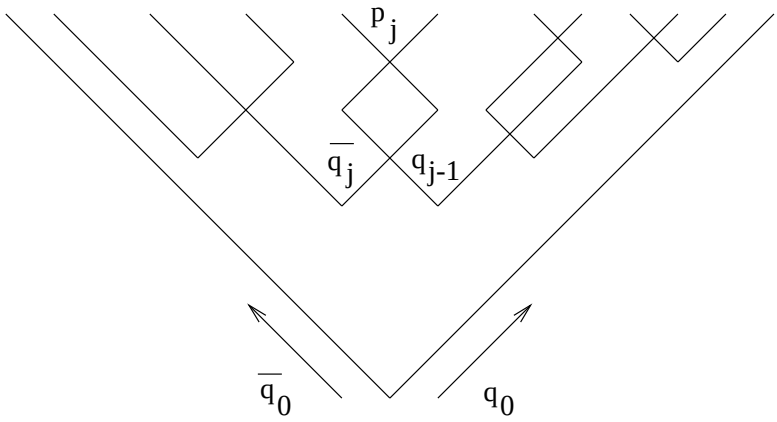

Figure 1.1: A high-energy string breakup of an original $q_0\overline{q_0}$ -pair, created at a single space-time point.

The massless relativistic string is in the Lund Model used as a model for the colour force fields with colour-3 quarks (q) and colour-$\bar{3}$ antiquarks ($\bar{q}$) at the endpoints. Finally, the colour-8 gluons (g) are in the Lund Model interpreted as internal excitations on the string. We will, in this note, treat all the ($q\bar{q}$)-particles as massless and moving along the lightcones. However, the final result is independent of this assumption, cf. [2], (massive q and $\bar{q}$ would in a semi-classical scenario move along hyperbolas with the lightcones as asymptotes). Further, we will as examples of the formalism consider only e^+e^--annihilation reactions and refrain other processes as well as gluonic bremsstrahlung to future work.

Then an original $q_o\bar{q}_o$-pair is assumed to be created at a single space-time point and start to go apart thereby stretching the string field in between them (cf. Fig 1.1). The field will break up into new pairs at the vertices $x_j = (x_{j+}, x_{j-})$ (we use lightcone coordinates) and a $q \equiv q_{j-1}$ will together with a $\bar{q} \equiv \bar{q}_j$ from the adjacent vertex form a final state hadron with the energy-momentum p_j.

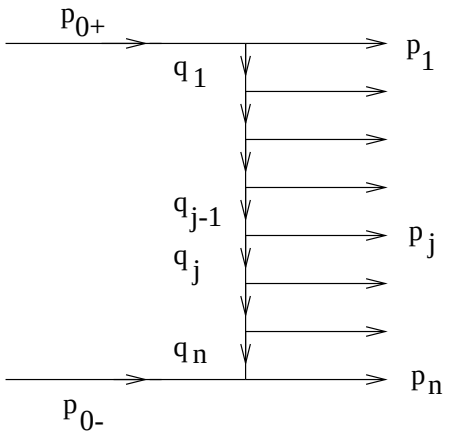

Figure 1.2: The production process described in terms of momentum transfers in a chain.

In this way we have introduced a convenient ordering in the form of rank: the first rank particle is formed by $(q_o\bar{q}_1)$, the second rank by $(q_1\bar{q}_2)$ etc. It is also possible to introduce a rank-ordering from the $\bar{q}_o$ side, i.e. along the opposite lightcone starting with $(\bar{q}_o q_{n-1})$ in an n-particle final state. The dynamical results should of course be independent of the ordering. Actually, it is easy to convince oneself that it is necessary that all the vertices must be space-like with respect to each other. One finds that the energy-momentum of the j-th particle is given by $p_j = \kappa(x_{j-1+} - x_{j+}, x_{j-} - x_{j-1-})$ (here $\kappa \simeq 1$ GeV/fm is the string constant and we will for simplicity put it equal to unity). As the vector p_j must be time-like (with squared mass equal to $m_j^2 = p_j^2$) we conclude that the two adjacent vertices are space-like.

There is immediately a second conclusion. If we define the vectors $q_j = (x_{j+}, -x_{j-})$ then we obtain that $p_j = q_{j-1} - q_j$. This means that the Lund fragmentation process also can be described by means of a ladder graph as in Fig. 1.2. Thus the energy-momentum transfers between the particles along the ladder is in a dual relationship to the production vertices in the description in Fig. 1.1. We will use this relationship in Section 1.3 to derive the results of this paper.

The derivation of the Lund Model formulas is based upon these observations and a final assumption: even if the energy of the original pair (in the cms denoted conventionally $W = \sqrt{s}$) will increase without limit the distribution of the proper times of the production vertices $\Gamma_j = x_j^2 = x_{j+}x_{j-}$ will stay finite. In terms of the momentum transfers this "saturation assumption" evidently

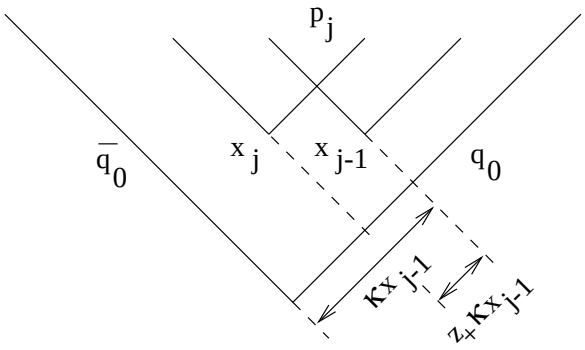

Figure 1.3: Two adjacent vertices with coordinates x_j and x_{j-1} (in the center of the process) and a hadron with energy-momentum p_j produced in between.

corresponds to (one of) the ordinary assumptions behind Gribov's Reggeon theory, that the momentum transfers stay finite in this limit.

To see the details, we will concentrate on two adjacent vertices in the center of the process with the coordinates x_j and x_{j-1} such that the above-mentioned hadron with p_j is produced in between, cf. Fig. 1.3. It is convenient to introduce the coordinates $z_+ = 1 - x_{j+}/x_{j-1+}$ and $z_- = 1 - x_{j-1-}/x_{j-}$ that are Lorentz invariants and will have the range $0 \leq z_\pm \leq 1$ independent of the other variables. We also describe the vertices by the hyperbolic coordinates (Γ_ℓ, y_ℓ), $\ell = j-1, j$ and note that due to Lorentz covariance the process can only depend upon the Γ's (i.e. the proper times squared) and the relative hyperbolic angles $\delta y_j = y_{j-1} - y_j$ (note that the δy's will be fixed by the mass requirements).

We will then consider the breakup vertex x_{j-1} to be the last in a long row of production points along the positive lightcone and using the saturation assumption we expect that the probability distribution is

$$H(x_{j-1})dx_{j-1+}dx_{j-1-} \equiv H(\Gamma_{j-1})d\Gamma_{j-1}dy_{j-1} \tag{1.1}$$

In the second line we have made use of Lorentz invariance to claim that the function H only depends upon Γ_{j-1}. The production of the particle p_j is then given by another "step" along the positive lightcone with the probability $f(z_+)dz_+$ to take the fraction z_+ of the remainder. Then the combined probability is given by

$$H(\Gamma_{j-1})d\Gamma_{j-1}dy_{j-1}f(z_+)dz_+ \tag{1.2}$$

In the same way we may consider the production of the particle as the last in a long row of steps along the negative lightcone, firstly arriving at the vertex

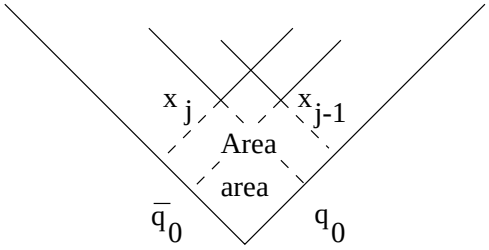

Figure 1.4: The two areas used in Eq. (1.5). The large area is the one spanned below the first meeting point of the two constituents from the adjacent vertices.

x_j with the probability H and then taking another step along the negative lightcone. In this way we obtain the joint probability

$$H(\Gamma_j)d\Gamma_j dy_j f(z_-)dz_- \tag{1.3}$$

The basic assumption in the Lund Model is then that the two probability distributions in Eqs. (1.2) and (1.3) are equal and this defines in a unique way the distributions H and f [1, 2]

$$\begin{aligned} H_j(\Gamma) &= C_j \Gamma^{a_j} \exp(-b\Gamma) \\ f_{j-1,j}(z) &= N_{j-1,j}(1-z)^{a_j} z^{a_{j-1}-a_j-1} \exp(-bm^2/z) \end{aligned} \tag{1.4}$$

The parameters a_j (with the notation for $f_{j-1,j}$ meaning that the hadron with mass m is produced in a step from the point $j-1$ to the point j) may be different for different vertices (e.g. spin- and/or flavour dependent) but the parameter b should be the same, i.e. it must correspond to a general colour dynamical property. (Speculations on its origin can be found in e.g. [2]). In the phenomenological applications of the Lund Model there has (besides the first particle in a heavy quark jet according to a suggestion by Bowler, [4]) been no use for more than a common a-value. We will in general in this paper treat this simpler case and only when it is useful exhibit the differences to the general case. Finally, the parameters C_j and $N_{j-1,j}$ are normalisation constants.

The joint probability distribution $H(\Gamma)f(z)$ can then be written as

$$H(\Gamma)f(z) \propto CN[(1-z)\Gamma]^a \exp(-b(\Gamma + m^2/z)) \equiv (area)^a \exp(-b(Area)) \tag{1.5}$$

where the two areas, the large and the small one, are shown in Fig. 1.4. Evidently, the opposite production direction will produce the same result and the areas play therefore due their simple factorisation properties (just as they do in general for gauge field theories) a fundamental role in the process. (If

there are different values of the a-parameter the result is similar with different areas represented, one typical of each vertex).

We will next consider the probability to produce a rank-connected N-particle set $\{p_j\}$, for definiteness along the positive lightcone starting at the turning point of the original q_o (cf. Fig. 1.5). The first rank particle will then take a fraction z_1 of the total lightcone energy momentum, the second will take a fraction z_2 of what is left, i.e. $(1-z_1)$ etc. The observable fractions are then $\zeta_1 \equiv z_1$, $\zeta_2 = z_2(1-\zeta_1)$, $\zeta_3 = z_3(1-\zeta_1-\zeta_2) = z_3(1-z_1)(1-z_2)$ etc. In this way we obtain in easily understood notations, [1, 2]:

$$\begin{aligned}
&\prod_1^N N_j \frac{dz_j}{z_j}(1-z_j)^a \exp(-bm_j^2/z_j) = \\
&\prod_1^N N_j \frac{d\zeta_j}{\zeta_j}(1-\sum_1^N \zeta_j)^a \exp(-b(A+\Gamma)) = \\
&ds\frac{dz}{z}(1-z)^a \exp(-bs(1-z)/z)\prod_1^N N_j \frac{du_j}{u_j} \times \\
&\exp(-bA)\delta(1-\sum_1^N u_j)\delta(s-\sum_1^N m_j^2/u_j) \equiv dP_{ext}dP_{int} \qquad (1.6)
\end{aligned}$$

In the second line, we have introduced the variables ζ_j defined above and in the third the common variable $z = \sum_1^N \zeta_j$ and finally rescaled the fractions into $u_j = \zeta_j/z$. We have also introduced the total area (according to Fig. 1.5) $A_{tot} = A + \Gamma$ and the total cms energy $\sqrt{s}$ of the N-particle cluster. We note that the "final" vertex proper time squared is $\Gamma = (1-z)s/z$.

The final result is then that the probability distribution can be factorised into two parts. One of them (dP_{ext}) (note that it is independent of the multiplicity N) is the probability to make a cluster of mass $\sqrt{s}$ and lightcone fraction z. We note the close similarity to the fragmentation function for a single particle f in Eq.(1.4). The other one (dP_{int}) is the probability that the cluster will decay into just these particular particles with the fractional energy momenta u_j in the cluster cms.

The distribution dP_{ext} for the general case when several values of a occurs will only depend upon the first and the last a-values:

$$dP_{ext} = ds\frac{dz}{z}z^{a_0}(\frac{1-z}{z})^{a_n}exp(-b\Gamma) \qquad (1.7)$$

The distribution dP_{ext} can be used to study the convergence of the "saturation assumption" on the distribution H. One finds, [2] that for squared cms-energies s larger than a few times the inverse of the parameter b there is an exponential convergence.

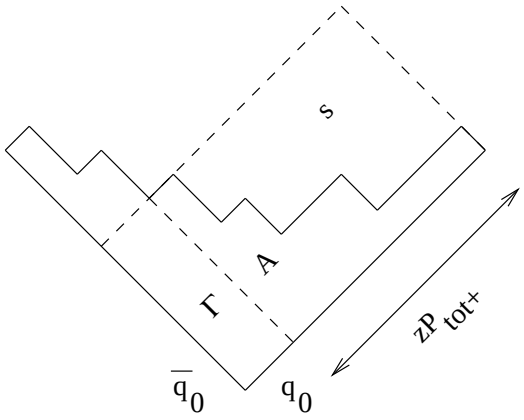

Figure 1.5: An N-particle cluster with notation as explained in the text.

The distribution dP_{int} can be reformulated using that du_j/u_j is equivalent to $d^2p\delta(p^2 - m^2)$ and that the two delta functions in the same way can be written in terms of the particle energy momenta ($p_j = (u_j P_{tot+}, m^2/u_j P_{tot+})$), $P_{tot} = (P_{tot+}, s/P_{tot+})$

$$\delta(1 - \sum_1^n u_j)\delta(s - \sum_1^n m_j^2/u_j) = \delta^2(\sum_1^n p_j - P_{tot}) \tag{1.8}$$

Putting this together we obtain the Lund Model area law:

$$dP_{int} = \prod_1^n N_j d^2p_j \delta(p_j^2 - m_j^2)\delta(\sum_1^n p_j - P_{tot}) \exp(-bA) \tag{1.9}$$

In the case of different a-parameter values we obtain an extra factor for each j: $u_j^{(\delta a)_j}$ with $(\delta a)_j = a_{j-1} - a_j$, i.e. only the differences of the adjacent a-values occur. (It is useful to note that $u_{+j}u_{-j} = m_j^2/s$ in order to see that the formula is symmetric between the forward and backward lightcones).

1.3 The Transition Operator and its Eigenfunctions

We will in this section rearrange the Lund Model area law , cf. Eq. (1.9), in another form i.e. as a product of a set of step operators taking us from one vertex to the next thereby producing a particle in between. We will after that show that this transition operator has a well-defined set of eigenfunctions with discrete eigenvalues.

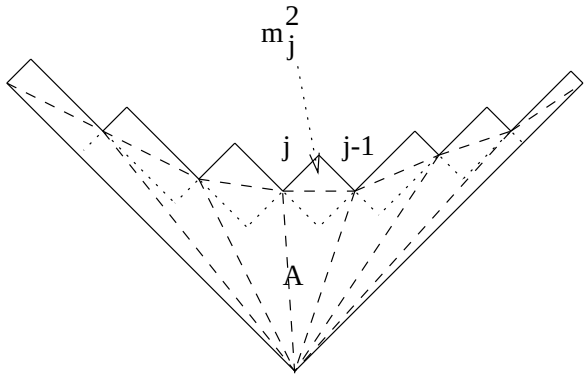

Figure 1.6: The area A subdivided into triangular regions as described in the text.

To do that, we note that the area A can according to Fig. 1.6 be subdivided into (hyperbolic) triangular regions (each with an extra "tip" corresponding to half of the squared mass; we neglect them for the moment and note that they can be included in the particle production constants N_j). The size of these regions are given by $(\delta A)_j = \sqrt{\Gamma_{j-1}\Gamma_j}|sinh(\delta y_j)|$ (we are using the notations from the earlier section) and one finds by direct calculation that

$$\begin{aligned}(\delta A)_j &= \sqrt{\lambda(\Gamma_{j-1},\Gamma_j,-m_j^2)}/2 \\ \lambda(a,b,c) &= a^2+b^2+c^2-2ab-2bc-2ac \end{aligned} \tag{1.10}$$

If we introduce the lightcone fraction z according to Fig. 1.6, then we can write

$$\begin{aligned}\Gamma_{j-1} &= (1-z)(\Gamma_j + m_j^2/z) \\ (\delta A)_j &= (z\Gamma_j + m_j^2/z)/2 \end{aligned} \tag{1.11}$$

We also note the vectors $q_j = (x_{j+}, -x_{j-})$ (with $-q_j^2 = \Gamma_j$) that fulfil $p_j = q_{j-1} - q_j$, thereby "solving" the energy-momentum conservation conditions in

Eq.(1.9). If we introduce them instead of the particle vectors $\{p_j\}$, then we find the Jacobian

$$d^2p_j\delta(p_j^2 - m_j^2) = d\Gamma_j/\sqrt{\lambda(\Gamma_{j-1}, \Gamma_j, -m_j^2)} \tag{1.12}$$

We can consequently subdivide the whole process according to the arealaw as

$$\begin{aligned} dP_{int} &= \prod_1^n K(\Gamma_{j-1}, \Gamma_j, m_j^2)d\Gamma_j \\ K(\Gamma_{j-1}, \Gamma_j, m_j^2) &= N_j \frac{\exp(-b/2\sqrt{\lambda(\Gamma_{j-1}, \Gamma_j, -m_j^2)})}{\sqrt{\lambda(\Gamma_{j-1}, \Gamma_j, -m_j^2)}} \end{aligned} \tag{1.13}$$

A useful representation of the kernel function K is (it is easily obtained from the considerations above)

$$\begin{aligned} &K(\Gamma_{j-1}, \Gamma_j, m_j^2) = \\ &\int_0^1 \frac{dz \exp(-b(z\Gamma_j + m_j^2/z)/2)}{z} \delta(\Gamma_{j-1} - (1-z)(\Gamma_j + m_j^2/z)) \end{aligned} \tag{1.14}$$

(To be precise the result in Eq.(1.13) must be supplemented by boundary conditions but we will neglect them because in this paper we will only be interested in results outside the fragmentation regions). It is useful to consider the eigenfunctions of the transition operator K. For simplicity we will introduce the dimensionless variables $\Gamma_\ell \to b\Gamma_\ell \equiv x_\ell$ and $m_\ell^2 \to bm_\ell^2 = y_\ell$ and consider the solution to the equations

$$\lambda_n g_n(x) = \int K(x, x', y) g_n(x')dx' \tag{1.15}$$

The surprising and very gratifying result we obtain is that the functions g_n are well-known in mathematical analysis. We are going to call them the Laguerre functions (noting that the Laguerre polynomials L_n are orthonormal in the measure $dx\exp(-x)$)

$$g_n(x) = L_n(x)\exp(-x/2) \tag{1.16}$$

They are orthonormal on the positive real axis $0 \le x \le \infty$ in the measure dx (we use the notations from [5])

$$\begin{aligned} &\int_0^\infty dx g_n(x) g_m(x) = \delta_{n,m} \\ &\sum_n g_n(x) g_n(x') = \delta(x - x') \end{aligned} \tag{1.17}$$

Further, the Laguerre functions are the eigenfunctions of the two-dimensional harmonic oscillator corresponding to angular momentum equal to zero. In fact, it is easy to prove that the eigenfunctions g_n will fulfil the following equation because of the well-known properties of the Laguerre polynomials L_n

$$\begin{aligned} & x\frac{d^2L_n}{dx^2} + (1-x)\frac{dL_n}{dx} + nL_n = 0 \\ & (-\triangle + bQ^2)g_n(bQ^2) = 2(2n+1)g_n(bQ^2) \end{aligned} \tag{1.18}$$

In the second line, we have considered the two-component vector Q with the scalar product $Q^2 = Q_1^2 \pm Q_0^2$. The differential operator is correspondingly defined as $\triangle = \frac{\partial^2}{\partial bQ_1^2} \pm \frac{\partial^2}{\partial bQ_0^2}$ i.e. the equation is valid both for Euclidian metric and for space-like directions in two-dimensional Minkowski space.

We note in particular, that the eigenfunctions are independent of the mass m of the particle produced in between, this mass-dependence comes solely in the eigenvalues

$$\lambda_n(y) = N\exp(y/2)\int_0^1 dz/z\exp(-y/z)(1-z)^n \tag{1.19}$$

Here we have kept to the definition of the hyperbolic triangle, without the "tip", in the kernel function K (cf. the remarks before the Eq.(1.10)). We will be concerned with the properties of the eigenvalues in the next section but we note at this point their close relationship to the Lund fragmentation function f (for equal a-values) in Eq.(1.4). It is also obvious from Eq.(1.19) that the eigenvalues will be discrete and decrease quickly with n.

To obtain these results from Eq.(1.15), we make use of the representation of the kernel function K in Eq.(1.14) and find the following necessary (and sufficient) requirements on the Laguerre polynomials:

$$\lambda_n L_n(x) = \int_0^1 dz/z\exp(-y/z)L_n((1-z)(x+y/z)) \tag{1.20}$$

It is easy to see that for a polynomial of the n:th degree the eigenvalues λ_n will have to fulfil Eq.(1.19). However, to prove the general result in Eq.(1.20) we have expanded both sides in powers, performed for the m:th term inside the integral $0 \le \ell \le m$ partial integrations (to get rid of the powers of y) and then gathered the powers in x. We feel that there must be a simpler way but we have not found it yet.

Given these results, we note that a theorem attributed to Mercer (private information, [6]) provides the following representation for the transition operator K:

$$K(x,x',y) = \sum_{n=0}^{\infty} g_n(x)\lambda_n(y)g_n(x') \tag{1.21}$$

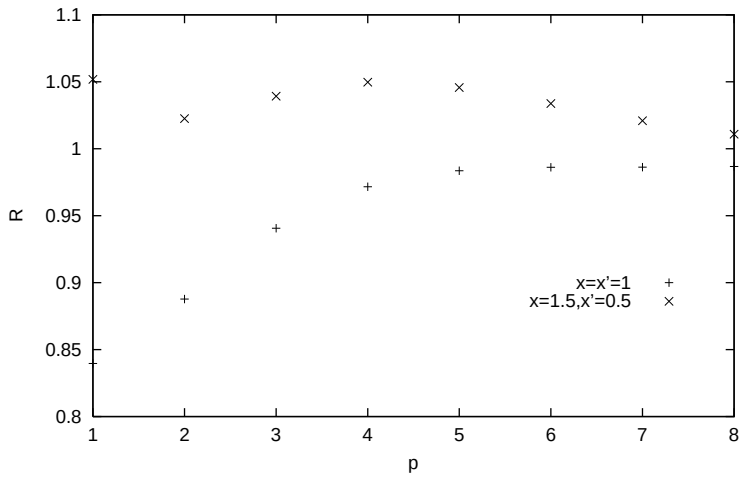

Figure 1.7: The ratio R=$\frac{\exp(-\frac{1}{2}\sqrt{\lambda(x,x',-y)})}{\sqrt{\lambda(x,x',-y)}}$/ $\sum_{n=0}^{p} g_n(x)\lambda_n(y)g_n(x')$ for different values of p,x and x' when y=0.5.

In order to check the convergence properties of Eq.(1.21), we show in Fig. 1.7 the results for the ratio of the left-hand to the right-hand side of the equation. It is evidently in general only necessary to keep a few terms to obtain a good approximation.

Due to the orthonormality of the Laguerre functions, it is further immediately obvious that while Eq.(1.21) represents the distribution after a single particle production between x' and x the result for the production of N particles in between them is given by

$$K_N(x,x') = \sum_{n=0}^{\infty} g_n(x)(\lambda_n(y))^N g_n(x') \tag{1.22}$$

In the next section, we will show how to provide a formula for a fixed invariant mass-square s and/or a fixed lightcone fraction z (thereby completely defining the relationships) between the points labelled by x' and x.

1.4 The Properties of the Eigenvalues

We will in the following discussion for simplicity put the normalisation constant N equal to unity but we will insert it in the end formulas. Then the eigenvalues $\lambda_n(y)$ (with $y = bm^2$) defined in Eq.(1.19) will have the following property:

$$\exp(y/2)\lambda_n(y) = \int_0^1 dz(1-z)^n \frac{\exp(-(1-z)y/z)}{z} =$$
$$\int_0^1 dz \sum_m (1-z)^{m+n} L_m(y) = \sum_m \frac{L_m(y)}{m+n+1} \tag{1.23}$$

We have here in going from the second to the third line in Eq. (1.23) made use of the generating function for the Laguerre polynomials ([5]):

$$\sum_n L_n(y) z^n = \sum_k \frac{(-y)^k}{k!} \sum_m \frac{z^{m+k}(m+k)!}{m!k!} = \frac{\exp[-yz/(1-z)]}{(1-z)} \tag{1.24}$$

In the second line, we have introduced the series expansion for the Laguerre polynomials, rearranged it by changing the original index $n \to m+k$ and then summed up firstly a negative binomial and then an exponential series.

Consequently, the eigenvalue for n can be written as a series in the eigenfunctions g_m and we may from this representation immediately conclude (using the differential equation in Eq.(1.18)) that the eigenvalues will fulfil

$$(-\triangle + bp^2)\lambda_n(bp^2) = -2(2n+1)\lambda_n(bp^2) + 4\delta(bp^2) \tag{1.25}$$

Here we have introduced the timelike vector p with length equal to the mass (and the differential operator $\triangle$ is defined in terms of p:s components). We have also used the result in Eq.(1.17) noting that $g_m(0) = 1$ for all values of m. We conclude that also the eigenvalues are governed by the harmonic oscillator equation and that they correspond to a particular analytic continuation of these functions from spacelike to timelike vectors.

Actually, the eigenvalues $\lambda_n(y)$ are solutions to the (degenerate) hypergeometric differential equation and in conventional notations, [5] in terms of Whittaker functions we have $\lambda_n(y) = n! W_{-n-1/2,0}(y)/\sqrt{y}$. Using either the differential equation in Eq.(1.25) or the formulas in [5] we obtain another useful representation that bears out these analyticity properties:

$$\lambda_n(y) = \int_0^\infty dt \frac{g_n(t)\exp(-(t+y)/2)}{t+y} \tag{1.26}$$

Next we will consider the correlation coefficients for the case when we produce N particles in between the vertices denoted x and x' in Eq. (1.22). Using the

same procedure as in connection with the derivation of the N-particle cluster in Eq.(1.6), we can immediately write

$$\begin{aligned}
\lambda_n^N(y) &= \int ds R_N(s)\hat{\lambda}_n(bs) \\
R_N(s) &= \int \prod_1^N N_j d^2p_j \delta(p_j^2 - m_j^2)\delta(\sum_1^N p_j - P_{tot})\exp(-bA) \\
\hat{\lambda}_n(bs) &= \exp(bs/2)\lambda_n(bs)
\end{aligned} \tag{1.27}$$

The quantity $\hat{\lambda}_n(bs)$ is the probability (in the nth harmonic oscillator state) to produce a cluster with the energy s. It is the integral over all z values of dP_{ext} in Eq. (1.6) (with the Lund parameter a exchanged for n). In the same way $R_N(s)$ is related to the integral over dP_{int} in Eq. (1.6), i.e. it is the phase space integral (including the area law) of the N particles. We have brought back the normalisation constants N_j in the expression for R_N.

It is now evident how to obtain the distributions of x and x' when there are N particles with a fixed squared mass s in between:

$$\sum_n g_n(x)\hat{\lambda}_n(bs)R_N(s)g_n(x') \tag{1.28}$$

We will next turn to the properties of the phase space integrals R_N but before that we make the following observation. The model has very simple factorisation properties both in the energy-momentum fractions and, as we have shown in this note, in the energy-momentum transfers (or in the dual language, in the vertex positions). Consequently, it is in the same way as in Eq.(1.28) possible to pick out any other variables, like particular energy-momentum fractions somewhere "in between" and reformulate the remaining correlation coefficients accordingly. (It is of course necessary to define the scaling variables properly). As every possible observable is either related to the energy momentum transfers or to the energy-momentum of the observed particles we have in this way a complete analytical description of the process.

We will show two particularly simple and useful properties of the phase space integrals R_N. They fulfil a set of iterative integral equations and there are very simple formulas for the analytic function $\mathcal{R}_N$ which is defined by

$$\mathcal{R}_N(u) = \int ds \frac{R_N(s)}{s+u} \tag{1.29}$$

To see these properties we note that if we "pick out" the first rank particle from the N-particle cluster that defines R_N we obtain, cf. Eqs. (1.6) and (1.27) $N_1 du_1/u_1 \exp(-bm^2/u_1)$. The remaining $(N-1)$ particles will give the same contribution but the energy is reduced to $s_1 = (P_{tot}-p_1)^2 = (1-u_1)(s-m^2/u_1)$.

We have consequently the integral equation

$$R_N(s) = \int_0^1 \frac{N_1 du_1}{u_1} R_{N-1}((1-u_1)(s-m^2/u_1)) \exp(-bm^2/u_1) \qquad (1.30)$$

We note the similarity to the original integral equations for the harmonic oscillator functions $g_n(x)$, but there are two major differences. The first is the change of sign in front of the term m^2/u_1 in the integral (reflecting the fact that we are going from the space-like vectors q_j to the timelike vector P_{tot}). The second difference is that the argument in the functions R_N and R_{N-1} do not have the same range. It is evident that the threshold for producing N particles is $s_{N,thresh} = N^2 m^2$ which is larger than the threshold for $N-1$ particles.

There is, however, another relation which will make it possible to calculate the functions R_N analytically at least as a perturbation series. In order to see that, we consider the following sum and use the results from Eq.(1.27):

$$\begin{aligned}
&\sum_n (\lambda_n(y))^N L_N(bu) = \\
&\int ds R_N(s) \int \frac{dz}{z} \exp -bs(1-z)/z \sum_n (1-z)^n L_n(bu) = \\
&\int ds R_N(s) \int \frac{dz}{z^2} \exp -(bs+bu)(1-z)/z = \mathcal{R}_N(u)/b
\end{aligned} \qquad (1.31)$$

We have once again used the generating function in Eq.(1.24) and performed the z integral. In this way we have a representation of the analytic function $\mathcal{R}$ along the positive real u-axis. It is , however, necessary to extend this function to the negative real axis in order to obtain the properties of R_N. We note in passing that the first line in Eq.(1.31) is (besides a factor $\exp(-bu/2)$ the contribution for the case when we would start out at the lightcone $x = 0$ and consider N steps to the point $x' = bu$ ($g_n(0) = 1$ for values of n). This result can be used in a perturbation theory by noting that for large values of n we have the following behaviour of our functions:

$$g_n(x) \simeq J_0(2\sqrt{nx}) \quad \text{and} \quad \lambda_n(y) \simeq \sqrt{2/\pi} K_0(2\sqrt{ny}) \qquad (1.32)$$

We can then in this approximation write

$$\begin{aligned}
\sum_n g_n &\to \int \frac{d^2 v}{2\pi} \exp(i2\vec{v}\vec{\mu}) \\
\lambda_n(y) &\to \int \frac{d^2 t}{(2\pi)^{3/2}} \frac{\exp(i2\vec{v}\vec{t})}{\vec{t}^2 + y}
\end{aligned} \qquad (1.33)$$

We have then defined two-dimensional Euclidian vectors with $\vec{\mu}^2 = u$ and with

$\vec{v}^2 \to n$. Therefore the whole expression can approximately be written

$$\exp(-bu/2)\mathcal{R}(u) = \sum_n (\lambda_n(y))^N g_n(bu) \to$$
$$\int \prod_{j=1}^{N} \frac{d^2 t_j}{(2\pi)^{3/2}(\vec{t}_j^2 + y)} \int \frac{d^2 v \exp(i2\vec{v}(\vec{\mu} - \sum \vec{t}_j))}{2\pi} =$$
$$\int \prod_{j=1}^{N} \frac{d^2 t_j}{(2\pi)^{3/2}(\vec{t}_j^2 + y)} \delta(\vec{\mu} - \sum \vec{t}_j)/4 \tag{1.34}$$

In this way we have exhibited the analytical function $\exp(-bu/2)\mathcal{R}_N(u)$ for values of $u \geq 0$ as the contribution from a simple expression obtainable in a two-dimensional Euclidian field theory. (Note that we use the Laguerre functions g_n and not the Laguerre polynomials L_n in our approximations).

We note that the approximation corresponds to the large n-limit of the harmonic oscillator function, i.e. we are far away from the ground state and consequently "the motion" behaves as almost free oscillations.

It is possible inside the same formalism to take the neglected terms in the approximation into account as further contributions in the model. We can use the present results to show that the convergence radius in an expansion of $\mathcal{R}_N$ around $u = 0$ is given by $N^2 m^2$ (just as expected). But further terms in the expansion are necessary in order to obtain the precise threshold behaviour. We will present such results in future publications.

1.5 Concluding Remarks

Due to its simple factorisation properties, the Lund Fragmentation Model can as we have shown in here be diagonalised in terms of harmonic oscillator functions. We have, up to now, only treated the $1 + 1$-dimensional version of the model but we will, in future publications, continue the work into the $3 + 1$-dimensional real world.

Transverse momentum is in the fragmentation process of the Lund Model produced via a tunneling mechanism, leading to a gaussian spectrum. In the simplest version of the model, there are no correlations between the transverse momentum generated at one vertex and at the next but the experimental data show, [7], that such correlations occur at least in the production of the light pions. A mechanism, with strong similarities to the Ornstein-Uhlenbeck process for the velocity distribution of a Brownian motion particle, has been proposed and succesfully applied to the data, [8].

As this process again is of a gaussian character, we may use very similar methods to diagonalise it, cf. also [9]. There is, however, a small subtlety. If the transverse momentum is firstly generated and afterwards the string-field

used to provide longitudinal momentum (as in JETSET) then the transverse mass is used instead of the ordinary mass. This would provide a particular correlation between transverse and longitudinal motion. We will come back in a later publication to a general investigation of the dynamics.

Gluon radiation is in the Lund Model treated in terms of internal excitations of the string field and this will lead to a bent string surface, [2]. The fragmentation of states containing one or more gluons has been introduced into the Lund Model by Sjöstrand, [10], using a particular generalisation of the process described above. This process is implemented into JETSET and has been very succesful to describe the experimental data. The method we have introduced above for a flat string surface can be almost directly applied (there is a minor change, that we feel may have some implications for the description of the fastest particles in a gluon jet) to the method introduced by Sjöstrand.

Bose-Einstein correlations has been introduced into the Lund Model by interpreting the Lund Area Law as stemming from the square of a quantum mechanical transition matrix element, [11, 12]. This means that the Area Law for production of two or more identical particles, obtains a weight factor depending upon area differences. One problem in this respect is that with n identical particles the weight factor will obtain contributions from the $n!$ different permutations of the particles. The mathematicians call these problems exponential in n and they are very time-consuming (although we were in [12] able to bring them down considerably). As the area differences are directly expressible in terms of the variables we have discussed above we have some hope to be able to reexpress the full result by means of our formalism.

Finally, we have obtained a new set of tools to study the energy dependence of quantities like $R_N(s)$ and even more interestingly the sum over all the multiplicities $R(s) = \sum_N R_N$. This dependence will necessarily be of the kind s^a. This is known from before, [1, 2], but the power a, that corresponds to a "Regge intercept" in quark scattering, in accordance with Gribov's Reggeon theory, will in this way be accessible for analytical treatment. Evidently the corresponding power obtained for a "gluon fragmentation process" will have some meaning for the soft Pomeron intercept.

1.6 Acknowledgements

One of us, Bo Andersson, would like to thank Eddi de Wolfe for suggesting that the Lund Model should be treated by transfer matrix techniques and for providing helpful material.

References

[1] B. Andersson, G. Gustafson, B. Söderberg, Z. Phys. **C20** (1983) 317.

[2] Bo Andersson, The Lund Model, (Cambridge University Press, 1998).

[3] T. Sjöstrand, Computer Physics Commun. **82** (1994) 74.

[4] M.G. Bowler, Z. Phys. **C29** (1985) 617.

[5] W. Magnus, F. Oberhettinger and R.P. Soni, Formulas and Theorems for the Special Functions of Mathematical Physics, (Springer, 1966).

[6] Eddi de Wolf, private information.

[7] E.A. de Wolf, Contrib. to Proc. XXII Symp. on Multiparticle Dynamics, ed. A.Pajares World Scientific.

[8] B. Andersson, G. Gustafson, J. Samuelson, Nucl. Phys. **B463** (1996) 217.

[9] C. Michael, Nucl. Phys. **B103** (1976) 296.

[10] T. Sjöstrand, Nucl. Phys. **B248** (1984) 469.

[11] B. Andersson, W. Hofmann, Phys. Lett. **B169** (1986) 364.

[12] B. Andersson, M. Ringnér, Nucl. Phys. **B513** (1998) 627, Phys. Lett. **B421** (1998) 283.

The Lund Fragmentation Process for a Multi-gluon String According to the Area Law

Paper II

LU TP 01-22
June 2001

The Lund Fragmentation Process for a Multi-gluon String According to the Area Law

Bo Andersson[1]
Sandipan Mohanty[2]
Fredrik Söderberg[3]
Department of Theoretical Physics, Lund University,
Sölvegatan 14A, S-223 62 Lund, Sweden

Abstract
The Lund Area Law describes the probability for the production of a set of colourless hadrons from an initial set of partons, in the Lund string fragmentation model. It was derived from classical probability concepts but has later been interpreted as the result of gauge invariance in terms of the Wilson gauge loop integrals. In this paper *we will present a general method to implement the Area Law for a multi-gluon string state.* In this case the world surface of the massless relativistic string is a geometrically bent $(1+1)$-dimensional surface embedded in the $(1+3)$-dimensional Minkowski space. The partonic states are in general given by a perturbative QCD cascade and are consequently defined only down to a cutoff in the energy momentum fluctuations. *We will show that our method defines the states down to the hadronic mass scale inside an analytically calculable scenario.*

We will then show that there is a differential version of our process which is closely related to the generalised rapidity range λ, which has been used as a measure on the partonic states. We identify λ as the area spanned between *the directrix curve* (the curve given by the parton energy momentum vectors laid out in colour order, which determines the string surface) and the average curve (to be called the $\mathcal{P}$-curve) of the stochastic X-curves (curves obtained when the hadronic energy-momentum vectors are laid out in rank order). Finally *we show that from the X-curve corresponding to a particular stochastic fragmentation situation it is possible to reproduce the directrix curve* (up to one starting vector and a set of sign choices, one for each hadron). This relationship provides an analytical formulation of the notion of Parton-Hadron Duality. The whole effort is made in order to get a new handle to treat the transition region between where we expect perturbative QCD to work and where the hadronic features become noticeable.

[1]bo@thep.lu.se
[2]sandipan@thep.lu.se
[3]fredrik@thep.lu.se

2.1 Introduction

The Lund String Fragmentation Model was developed many years ago, [1, 3], and as implemented in the well-known Monte Carlo simulation program JETSET, [4], it has been very successful in reproducing experimental data from high energy multi-particle processes.

The model is based upon a few general assumptions: (i) the final state particles stem from the breakup of a string-like force field spanned between the coloured constituents, (ii) there is causality and Lorentz invariance and (iii) the production of the particles can be described in terms of a stochastic process which obeys a saturation assumption. We have, in a recent paper [5], re-derived the major result for the (1+1)-dimensional model, which is applicable for events with a quark (q, a colour-3) and an antiquark ($\bar{q}$, a colour-$\bar{3}$) at the endpoints of the string but with no interior gluonic (g, colour-8) excitations. The result is that the (non-normalised) probability for the production of an n-particle final state of hadrons with energy momenta $\{p_j\}$ and masses $\{m_j\}$ is given by the Lund Area Law:

$$dP_n(\{p_j\}; P_{tot}) = \prod_{j=1}^{n} N_j d^2p_j \delta(p_j^2 - m_j^2) \delta(\sum_{j=1}^{n} p_j - P_{tot}) \exp(-bA) \qquad (2.1)$$

where A is the area spanned by the string "before" the breakup, cf. Fig.2.1, P_{tot} is the total energy-momentum of the state and $\{N_j\}$ and b are parameters related to the density of hadronic states and the breakup properties of the string field, respectively.

The result in Eq. (2.1) is evidently similar to a quantum mechanical transition probability. It is the final state phase space multiplied by a squared matrix element, which in this case would correspond to the negative area exponential. In [5] we have shown that it is possible to "diagonalise" the model, i.e. to express the result in Eq. (2.1) as a product of (diagonal) transition operators (in quantum mechanical language it would correspond to density operators). It turns out that in this way the dynamics can be described in terms of $(1+1)$-dimensional (space-like) harmonic oscillators.

Shortly after the original derivation of the Area Law, [1], Sjöstrand, [6], provided an implementation of the model applicable also for multi-gluon states, i.e. when the string surface is no longer flat but geometrically bent due to the internal excitations. Sjöstrand's method is to project the positions of the breakup points (the vertices) from the (flat) (1+1)-dimensional model as given by Eq. (2.1) onto the surface of the bent string. The projection is done so that the proper times of the vertices and the squared masses of the particles produced between them are the same. Unfortunately this method does not fulfil the Area Law on the bent surface because it is a geometrical fact that the

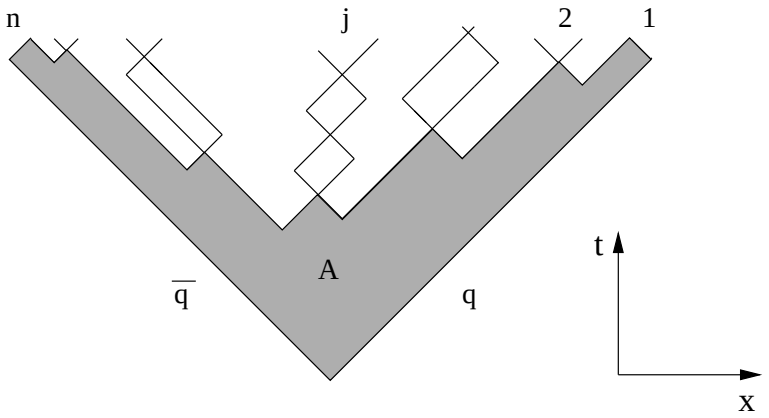

Figure 2.1: A high-energy string breakup.

areas "below the vertices" are not invariant under such a projection from a flat to a bent surface.

Although the Area Law is not fulfilled on an event to event basis by the method in [6] we will show that it is fulfilled in an average sense, i.e. the predicted inclusive distributions are little affected by the differences. It is well-known that the experimental results for these distributions are well described by JETSET even up to the largest available energies of today.

The intention of this note is to implement another method for particle production in multi-gluon states which fulfils the Area Law at every single step in the production process. We will find that it is necessary to tackle a set of problems in the definition of the states which we apply the process to. We note that the states defined by perturbation theory are resolved only to the scale of some virtuality cutoff. We will find that our method provides a set of excitations on the hadronic mass scale, in the string field. We will investigate the properties of these "soft hadronisation gluons" in future work.

The states of the massless relativistic string fulfil a minimum principle, i.e. the surface spanned in spacetime by the string during its motion is a minimal surface. This means on the one hand, that the states should be stable against small-scale variations and on the other hand that the surface is fully determined by the boundary curve. In this case the boundary curve corresponds to the orbit of one of the endpoints, conventionally chosen as the q-endpoint. Therefore, the process we are going to define is a process along this curve, to be called the *directrix curve*, which is completely defined by the perturbative cascade. In this paper we will treat the partons as massless, although both the process and the directrix curve can be defined for a general case with massive quarks.

One property which can be derived from Eq. (2.1) is that the average decay region is a typical hyperbola. On the average, the final state hadrons in our process will be produced in the same way, albeit this time along a set of connected hyperbolae. In [2] we have defined such an average curve and we will, in this paper, call it the $\mathcal{X}$-curve. Just as a simple hyperbola has a length proportional to the hyperbolic angle that it spans (this corresponds to the available rapidity range along the mean decay region, in a two-jet system of hadrons) the $\mathcal{X}$-curve has a length corresponding to a generalised rapidity range, usually called the λ measure, [2, 3]. The $\mathcal{X}$-curve is defined in terms of differential equations and we will show the close relationship between the $\mathcal{X}$-curve and our process in the limit of a vanishing hadron mass.

There are several reasons to undertake this investigation. One is to compare the precise implementation of the Area Law to the approximate process in [6]. We will do this both in this paper and in future publications.

Another reason is to get a handle on the general structure of fragmentation, in particular to be able to treat also the multi-gluon fragmentation states by the analytical methods introduced in [5]. This is of particular interest for the transition region, i.e. the region in between where we expect perturbation theory to work and where we know that the non-perturbative fragmentation sets in.

A final reason is to investigate the stability of the states in QCD under fragmentation, i.e. given a multi-gluon state defined according to the rules of perturbation theory (with cut-offs as mentioned above) to find out to what extent it can be modified so that the observable results after fragmentation are still in agreement with the experiments. In the Lund interpretation of fragmentation where the particles stem from the energy of the force field it is tacitly assumed that modifications of the perturbative state below and up to the scale of the hadronic masses should have no effects. We will find that it is necessary to take into account the coherence properties of the radiation in any modification.

Although the methods presented in this paper are applicable to any multi-gluon state, for definiteness we will concentrate on the states obtained in e^+e^--annihilation processes where we expect an original colour singlet $(q\bar{q})$-state to form and start to go apart, producing a set of bremsstrahlung gluons inside an essentially point-like region. We will also be satisfied to treat a single kind of hadron with mass m. Finally, in this paper we will not introduce gaussian transverse momentum fluctuations (which we expect in a tunneling scenario [3]) in the fragmentation process. We will investigate the influence of such fluctuations in a future publication.

In Section 2.2, we provide a set of necessary formulae from the $(1 + 1)$-dimensional Lund Model. In Section 2.3, we consider the motion of strings containing internal excitations. We also provide a description of the coherence

properties of QCD and some necessary formulae to understand the $\mathcal{X}$-curve. In Section 2.4, we define the properties of the string breakup in general. We find that the most general implementation of the Area Law leads to a highly intractable process and therefore in Section 2.5 we define another approach which mends all the problems with the earlier one. In particular, in Section 2.5.3 we show a close relationship between a differential version of this process and the $\mathcal{X}$-curve. In Section 2.6, we present a set of results from our method, followed by some concluding remarks on future work in Section 2.7.

2.2 Some results from the $(1+1)$-dimensional model

2.2.1 The Area Law

The Lund Model contains a non-trivial interpretation of the QCD force-field in terms of the massless relativistic string with the quarks (q) and the anti-quarks ($\bar{q}$) at the endpoints and the gluons (g) as internal excitations on the string field. It is assumed that the force field can break up into smaller parts in the fragmentation process by the production of new ($q\bar{q}$)-states (i.e. new endpoints). A q from one such breakup point ("vertex"), together with a $\bar{q}$ from an adjacent vertex and the field between them, can form a hadron on mass shell.

For the simple case when there are no gluons, the string field only corresponds to a constant force field (with a phenomenological size $\kappa \simeq 1GeV/fm$) spanned between the original $q\bar{q}$-pair. In a semi-classical picture, conservation of energy-momentum allows the creation of a new massless pair at some point along the field. The pair will then go apart along opposite light-cones, using up the energy in the field in between (in this way the confined fields will always end on the charges). In order that the hadron produced between two adjacent vertices should have a positive squared mass, it is necessary that the vertices are placed in a space-like manner with respect to each other. Consequently, time-ordering will be a frame-dependent statement (in any Lorentz frame the slowest particles will be the first to be produced, thereby fulfilling the requirements in a Landau-Pomeranchuk formation time scenario). It is possible to order the production process instead, along the light-cones and introduce the notion of *rank* so that the first rank hadron along the original q-light-cone will contain that q together with a $\bar{q}$ from the first vertex along the light-cone, the second rank hadron a q from the first vertex and a $\bar{q}$ from the next etc.; cf. Fig.2.1. Rank ordering is a frame independent procedure. It is of course possible to introduce a rank-ordering also from the end containing the original $\bar{q}$. One obtains , [1, 3, 5], the unique process described by Eq. (2.1)

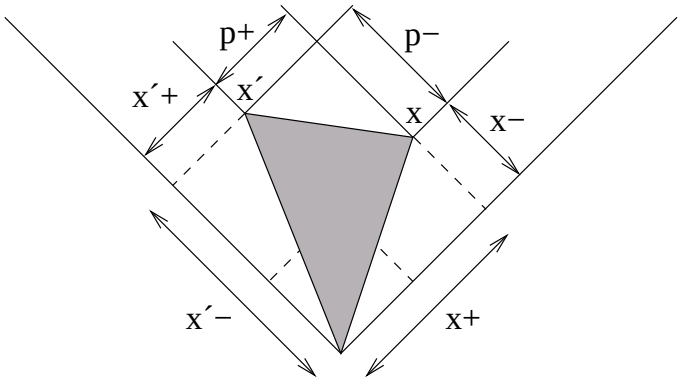

Figure 2.2: Two adjacent vertices of the string breakup process.

from these observations and an assumption that the breakup process obeys a saturation assumption, i.e. that after many steps when we are far from the endpoints the proper times of the vertices will be distributed according to an energy-independent distribution.

A particular feature is that if a particle with energy-momentum $p = (p_+, p_-)$ and with squared mass $m^2 = p^2 = p_+ p_-$ is produced between the two vertices with $x = (x_+, x_-)$ and $x' = (x'_+, x'_-)$ then we have (cf. Fig.2.2):

$$\begin{aligned} p_+ &= \kappa(x_+ - x'_+) \equiv q_+ - q'_+ \\ p_- &= \kappa(x'_- - x_-) \equiv q_- - q'_- \end{aligned} \tag{2.2}$$

Thus we find that on a flat string surface the difference between the vertex points will fulfil :

$$(x - x')^2 = -m^2/\kappa^2 \tag{2.3}$$

Eq. (2.2) implies that the $(1+1)$-dimensional Lund Fragmentation Model may also be described by means of a multi-peripheral chain diagram as in Fig.2.3 or in an energy-momentum space picture as in Fig.2.4.

This is used in [5] in order to subdivide the Area Law process into steps in between the vertices. The energy-momentum conserving δ-distribution in Eq. (2.1) can be "solved" by introducing the momentum transfers $\{q_j\}$ instead of the hadron momenta $\{p_j\}$. Then the mass-shell condition means that the hyperbolic angle between the vertices and the size of the area slit, exhibited in Fig.2.2 are fixed by the squared sizes $q^2 = -\Gamma$, $(q')^2 = -\Gamma'$ and $(q - q')^2 = m^2$.

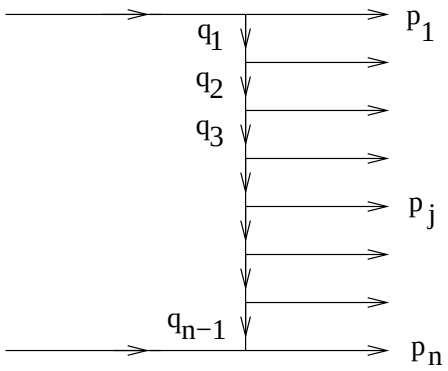

Figure 2.3: A ladder diagram describing multi-particle production.

The result is that Eq. (2.1) can be rewritten as a product of steps between the $\{\Gamma_j\}$:

$$\begin{aligned} dP_n(\{p_j\}, P_{tot}) &= \prod K(\Gamma_j, \Gamma_{j-1}, m^2) d\Gamma_j \\ K(\Gamma, \Gamma', m^2) &= N \frac{\exp(-\frac{b}{2}\sqrt{\lambda(\Gamma, \Gamma', -m^2)})}{\sqrt{\lambda(\Gamma, \Gamma', -m^2)}} \\ \lambda(a, b, c) &= a^2 + b^2 + c^2 - 2ab - 2ac - 2bc \end{aligned} \tag{2.4}$$

It is a remarkable fact that the transfer operators K can be diagonalised in terms of the eigenfunctions of the harmonic oscillator (those which are boost-invariant in a $(1+1)$-dimensional space-like Minkowski space. in a two-dimensional Euclidean space they correspond to a vanishing angular momentum) $g_n(\Gamma)$ with the eigenvalues solely determined by the squared mass of the hadrons produced in between:

$$K(\Gamma, \Gamma', m^2) = \sum_{n=0}^{\infty} g_n(\Gamma) \lambda_n(m^2) g_n(\Gamma') \tag{2.5}$$

The eigenvalues λ_n are analytic continuations of the harmonic oscillator eigenfunctions to time-like values of the argument, [5]. Useful representations of K and the eigenvalues λ_n are :

$$\begin{aligned} K(\Gamma, \Gamma', m^2) &= \int_0^1 \frac{dz}{z} \exp(-\frac{b}{2}(z\Gamma + \frac{m^2}{z})) \delta(\Gamma' - (1-z)(\Gamma + \frac{m^2}{z})) \\ \lambda_n(m^2) &= N \exp(\frac{bm^2}{2}) \int_0^1 \frac{dz}{z} (1-z)^n \exp(-\frac{bm^2}{z}) \end{aligned} \tag{2.6}$$

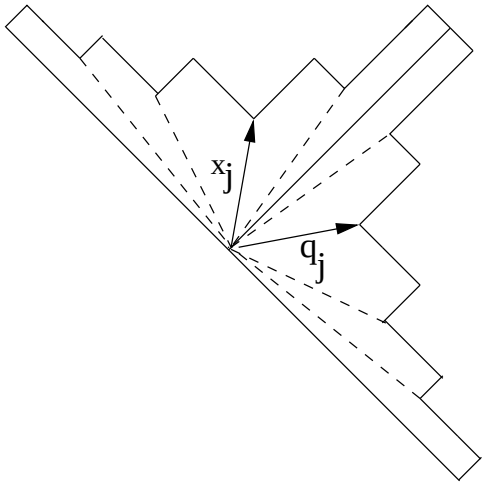

Figure 2.4: The energy-momentum space picture (q_j) and the spacetime picture (x_j) respectively.

We have introduced the positive light-cone fraction of the produced hadron z defined by $(x_+ - x'_+) = zx_+$. It is straight forward algebra to prove that the shaded area, exhibited in Fig.2.2 is given by the exponent $\frac{1}{2}(z\Gamma + \frac{m^2}{z})$ in the representation of the kernel K. We also note that the area obtained by summing the areas of the regions marked I, II and III in Fig.2.5 is equal to twice this area and that m^2/z equals the sum of the areas of regions I and II. There is a simple relationship between the two adjacent values of Γ in the representation of K:

$$\Gamma' = (1-z)(\Gamma + \frac{m^2}{z}) \tag{2.7}$$

Finally we note the identity (in easily understood notation) :

$$(I)(III) = (II)(IV) \tag{2.8}$$

Eq. (2.8), just as Eq. (2.3), is only valid for a flat string surface and a particular consequence is that the region IV is non-vanishing for the $(1+1)$-dimensional model. As the area of the region IV is proportional to $(1-z)$, the variable z must always be smaller than unity, i.e. there is a built in requirement that a typical step of the process can never use up all the available light-cone energy-momentum.

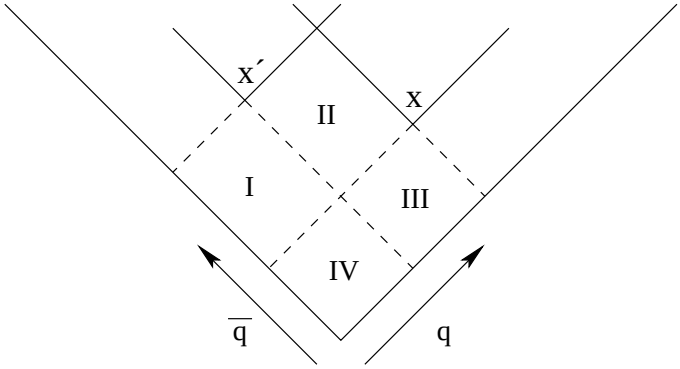

Figure 2.5: The figure shows the two vertices and the regions I, II, III and IV described in the text.

Such a requirement also comes out of the following argument. Suppose that we would integrate dP_n in Eq. (2.1) over all possible energy momenta and then sum over all multiplicities. Due to Lorentz invariance, we will obtain a function $R(s)$ which can only depend upon the total squared energy-momentum $s = P_{tot}^2$. If we pick out the dependence on the first particle and sum and integrate over all the rest we obtain an integral equation for the function R :

$$R(s) = (B.T) + \int_0^1 N\frac{dz}{z}\exp(-b\frac{m^2}{z})R(s')$$
$$s' = (1-z)(s-\frac{m^2}{z}) \qquad (2.9)$$

where $(B.T)$ stands for "boundary condition term" and the variable s' is equal to the squared mass of all the remaining particles if the first hadron takes the light-cone fraction z (we note the similarity to the Eq. (2.7)). The integral equation (2.9) has an asymptotic solution $R \propto s^a$ (with the parameter a being a function of N and bm^2 ,cf. [5]) with the requirement :

$$\int_0^1 N\frac{dz}{z}(1-z)^a\exp(-b\frac{m^2}{z}) = 1 \qquad (2.10)$$

Consequently while the exclusive formula for the production of a particular hadron with the light-cone fraction z is given by the Area Law, the inclusive probability to produce this hadron (irrespective of what comes after it in the process) must be weighted with $R(s')/R(s) \simeq (1-z)^a$. Therefore, the well-known Lund fragmentation formula is given by the integrand in Eq. (2.10) and there is a power suppression for large values of the fragmentation variable.

The formulae presented above correspond to an ordering along the positive light-cone, i.e. the variable z is defined as the positive light-cone momentum fraction of the particle. It is possible to redefine everything in terms of an ordering along the negative light-cone, i.e. to introduce the corresponding negative light-cone component ζ by writing $(x'_- - x_-) = \zeta x'_-$. It is straightforward to prove that

$$\zeta = \frac{m^2}{m^2 + z\Gamma} \quad \text{and} \quad z = \frac{m^2}{m^2 + \zeta\Gamma'} \tag{2.11}$$

and from this we find that the integrand in the representation of the kernel K can be reformulated from $(z, \Gamma) \to (\zeta, \Gamma')$ to exhibit the symmetry between the descriptions along the positive and the negative light-cone directions

$$\begin{aligned} &\frac{dz}{z}\delta(\Gamma' - (1-z)(\Gamma + \frac{m^2}{z}))\exp(-\frac{b}{2}(z\Gamma + \frac{m^2}{z})) \to \\ &\quad \frac{d\zeta}{\zeta}\delta(\Gamma - (1-\zeta)(\Gamma' + \frac{m^2}{\zeta}))\exp(-\frac{b}{2}(\zeta\Gamma' + \frac{m^2}{\zeta})) \end{aligned} \tag{2.12}$$

2.3 The description of a multi-gluon string state

The dynamics of the massless relativistic string is based upon the principle that *the surface spanned by the string during its motion is a minimal surface.* This means that *the surface is completely determined by its boundary.* In the Lund Model the string is used as a model for the confined colour force field in QCD and the above property then has the further important implication that the dynamics will be infrared stable, i.e. *all predictable features from the decay of the force field should be stable against minor deformations of the boundary.*

For an open string a single wave moves across the spacetime surface and bounces at the endpoints. *The wave motion is determined by a (four-)vector-valued shape function, which we will call the directrix,* $\mathcal{A}$. Thus a point on the string, parametrized by the amount of energy σ, between the point and (for definiteness) the q-endpoint is, at the time t, at the position

$$x(\sigma, t) = \frac{1}{2}(\mathcal{A}(t + \frac{\sigma}{\kappa}) + \mathcal{A}(t - \frac{\sigma}{\kappa})) \tag{2.13}$$

We will from now on put the string constant κ equal to unity in order to simplify the formulae.

While the tension $\vec{T} = \partial\vec{x}/\partial\sigma$ is directed along the string, the velocity $\vec{v} = \partial\vec{x}/\partial t$ is directed transversely so that $\vec{T} \cdot \vec{v} = 0$. The definition of σ also implies that $\vec{T}^2 + \vec{v}^2 = 1$ (all the three-vector relations are valid in the local rest-frame). Together this means that the directrix function has an everywhere

light-like tangent

$$\left(\frac{d\vec{\mathcal{A}}}{d\xi}\right)^2 = 1 = \left(\frac{d\mathcal{A}_0}{d\xi}\right)^2 \tag{2.14}$$

The tension must vanish at the endpoints ($\sigma = 0$ and $\sigma = E_{tot}$) and this implies that the directrix must be a periodic function with the property

$$\mathcal{A}(\xi + 2E_{tot}) = \mathcal{A}(\xi) + 2P_{tot} \tag{2.15}$$

where P_{tot} (E_{tot}) is the total energy-momentum (energy) of the state. While according to Eq. (2.13), the directrix $\mathcal{A}(t)$ describes the motion of the q-end, from Eq. (2.15) it is evident that

$$\mathcal{A}_{\bar{q}}(t) = \mathcal{A}(t + E_{tot}) - P_{tot} \tag{2.16}$$

will describe the motion of the $\bar{q}$-end. Finally, if the string starts out from a point (at the time $t = 0$) then we must have the symmetry :

$$\mathcal{A}(\xi) = -\mathcal{A}(-\xi) \tag{2.17}$$

Using the Lund interpretation of the gluons as internal excitations on the string it is easy to construct the first half period of the directrix curve: it starts with the quark energy-momentum k_1 and then the gluon energy-momenta $\{k_j\}$ are laid out in colour order and it ends with the $\bar{q}$ energy-momentum k_n, for a string with $(n-2)$ gluons. In this way the q-endpoint will be acted upon by the colour-ordered excitations as they arrive in turn. From Eqs. (2.15) and (2.17) it follows that we obtain the directrix of the second half period by reversing the order, starting with the $\bar{q}$ energy-momentum and ending with the q energy-momentum (besides the translation this is the way the $\bar{q}$-endpoint will move according to Eq. (2.16)).

The energy-momentum content in the string at a certain time t, between the point σ and the q-end is given by :

$$\int_0^\sigma d\sigma' \frac{\partial x}{\partial t} = \frac{1}{2}(\mathcal{A}(t+\sigma) - \mathcal{A}(t-\sigma)) \tag{2.18}$$

2.3.1 The coherence conditions in QCD

The properties of the directrices which are described above are common to all states of the massless relativistic string. On the other hand the use of the string as a model for the force fields of QCD may single out a particular class of all possible states. We will briefly discuss *the conditions which correspond to the coherence conditions of bremsstrahlung radiation in a gauge field theory.*

Multi-gluon radiation is in general described by means of perturbative cascade models. In order to consider the properties of the states, we will make use of the ideas behind the Lund Dipole Model. To see the emergence of a multi-gluon state we start out with the following two basic results from QCD bremsstrahlung, (cf. [3, 7, 8]).

B1 The original $(q\bar{q})$-state emits bremsstrahlung radiation according to the ordinary dipole formula, i.e. there is an inclusive density of gluon quanta which is flat in rapidity y and the logarithm of the squared transverse momentum $\kappa = \log(k_\perp^2)$ with a density given by the coupling, $\bar{\alpha} \equiv C\alpha_s/2\pi$:

$$dn = \bar{\alpha} d\kappa dy \tag{2.19}$$

B2 After the first ("hardest") gluon (g_1) is emitted there are two dipoles available, one between the (qg_1) and one between the $(g_1\bar{q})$ with squared masses $s_{12} \equiv (k_q + k_{g_1})^2$ and $s_{23} \equiv (k_{g_1} + k_{\bar{q}})^2$. The second gluon may be emitted independently inside the angular (rapidity) range of the first or the second dipole. We note that the two dipoles (each spanned by two light-like parton energy momenta) move apart in the total cms.

After the emission of the second gluon, according to the Lund Dipole Model [8], there are three independent dipoles for further emission, and so on. The masses of the dipoles will quickly decrease and therefore also the transverse momentum size of the emitted gluons. The cascades are stopped by some "virtuality" cutoff, either in the dipole mass or in the transverse momentum. The Dipole Model is implemented in the Monte Carlo simulation program ARIADNE [9].

In terms of the directrix, the original state is described by the light-like energy momenta of the original $(q\bar{q})$-pair. After the emission of the first gluon the state, in space (in the cms), will be described by a (connected) triangle, cf. Fig.2.6, where the vectors $\vec{k}_q \equiv \vec{k}_1$ and the vectors $\vec{k}_g \equiv \vec{k}_2$ constitute one of the dipoles and the $\vec{k}_2$ and $\vec{k}_{\bar{q}} \equiv \vec{k}_3$ the second dipole, as discussed above. (We note that for light-like vectors the space part length is equal to the time component) Emission of the second gluon will then occur in between the two vectors describing the dipole and this evidently means that the second gluon vector will "cut off" one of the triangular corners, making the directrix into a quadrangle etc. (Note that already with the emission of two gluons, the vectors shown in Fig.2.6 no longer need to be in a plane)

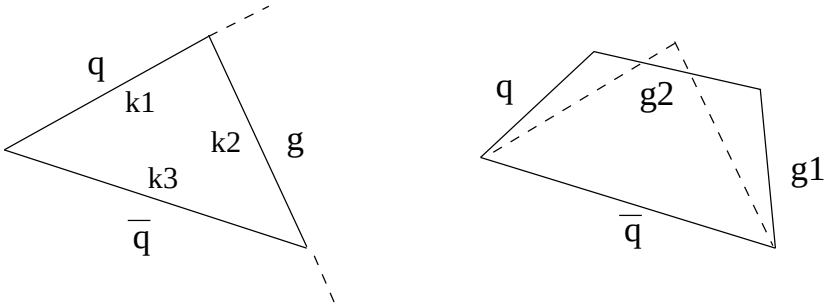

Figure 2.6: The emission of the first and the second gluon respectively.

In general, there will be an emission of a set of "hard" gluons which will determine the general shape of the directrix. The remaining emissions will then make the directrix smoother and smoother as each new emission will correspond to a gluon vector which cuts off an earlier corner. This means that the angle between the energy-momentum vectors of colour-connected partons becomes smaller (along the main directions, determined by the hard emissions) the longer the cascade continues. This is the way that the coherence properties of the bremsstrahlung radiation work, and it is sometimes referred to as the "strong angular condition". Later on, we will find that this angular condition will play an important role when we consider the deviations in the partonic states which are allowed by the fragmentation process.

2.4 The General Breakup of a String Field

We will now consider the partitioning of a general string state at a point $x(\sigma, t)$ and after that define the most general process possible for the Area Law.

According to Eq. (2.13) the breakup will occur at the middle point $\frac{1}{2}(\mathcal{A}(\xi_1)+\mathcal{A}(\xi_2))$ between two positions on the directrix, determined by $\xi_1 > \xi_2$ with $t = \frac{1}{2}(\xi_1 + \xi_2)$ and $\sigma = \frac{1}{2}(\xi_1 - \xi_2)$, cf. Fig.2.7. There will be two parts of the string left over and we will now describe their motion after the breakup.

The first part (to be denoted "(12)") can be described by the "new"directrix $\mathcal{A}_{12}(\xi) \equiv \mathcal{A}(\xi)$ for $\xi_2 \leq \xi \leq \xi_1$. It will contain the energy-momentum $P_{12} = (\mathcal{A}(\xi_1) - \mathcal{A}(\xi_2))/2$, cf. Fig.2.7, so that it can be continued as in Eq. (2.15) with $P_{tot} \to P_{12}$. Starting it out from the position $\mathcal{A}_{12}(\xi_2) \equiv \mathcal{A}(\xi_2)$, it is the "new" orbit of the (original) q-particle in the string (12). To obtain the corresponding orbit for the "new" $\bar{q}$-end we use Eq. (2.16) to obtain $\mathcal{A}_{12\bar{q}} \equiv \mathcal{A}_{12}(t + (\xi_1 - \xi_2)/2) - P_{12}$.

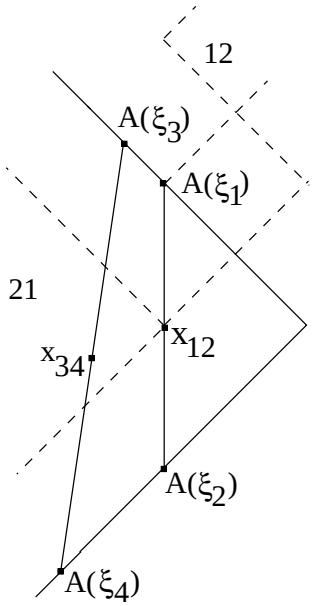

Figure 2.7: The system (12) is shown as a string piece which is moving away, while the system (21) is translated to x_{12}. The second break-up point x_{34} is the middle point between $A(\xi_3)$ and $A(\xi_4)$. In this way, the particle produced in between x_{12} and x_{34} can be taken either as the second particle in the break-up of the original system or the first in the system (21).

If we start at the "breakup" time $t = \frac{1}{2}(\xi_1 + \xi_2)$, it will evidently behave just as if we had adjoined the directrix $\mathcal{A}_{12}$ to the point $x(\sigma, t)$ (note that $\mathcal{A}_{12}(\xi_1) = 2P_{12} + \mathcal{A}_{12}(\xi_2)$).

The second part (denoted "(21)") can be described as the remainder, i.e. $\mathcal{A}_{21} = \mathcal{A}(\xi)$ with $\xi_1 \leq \xi \leq 2E_{tot} + \xi_2$ (noting that the original directrix is continued according to Eq. (2.15)) . The directrix $\mathcal{A}_{21}$ contains the energy $P_{21} = P_{tot} - P_{12}$ and is continued accordingly. To find the orbit of the produced q-end in the part (21) we adjoin the directrix $\mathcal{A}_{21}$ to the point $x(\sigma, t)$ starting it at $\xi = \xi_1$. The (original) $\bar{q}$ will again move according to Eq. (2.16).

The most noticeable property is that for a multi-gluon force field the directrices of the two new string parts will not fulfil Eq. (2.17). This implies that the endpoints of the new strings never meet but instead turn around each other so that each of the two states will contain angular momentum.

It is only in the $(1+1)$*-dimensional case that the two new string parts will have the same properties as the original string* (though they will be scaled down in size and have different rest-frames due to the momentum transfer at the breakup). The conclusion is that *the final state in a multi-gluon string fragmentation in general depends upon the ordering of the different breakups.*

2.4.1 A general process based upon the Area Law

We may nevertheless devise a string breaking process on a "frozen" string surface, i.e. under the assumption that the string surface is once and for all a given device (this is also the way Sjöstrand treated the problem exhibited above). Assume that the system (12) is a hadron on the mass-shell, produced as the "first" hadron along the original q-direction (i.e. the point $\mathcal{A}(\xi_2)$ is along the q energy-momentum vector and $\mathcal{A}(\xi_1)$ on the other side of the corner in the directrix between the q and the first gluon). Then we may choose two new points $\xi_3 > \xi_1$ and $\xi_4 < \xi_2$ to obtain the second rank hadron (34) with energy-momentum $p_{34} = \frac{1}{2}(\mathcal{A}(\xi_3) - \mathcal{A}(\xi_1) + \mathcal{A}(\xi_2) - \mathcal{A}(\xi_4))$ with the production vertex at $x_{34} = \frac{1}{2}(\mathcal{A}(\xi_3) + \mathcal{A}(\xi_4))$. We may evidently continue this process across the string surface and we note that at every step it is only necessary to choose two numbers: $(\delta\xi)_+ = \xi_3 - \xi_1$ and $(\delta\xi)_- = \xi_2 - \xi_4$. They must be chosen so that the corresponding p_{34} is the energy-momentum of a particle on the mass-shell. It is necessary to have a second condition, however, and we may then use the Area Law.

For the $(1+1)$-dimensional model the numbers $(\delta\xi)_\pm$ evidently correspond to the light-cone coordinates z and ζ in Section 2.2. The indices $\pm$ can be given a further meaning for the general directrix. According to Eq. (2.13) there is a left-moving and a right-moving wave spanning the string surface and according to Eq. (2.15) the fixed phase parts (from now on we will call them "grains") "stream" across and bounce back (thereby turning from left- to right-movers) at the q and $\bar{q}$ ends.

We may describe the situation in a (σ, t)-plane, cf. Fig.2.8, with the right- and left moving grains moving along fixed "light-cone lines". The whole string is, at the time $t = 0$, gathered into a single point at the origin. The boundary values at $\sigma = 0$ and $\sigma = E_{tot}$ are the directrix $\mathcal{A}(t)$ and the orbit of the $\bar{q}$, i.e. $\mathcal{A}_{\bar{q}}(t)$, respectively. A breakup point $x \equiv x_{12}$ is reached by the meeting of the left-moving grain indexed ξ_1 and the "right-mover" ξ_2 and the breakup at x_{34} by the left-mover ξ_3 and right-mover ξ_4. The energy-momentum p_{34}, streaming into the hadron produced between x_{12} and x_{34}, is evidently $\frac{1}{2}(\mathcal{A}(\xi_3) - \mathcal{A}(\xi_1))$ from the left and $\frac{1}{2}(\mathcal{A}(\xi_2) - \mathcal{A}(\xi_4))$ from the right. If we use $\pm$ as indices for the left- and the right-movers respectively we obtain a useful parametrisation.

With regard to surface areas there is an obvious (scalar) surface element defined by the surface spanned by the (incremental) grains coming from the

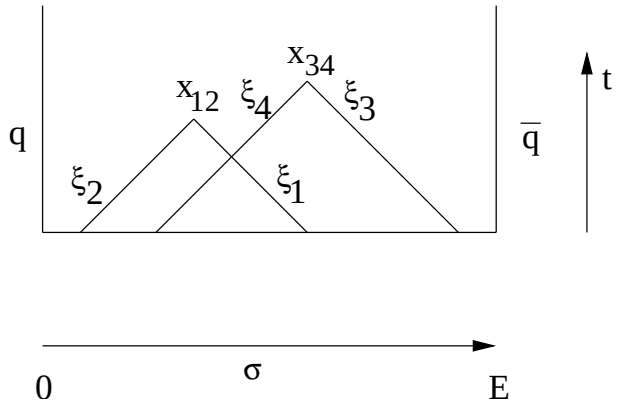

Figure 2.8: The break-up points and the corresponding right and left-moving grains in the (σ,t)-plane, as described in the text.

left and the right.

$$dA \propto d\mathcal{A}_+ \cdot d\mathcal{A}_- \tag{2.20}$$

Using this we may easily calculate the area "below the vertices" x_{12} and x_{34} (cf. Fig.2.8) as they are defined above. They are the correspondence to the squared proper times Γ considered in Section 2.2 (in the Fig. 2.5 they would correspond to the areas $I + IV$ and $III + IV$).

$$\Gamma_{12} = x_{12}^2 \quad \text{and} \quad \Gamma_{34} = x_{34}^2 \tag{2.21}$$

So, for the vertices shown in Fig.2.8, these areas are just the squared proper times of the vertices. But we note that they can not be expressed as the products of light-cone components or even in terms of products of sets of left- and right-movers solely, for general multigluon strings.

The area below the vertices (if we neglect the squared mass term in the Area Law, which can evidently be included in the normalisation constants N in Eq. (2.1)) can be expressed as

$$A_{1234} = x_{12}^2 + x_{34}^2 - x_{14}^2 \tag{2.22}$$

(this is the correspondence to the area called $I + III + IV$ in connection with Eq. (2.8)). We note that the area corresponding to IV, i.e. x_{14}^2 in Eq. (2.22), may vanish in this case, i.e. the left-mover indexed 1 and the right-mover indexed 4 may meet "before" $t = 0$. This means that the condition in Eq (2.8) can not be met for the general situation.

We may nevertheless include these considerations to devise an exact version of the Area Law in Eq. (2.1). We write, in an obvious way, the differentials $d^2p \to (dp_+ \cdot dp_-)$ and include the mass-shell condition by a δ-distribution as in Eq. (2.1). The result is, however, very complex to treat and for our purposes there are three shortcomings:

1 If we treat the process in an iterative way, at every step, just as we mentioned above, there are two numbers $(\delta\xi)_\pm$ to be solved for. One is fixed by the mass-shell condition and the other can be fixed by the area exponential; but the distribution functions are very complex (cf. the remarks under 2 below). In principle everything can be done by Monte Carlo simulation methods but even with very fast computers and the best possible computer routines this model will always be much slower than a process where there is only one number to be solved for, at every step.

2 Due to the complexity of the formulae there is no way we can obtain useful analytical tools to study the behaviour of the correspondences to the transition operators as in e.g. Eq. (2.5). This also implies that there is no way that we can define the total integral and sum over the produced hadronic states (as we could do for the $(1+1)$-dimensional model in Eqs. (2.9) and (2.10)) so as to be able to obtain the correct weighting in every step of an inclusive cascade.

3 Although this implementation of the Area Law is an "exact" procedure, fulfilling at every step the mass-shell condition and taking the "true" area below the vertices into account, it nevertheless starts out from the assumption that the partonic state is so well defined that there are reasons to implement an "exact" theoretical fragmentation procedure on it. This is in general not the case, i.e. the partonic state defined by perturbation theory is only well-defined down to some virtuality cut-off as we have discussed before.

We use quotation-marks on the word "exact" in order to indicate that the use of a "frozen surface" is in itself an assumption introduced to mend the problems obtained from the use of classical physics and neglect of the subsequent angular momentum production. In the third item above, we are coming back to the statement at the beginning of the section, that infrared stability should imply that minor deformations of the boundary (in this case changes in the partonic state as defined by the directrix $\mathcal{A}$ up to the order of the hadronic mass scales) should not be noticable in the results. In the next section we will define a procedure which will mend all the three shortcomings mentioned above.

2.5 The Lund String Fragmentation as a process along the directrix

In this section, we will consider a fragmentation process which is defined along the directrix and does not suffer from the three problems considered at the end of Section 2.4.1. In order to exhibit the idea we will start with the $(1+1)$-dimensional model and rewrite it in a useful way. After that we will extend it to the general case. In particular, we will allow modifications of the order of the hadronic mass-scale in the directrix in accordance with the discussion under point 3 above.

2.5.1 The directrix process for the $(1+1)$-dimensional case

In this case the directrix contains only two directions, given by the $\bar{q}$ energy-momentum vector (to be called $\mathcal{A}_+$ in accordance with the notation introduced in Section 2.4.1) and the q energy-momentum ($\mathcal{A}_-$). A vertex point x_j, obtained after the production of j hadrons from the q-side, $p_1, \ldots, p_j$ is then described (with respect to the origin) by

$$x_j = \frac{1}{2}(\mathcal{A}_{+j} + \mathcal{A}_{-j}) \tag{2.23}$$

We also know that

$$\sum_1^j p_\ell = \frac{1}{2}(\mathcal{A}_{+j} - \mathcal{A}_{-j}) \tag{2.24}$$

Using the symmetry of a directrix passing through a single point (Eq. (2.17)) we may find another point on the directrix with the property

$$\mathcal{A}_{-j} \equiv \mathcal{A}_-(\xi_j) = -\mathcal{A}_-(-\xi_j) \equiv -\mathcal{B}_{-j} \tag{2.25}$$

We will from now on drop the indices $\pm$ on $\mathcal{A}_+$ and $\mathcal{B}_-$ but we note that they do describe points on the same directrix in accordance with the left- and right-mover notation in Section 2.4.1. While $\mathcal{A}_-$ goes "backward" for increasing j-values, $\mathcal{B}$ follows the q-direction.

We may now consider the hadron energy momenta to define a curve from the origin "along the directrix" such that after j steps it has reached the point

$$\sum_1^j p_\ell \equiv X_j = \frac{1}{2}(\mathcal{A}_j + \mathcal{B}_j) \tag{2.26}$$

while the difference between the point $\mathcal{A}_j$ on the directrix and X_j is given by x_j in Eq. (2.23). The production of a new particle p_{j+1} then corresponds to

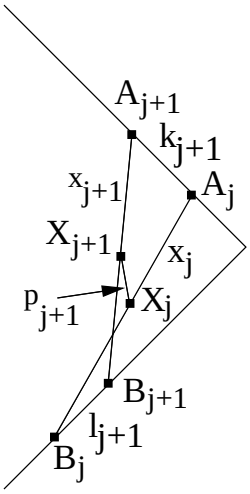

Figure 2.9: A description of the fragmentation process along the directrix with notations according to the text.

choosing two new points X_{j+1} and $\mathcal{A}_{j+1}$ (along the directrix) such that, cf. Fig.2.9

$$X_{j+1} - X_j = p_{j+1} \quad \text{and} \quad \mathcal{A}_{j+1} - \mathcal{A}_j \equiv k_{j+1} \tag{2.27}$$

We also obtain a new "vertex" vector x_{j+1} by the identity (cf. Fig.2.9):

$$p_{j+1} + x_{j+1} = x_j + k_{j+1} \tag{2.28}$$

In this way the vertex vector fulfils $x_{j+1} = \mathcal{A}_{j+1} - X_{j+1}$ just as $x_j = \mathcal{A}_j - X_j$. We have then arranged it so that the hadrons are produced along a curve, the X-curve, from the origin and the vertex vectors are the connectors for this curve going from the produced particle to the directrix. Before we consider the Area Law in this situation we note the symmetry between a reversed process and the process described above, i.e. when we go from X_j to X_{j+1} producing p_{j+1} by the use of a part k_{j+1} of the directrix along $\mathcal{A}$.

To see the reverse process we note that the vector x_j can just as well be reached by taking the difference between the point X_j on the hadron curve, Eq. (2.26), and "the backward point" on the directrix $\mathcal{B}_j$.

$$x_j = \frac{1}{2}(\mathcal{A}_j - \mathcal{B}_j) = \mathcal{A}_j - X_j = X_j - \mathcal{B}_j \tag{2.29}$$

Using this we could evidently consider the production of the particle p_{j+1} as a step from $\mathcal{B}_j$ to $\mathcal{B}_{j+1} = \mathcal{B}_j + \ell_j$ (cf. Eq. (2.27)) such that we have in

correspondence to Eq. (2.28) and Fig.2.9

$$p_{j+1} + x_j = x_{j+1} + \ell_{j+1} \tag{2.30}$$

In order to formalise the determination of the particle energy momentum p, we may then in "the k-process" (along $\mathcal{A}$) assume that we know the starting vertex vector x, connected to a point $\mathcal{A}_P$. We may then choose a piece k along $\mathcal{A}$ (of a size to be determined) and then define the other light-cone direction in the plane determined by (x, k) by

$$\hat{\ell} = x - k\frac{x^2}{2xk} \tag{2.31}$$

The vector p will be described in terms of $(k, \hat{\ell})$ as

$$p = z\hat{\ell} + \frac{k}{2} = zx + \frac{k}{2}(1 - \frac{zx^2}{xk}) \tag{2.32}$$

with the requirement that the particle should be on the mass-shell

$$p^2 = m^2 = zkx \quad \text{i.e.} \quad kx = \frac{m^2}{z} \tag{2.33}$$

From Eq. (2.28) we obtain the new vertex vector x' by

$$\begin{aligned} x' &= (1-z)x + \frac{k}{2}(1 + \frac{zx^2}{xk}) \\ (x')^2 &= (1-z)(x^2 + xk) = (1-z)(x^2 + \frac{m^2}{z}) \end{aligned} \tag{2.34}$$

In Fig.2.10 we show both the production as described in Section 2.2 and the k-process described above. In particular we note the two areas exhibited. It is straightforward to prove that

$$A = A_r + \Gamma' - \Gamma \tag{2.35}$$

with the obvious definition of e.g. $\Gamma = x^2$. The Area Law in Eq. (2.1) will be fulfilled both by the use of the area in Fig.2.1 and the area in between the directrix and the hadronic curve (the X-curve) if we choose the variable z from the fragmentation function in Eq. (2.10) and apply it as in Eqs. (2.32)-(2.34). This is so because the difference between the areas A and A_r for the single step exhibited above will vanish when we consider the whole process.

It is also obvious that we may define an ℓ-process similar to the k-process we have discussed above. We just write $z\hat{\ell} = \frac{1}{2}\ell$ and introduce the variable ζ such that $\frac{1}{2}k = \zeta\hat{k}$ with ζ chosen such that $m^2/\zeta = \ell x'$. Actually we obtain the same process (although "in the opposite order") under the assumption that we

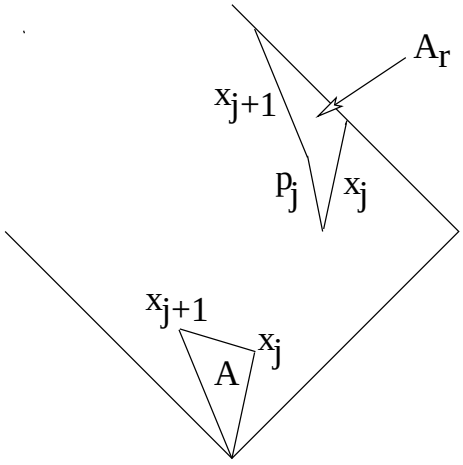

Figure 2.10: The figure shows both the production as described in Section 2.2 and the k-process described in the text.

start at x' and chose ℓ along the $\mathcal{B}$-part of the directrix with the variable ζ in accordance with Eq. (2.11). In this way the "backward" variable ζ evidently obeys the same distribution as the "forward" variable z and the Area Law is fulfilled.

We have reached a situation where a particle production step starts from a knowledge of a vector x connected to a light-cone-direction. Then we choose a light-like vector k such that Eq. (2.33) is fulfilled with a z-value stochastically chosen from the fragmentation function in Eq. (2.10). After that we construct the particle energy-momentum and a new vector x' according to Eqs. (2.32) and (2.34). We may start out choosing the "first" x-vector (x_0) equal to the q (light-cone) energy-momentum and then the $(1+1)$-dimensional model is defined.

2.5.2 The directrix process around a gluon corner

For a multi-gluon directrix however, we will reach situations when there are "corners", i.e. where the directrix changes direction between two colourconnected partons. Thus besides the vertex vector x, there will be a remaining light-cone vector (to the corner) c and a chosen number z such that

$$cx < \frac{m^2}{z} \tag{2.36}$$

We will now consider ways to pass over such a corner. Assuming that the directrix continues on the other side of the corner we may choose a light-cone vector k which fulfils Eq. (2.33) (we note that according to Eq. (2.36) k can not be chosen along c) and another light-cone vector c' such that

$$k + c' = c + \hat{Q} \equiv Q \tag{2.37}$$

with $\hat{Q}$, a vector pointing from the corner to a new point on the directrix, and Q describing that point from the point on the directrix where the vertex vector x is connected.

We note that with this definition the suggested way to pass the corner corresponds to an exchange of one "dipole", $c + \hat{Q}$ in the process for another $k + c'$, i.e. to make a detour onto a "new" directrix which is "close" to the original one. The choice of the new dipole corresponds to a definition of what we will mean by the allowed "minor deviations" of the original perturbative state.

In order to investigate what can be allowed under these conditions we will exhibit a few possible choices to fulfil Eq. (2.37). We will then find that all possible choices are not allowed if we would like to obtain reasonable results for the final state hadron distributions. A first set of possibilities is to choose c' as a new light-like connector that will bring us "closer" (than the vector c) to the original directrix in the next production step. One may then hope that after another step in the process the new connector becomes even "smaller" so that we are back at the original directrix after a few steps.

C1 The vector k can be chosen in the plane spanned by the vertex vector x and the directrix Q (then both c' and k are fully determined).

C2 A more general choice is to take the vector k in the three-space spanned by x, Q and the remainder vector c. In this case it is necessary to provide a second condition to determine k and c'. In the rest-frame of the vertex vector x the space parts of the vectors $\vec{c}$ and $\vec{\hat{Q}}$ span a triangle with the vector $\vec{Q}$ as baseline, cf. Fig.2.11. (For the case exhibited we assume that also $\hat{Q}$ is light-like. The situation can be easily generalised to the situation when there are one or more "corners" also on $\hat{Q}$.) The remaining degree of freedom will then be fixed by an angular condition. One such condition is indicated in the Fig.2.11. The two triangles $(\vec{c}, \vec{\hat{Q}}, \vec{Q})$ and $(\vec{c'}, \vec{k}, \vec{Q})$ in this construction are chosen congruent. This is a kind of minimal choice for the size of Q in this three-space. It is not difficult to see that in general the new connector will be smoothly connected to the original directrix.

For the case defined by the condition C1 we obtain that k and c' will be directed along the two light-cone directions in the plane spanned by (x, Q):

$$k = \frac{Q}{2} + \frac{((Qx)Q - Q^2 x)}{2\sqrt{(Qx)^2 - Q^2 x^2}} \quad \text{and} \quad c' = Q - k \tag{2.38}$$

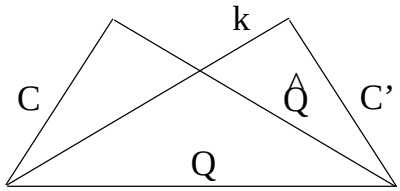

Figure 2.11: A possible construction (C2) for passing a gluon corner. The figure shows the space parts of the vectors, in the rest-frame of the vertex vector x, as described in the text.

(In Fig.2.11 they would be directed along the $\vec{Q}$-direction with the lengths $(Q_0 \pm |\vec{Q}|)/2$, respectively). The vector Q contains one degree of freedom which can be fixed by multiplying with x in Eq. (2.38), and using Eq. (2.33).

This means on the one hand that the situation corresponds to using up the smallest possible segment of the directrix in the construction according to Eq. (2.37). On the other hand we will obtain a very sharp "bend" on the new directrix segment, defined by the dipole (kc'). While the first result is desirable from an economy point of view, the second implies that we will break the coherence conditions for the directrix (the angular ordering) as discussed in Section 2.3.1.

The fragmentation distributions obtained with this choice are not very encouraging. After we "pass" the gluon corner the density of hadrons is much higher than the density before the corner. *We find that even for a small gluonic excitation a break of coherence may result in the production of too many hadrons over a large rapidity range.*

One might hope that the situation may be mended by a suitable angular choice. This is so for the situation described in C2 for a large part of the events and for simple gluonic configurations. In Fig.2.18 we show a Monte Carlo simulation of the (inclusive) final state hadron rapidities in a state containing a single gluon placed at the centre with a transverse momentum of 15 GeV. Even though for most fragmentation events the choice C2 performs well, on the level of a few percent it does happen that the directions of the connecting c' and the new vertex x' are such that we obtain a situation close to the one for C1. The new directrix (possibly after a few further steps in the process) will all the time come closer to the original one; but at the same time we obtain a sharp bend farther and farther away from the original gluon corner with each step. This causes too many particles to be produced over a large rapidity range (cf. Fig.2.18).

It is possible to make further changes in the procedure with more sophisticated angular choices, but we will instead go over to another and more successful choice, which we will call C3.

C3 A natural choice for the vector c' is to make it into the k-vector for the next particle production in the process, i.e. chose a new stochastic value z' and put $c' = k'$ with

$$k'x' = \frac{m^{2\,\prime}}{z} \tag{2.39}$$

in terms of the new vertex vector x' determined from (z, k, x) according to Eq. (2.34). In this way we are evidently getting back to the original directrix as fast as possible.

We may define the vector k still in the space spanned by (c, x, Q):

$$k = \alpha c + \beta x + \gamma Q \tag{2.40}$$

We obtain a solution for the coefficients (α, β, γ) from the requirements

$$\begin{aligned} k^2 &= 0 \\ kx = \frac{m^2}{z} \quad &\text{and} \quad kQ = \frac{1}{2}Q^2 \end{aligned} \tag{2.41}$$

(these conditions also imply that k' is light-like), and an equation for the vector Q along the directrix using Eqs. (2.41) and

$$\frac{m^2}{z'} = k'x' = (Q-k)((1-z)x + \frac{k}{2}(1 + \frac{zx^2}{kx})) \tag{2.42}$$

In the fragmentation distribution there is a factor $(1-z)^a$ (stemming from the density of states according to the discussion around Eq. (2.10). This implies that we may not use up all the energy-momentum along one of the light-cone directions in a single step. Small values of z correspond to $\zeta \simeq 1$ according to Eq. (2.11), i.e. to using up almost all the energy-momentum along the other light-cone direction in a step. Such values are suppressed by the area exponential in the distribution. Nevertheless it may happen that we obtain a very small z-value ($z \leq 0.1$), corresponding to a large (but not infinitely large) area. Sometimes for the general multi-gluon directrix however, there might be no possibility to accomodate such a large area due to energy-momentum conservation. Then the choice C3 can not be done. Instead of introducing a general projection of the two-particle distributions for all such cases, in the Monte Carlo simulation we have chosen to go back to the beginning and start a new fragmentation event. Such situations, when we can not use the choice C3, are infrequent enough to let this "restart strategy" be usable.

In order to test the influence of this feature on the model we investigate the influence on the single particle and two-particle distributions below in Section 2.6 and we find them negligible. In order to show that our changes in the directrices actually are of the hadronic mass scale we have defined a local

"bending parameter" closely related to the $k_\perp$ variable used in the ordering of the Lund Dipole Model, cf. Eq. (2.50)

$$k_{\perp 2}^2 = \frac{2(xk_1)(k_1k_2)}{x(k_1+k_2)+k_1k_2} \tag{2.43}$$

From the results in Section 2.6 we conclude that we are at most making local modifications on the order or below the hadronic scale in our directrices.

2.5.3 A Differential Process and its Relationship to the Generalised Rapidity

There is a direct connection between a differential version of our hadronisation process and the $\mathcal{X}$-curve that was referred to in the Introduction, [2]. In order to investigate this process we consider the limiting situation for a vanishing mass parameter. Then the distribution function will obviously develop a pole for $z \to 0$. We will assume that the model is defined by the incremental step size dz with the ratio $m/dz \to m_0$. The corresponding incremental k vector will be called $d\mathcal{A}$ and it will fulfil the mass-shell condition (we will use the notation q_P instead of x for the vertex vector in connection with the differential process)

$$q_P d\mathcal{A} = \frac{m^2}{dz} \to dz m_0^2 \tag{2.44}$$

From the model formulae for the change in q_P and the particle energy-momentum p (Eqs. (2.32) and (2.34)) we obtain the following differential equations defining a curve to be called the $\mathcal{P}$-curve

$$\begin{aligned} d\mathcal{P} &= dz q_P + \frac{d\mathcal{A}}{2}(1 - \frac{q_P^2}{m_0^2}) \\ dq_P &= -dz q_P + \frac{d\mathcal{A}}{2}(1 + \frac{q_P^2}{m_0^2}) \end{aligned} \tag{2.45}$$

Firstly we note that from the sum and differences of the Eqs. (2.45) we obtain

$$\begin{aligned} \mathcal{P} + q_P &= \mathcal{A} \\ \mathcal{P} - q_P &= \mathcal{L} \end{aligned} \tag{2.46}$$

where the vector $\mathcal{L}$ has a light-like tangent just as the directrix $\mathcal{A}$:

$$d\mathcal{L} = 2dz q_P - d\mathcal{A}\frac{q_P^2}{m_0^2} \tag{2.47}$$

In this way the $\mathcal{P}$-curve goes in between two curves with everywhere light-like tangents and the vector q_P connects to both of them.

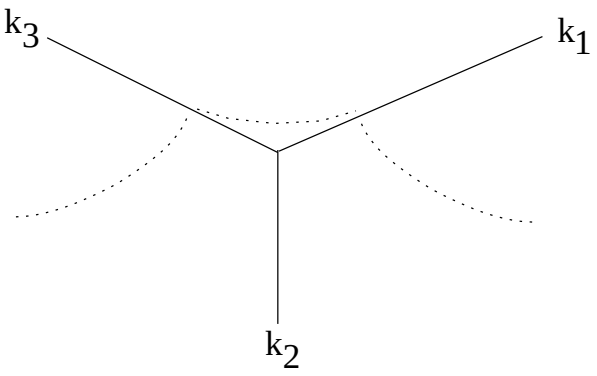

Figure 2.12: A string with a $q(k_1)$, $\bar{q}(k_3)$ and a single gluon excitation (k_2). The figure shows the connected region around the gluon "tip".

The vector q_P is time-like and quickly approaches the length m_0. To see that we multiply the second line of Eq. (2.45) by q_P and obtain

$$dq_P^2 = dz(-q_P^2 + m_0^2) \tag{2.48}$$

This means (remembering that $dz = q_P d\mathcal{A}/m_0^2$) that we may write:

$$q_P^2 = m_0^2(1 - T_P^{-1}) \quad \text{with} \quad T_P = \exp(\int (\frac{q_P d\mathcal{A}}{m_0^2})) \tag{2.49}$$

We have then assumed that $q_P = 0$ and $T_P = 1$ at the start of the process. We note that the integrand in the exponent for T_P is an area, more precisely the area betweeen the directrix and the $\mathcal{P}$-curve. This is very similar to the results we obtained in [2] for the generalised rapidity and we will now briefly connect to these results.

2.5.4 The $\mathcal{X}$-curve and its Properties

The distribution in Eq. (2.1) contains two terms, the phase space and the exponential area suppression. In order to obtain a large probability it is necessary for a given total energy-momentum on the one hand to make many particles on the other hand to make them in such a way that the area is small. The obvious compromise is that the decay region is around a typical hyperbola with an average squared distance to the origin $< \Gamma > \equiv \Gamma_0$. The length of the hyperbola is proportional to the available rapidity range for the final state particles, i.e. $\Delta y = \log(s/\Gamma_0)$ with s the squared cms energy.

In the Lund Model interpretation for a string with a single gluon excitation, there will be two parts of the string; one spanned between the q and the g and

one between the g and the $\bar{q}$. Each of them should break up in a similar way as the single string region described by Eq. (2.1). Besides that there will be a few particles produced in the connected region around the gluon "tip", cf. Fig.2.12. If the energy-momenta of the partons are k_j, $j = 1, 2, 3$ (with indices 1 (3) for the q ($\bar{q}$)), then there will be two hyperbolic angular ranges, $(\Delta y)_{12}$ and $(\Delta y)_{23}$. The sum of these ranges is

$$\begin{aligned} \lambda = (\Delta y)_{12} + (\Delta y)_{23} &= \log(\frac{s_{12}}{2\Gamma_0}) + \log(\frac{s_{23}}{2\Gamma_0}) \\ &= \log(\frac{s}{\Gamma_0}) + \log(\frac{s_{12}s_{23}}{4\Gamma_0 s}) \end{aligned} \tag{2.50}$$

Here $s_{j\ell} = (k_j + k_\ell)^2$ and $s = s_{12} + s_{23} + s_{13}$ and the factors 2 are introduced because only half of the gluon energy-momentum goes into each string region.

The quantity $k_\perp^2 \equiv s_{12}s_{23}/s$ is a convenient (and Lorentz invariant) approximation for the transverse momentum of the emitted gluon. From Eq. (2.50) we conclude that after the emission of a single gluon the phase space is increased from the single hyperbola result above by an amount corresponding to a "sticking-out tip" of length given by the logarithm of the emitted transverse momentum. In conventional notions this corresponds to the "anomalous dimensions" of QCD, i.e. the emission of a gluon increases the region of colour flow inside which more gluons can be emitted and hadronisation can take place. The whole scenario is easily visualised and used in the Lund Dipole Model, [8], and the corresponding Monte Carlo simulation program ARIADNE, [9].

It is straightforward to see that if there are many gluons then there is a corresponding quantity, a generalised rapidity $\lambda \simeq \log(\prod s_{jj+1})$ stemming from the hyperbolae spanned between the colour-connected gluons. But we note that this is not an infrared stable definition. We will now provide a convenient generalisation.

A closer examination of the region around the tip of a gluon reveals that there is a correction corresponding to a connected hyperbola in the region (k_1, k_3) between the "endpoint" of the hyperbola in the region spanned between $(k_1, k_2/2)$ and the one spanned between $(k_2/2, k_3)$, cf. Fig.2.12. In formulae we obtain for the average hyperbolae

$$\begin{aligned} (\alpha_1 k_1 + \frac{1}{2}\beta_1 k_2)^2 = \Gamma_0 \quad \text{and} \quad (\gamma_3 k_3 + \frac{1}{2}\beta_3 k_2)^2 = \Gamma_0 \\ (\alpha_2 k_1 + \gamma_2 k_3 + \frac{1}{2}k_2)^2 = \Gamma_0 \end{aligned} \tag{2.51}$$

with the ranges $1 \geq \alpha_1 \geq 2\Gamma_0/s_{12}$, $2\Gamma_0/s_{12} \geq \alpha_2 \geq 0$, $2\Gamma_0/s_{12} \leq \beta_1 \leq 1$ and similarly for the other variables. The length of the two hyperbolae in the segments $(k_1, k_2/2)$ and $(k_2/2, k_3)$ are then given by Eq. (2.50) but the third hyperbola provides an extra contribution (in the appropriate limit $s_{13} \simeq s$)

equal to $\log(1 + 4\Gamma_0 s/s_{12}s_{23})$. Then the total (generalised) rapidity length becomes

$$\lambda_{123} = \log(\frac{s}{\Gamma_0} + \frac{s_{12}s_{23}}{(2\Gamma_0)^2}) \tag{2.52}$$

This is evidently a nice interpolation between the situations with and without a gluon on the string and it is also an infrared stable definition of the notion of rapidity length. Eq. (2.52) is noted in [2] and led us to introduce a functional defined on a multigluon string directrix.

We may firstly define a set of connected integrals, [2]:

$$I_n = \int ds_{01} ds_{12} \cdots ds_{nE} \tag{2.53}$$

with the easily understood notation (cf. Eq. (2.18)) $s_{jj+1} = (\mathcal{A}(\xi_j) - \mathcal{A}(\xi_{j+1}))^2$, i.e. it is proportional to the squared mass between the points ξ_j and ξ_{j+1} along the directrix. By performing the integrals, we obtain that the argument in the logarithm in Eq. (2.52) is given by the sum $I_1/\Gamma_0 + I_2/(2\Gamma_0)^2$ and that we may in general define the functional T by :

$$T = 1 + \sum_{n=1}^{\infty} \frac{I_n}{(2m_0^2)^n} \tag{2.54}$$

as a suitable generalisation for any string state. For a finite number of partons N the terms with $n > N$ will all vanish and we also note that the highest degree term will always have the generic form :

$$2\frac{s_{12}}{4m_0^2}\frac{s_{23}}{4m_0^2} \cdots \frac{s_{N-1N}}{4m_0^2} \tag{2.55}$$

We also note that for a finite total energy E the contributions for very large degrees will become smaller and smaller compared to the scale m_0.

In order to study the functional T it is suitable to introduce a varying value ξ instead of the total energy E in the connected integrals. It is then evident that the functional $T(\xi)$ will fulfil the integral equation :

$$T(\xi) = 1 + \int_0^{\xi} \frac{ds(\xi, \xi')}{2m_0^2} T(\xi') \tag{2.56}$$

We will also introduce the vector-valued function $q_T(\xi)$ together with T so that we have

$$q_{T\mu}(\xi) = \frac{\int_0^{\xi} d\mathcal{A}_\mu(\xi') T(\xi')}{T(\xi)}$$

$$T(\xi) = 1 + \int_0^{\xi} \frac{q_T(\xi') d\mathcal{A}(\xi')}{m_0^2} T(\xi') \tag{2.57}$$

By differentiation and integration we obtain the results

$$T = \exp(\int_0^\xi \frac{q_T(\xi')d\mathcal{A}(\xi')}{m_0^2}) \equiv \exp(\lambda(\xi))$$
$$q_T^2(\xi) = m_0^2(1 - T^{-2}(\xi)) \tag{2.58}$$

The generalised rapidity λ corresponds to the result in Eq. (2.52) for the simple case described above and it provides an infrared stable definition for any multigluon state. Further the vector q_T is time-like and will quickly approach the finite length m_0.

2.5.5 The Correspondence between the $\mathcal{X}$-curve and the $\mathcal{P}$- curve

The similarity between these results and the results obtained for the $\mathcal{P}$-curve in Eqs. (2.48) and (2.49) are obvious (besides the power in T^{-1}) and there is a correspondence to the Eqs. (2.45) and (2.46) also. The interpretation of the $\mathcal{X}$-curve (as worked out in [2], cf. also [3]) is that there is a vector valued function $\mathcal{X}_\mu(\lambda)$ conveniently labelled by λ such that

$$\mathcal{X} + q_T = \mathcal{A}$$
$$\frac{d\mathcal{X}}{d\lambda} = q_T$$
$$\frac{dq_T}{d\lambda} = -q_T + \frac{d\mathcal{A}}{d\lambda} \tag{2.59}$$

i.e. the vector q_T is the tangent to the curve defined by $\mathcal{X}$ such that it reaches to the directrix. There is no direct correspondence to the $\mathcal{L}$-curve (unless the vectors q has reached its asymptotic length m_0).

It is useful to calculate the results from the differential equations for the case when there is a finite length light-like vector k_j in the directrix. By direct integration we find that if we have the vector q_{Tj} then "after" application of the parton energy-momentum k_j we obtain the vector q_{Tj+1} and will take a step along the $\mathcal{X}$-curve equal to $\delta\mathcal{X}_j$

$$q_{Tj+1} = \gamma_j q_{Tj} + \frac{(1+\gamma_j)}{2}k_j$$
$$\delta\mathcal{X}_j = (q_{Tj} + \frac{1}{2}k_j)(1-\gamma_j)$$
$$\gamma_j = \frac{1}{1 + \frac{q_{Tj}k_j}{m_0^2}} \tag{2.60}$$

(we also note that the products of the γ_j is equal to T^{-1}). The formulae

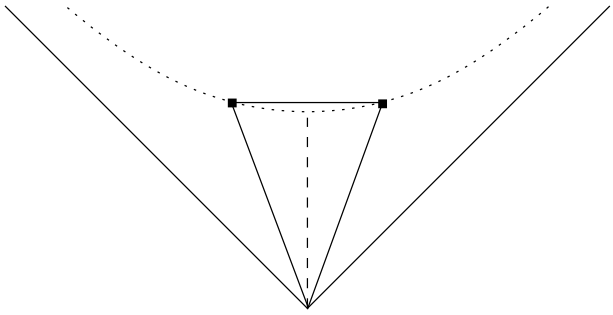

Figure 2.13: Two vertices placed symmetrically (around the rapidity y=0) at $m_0(\cosh(\delta y/2), \sinh(\delta y/2))$ and $m_0(\cosh(\delta y/2), -\sinh(\delta y/2))$ respectively, with a distance $2m_0 \sinh(\delta y/2))$.

corresponding to these results for the $\mathcal{P}$-curve are

$$\begin{aligned} q'_P &= \gamma q_P + \frac{(1 + \frac{q_P^2 \gamma}{m_0^2})}{2} k \\ \delta\mathcal{P} &= (1-\gamma) q_P + \frac{(1 - \frac{q_P^2 \gamma}{m_0^2})}{2} k \\ \delta\mathcal{L} \equiv \ell &= 2(1-\gamma) q_P - \frac{q_P^2 \gamma}{m_0^2} k \\ \gamma &= \frac{1}{1 + \frac{q_P k}{m_0^2}} \quad \text{and} \quad (T_P)^{-1} = \prod \gamma_j \end{aligned} \tag{2.61}$$

This means that while the length of a step along the $\mathcal{X}$-curve depends upon q_T^2 the corresponding step length along the $\mathcal{P}$-curve is

$$(\delta\mathcal{P})^2 \equiv M_j^2 = \frac{(1-\gamma_j)^2 m_0^2}{\gamma_j} \tag{2.62}$$

This has a very simple meaning for a step length M_j along a hyperbola with the parameter m_0, cf. Fig.2.13. If the vertices are placed symmetrically around the rapidity $y = 0$ at the positions $m_0(\cosh(\delta y/2), \pm\sinh(\delta y/2))$ then the step length is evidently $2m_0 \sinh(\delta y/2))$ which should be compared to M_j. Then if we square them and define $\gamma_j \equiv (1 - z_j) = \exp(-\delta y)$ the relationship in Eq. (2.62) will ensue.

The identification of γ and $(1 - z)$ is actually a very general feature of the process(we will come back to this aspect in the future). At this point we only

note that if the lengths (proper-times) of the two adjacent vertices are equal $\Gamma = \Gamma' = m_0^2 \equiv < \Gamma >$ then from Eq. (2.7) we obtain

$$m_0^2 = \frac{(1-z)m^2}{z^2} \tag{2.63}$$

which evidently coincides with the result in Eq. (2.62). Therefore, for this particular value of z, the fragmentation process will all the time proceed along the connected hyperbolae. It is in this way that the $\mathcal{P}$-curve can be considered the average of the hadronic X-curve.

In order to provide a precise relationship between the vectors q_P and q_T as well as the functionals T_P and T we make use of an interesting relationship for the $\mathcal{X}$-curve which is derived in [2]. If we define the $(1+4)$-dimensional vector $(Q_\mu \equiv T q_{T\mu}/m_0, T)$ (which has a length in the $(1+4)$ dimensional Minkowski metric equal to $Q^2 - T^2 = -1$) then the differential equation for q_T can be rewritten as

$$dT = Q\, d\mathcal{A} \quad \text{and} \quad dQ = T dA \tag{2.64}$$

i.e. as a group of special rotations in this space (corresponding to a subgroup of SO(1,4)) which are defined by the incremental changes along the directrix curve. The corresponding relationship for the $\mathcal{P}$-curve is, from the Eqs. (2.44) and (2.45) :

$$d(q_P T_P) = d\mathcal{A}(T_P - \frac{1}{2}) \quad \text{and} \quad dT_P = q_P d\mathcal{A} T_P \tag{2.65}$$

so that the $(1+4)$-dimensional vector $(2q_P T_P, 2T_P - 1)$ has both the same length and fulfils the same differential equations with respect to incremental changes along the directrix as (Q, T). In [2] we characterized the different directrices by means of the eigenvalues of the transfer matrix along the directrix and we found a simple and useful method to relate them to the generalised rapidity $\lambda = \log(T)$. We will come back to this formalism in a future publication and show the significance of the extended space.

In conclusion we have found a differential version of our stochastic process which corresponds to a curve of connected hyperbolae along the directrix function. The area in between the curve and the directrix (scaled by the single parameter m_0^2) has the interpretation of a generalised rapidity measure for the multigluon case. It is also related to a group of rotations with the incremental steps along the directrix as the generators. The curve may be interpreted as the average hadronic curve stemming from the hadronisation of the given directrix.

2.5.6 The Reverse Problem, to Find the Directrix from the Hadronic Curve

We will end this section by solving the reverse problem to the hadronisation process, i.e. to exhibit to what extent we can trace the directrix from a knowledge of the hadronic curve, which we will call the X-curve in accordance with the notation introduced in Section 2.5.1.

We will then assume that the X-curve is defined by the hadronic energy momenta $\{p_j\}$, ordered and laid out according to rank. (Note that this can not be done for a real event obtained from an experiment, since in general, rank is not an observable.) We will concentrate on the production of the hadron p_j, produced between the vertex vectors x_{j-1} and x_j with the directrix segment k_j, and an appropriately distributed stochastic number z_j. According to Eq. (2.28), in order to construct k_j it is sufficient to know p_j and the difference vector

$$(x_j - x_{j-1}) = \epsilon_j \hat{p}_j \tag{2.66}$$

It is straightforward to solve for $\hat{p}_j$ in terms of p_j and x_{j-1}

$$\hat{p}_j = \frac{(x_{j-1}p_j)p_j - p_j^2 x_{j-1}}{\sqrt{(p_j x_{j-1})^2 - p_j^2 x_{j-1}^2}} \tag{2.67}$$

The sign ϵ_j should be positive or negative depending upon whether m^2/z_j is larger or smaller than $z_j x_{j-1}^2$ (it is useful to note that $2(p_j x_{j-1}) = (m^2/z_j + z_j x_{j-1}^2)$). Therefore if we prescribe the first vertex vector x_0 (this is always chosen in our process as the original q energy-momentum vector) then the directrix vectors as well as the vertices are determined recursively up to a sign:

$$\begin{aligned} k_j &= p_j + \epsilon_j \hat{p}_j \\ x_j &= x_{j-1} + \epsilon_j \hat{p}_j \end{aligned} \tag{2.68}$$

It is evident that the other sign will determine the corresponding ℓ_j. We note however, that neither the necessary rank ordering of the hadrons, nor the colour ordering of the directrix gluons, are experimental observables. Therefore in this form the result has solely a theoretical meaning. It is also necessary to take the possible transverse fluctuations in the fragmentation process (mentioned before as stemming from tunneling) into account before any observables can be presented.

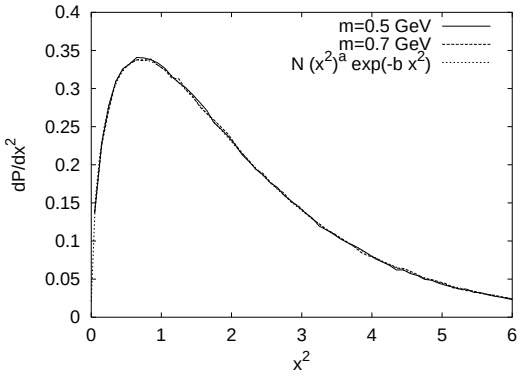

Figure 2.14: The x^2 distribution of the production vertices in our method for different values of the hadron mass, together with a plot of the Γ distribution in Eq.(2.69) with a=0.5 and b=0.7.

2.6 Results

In the previous section, we have proposed a method of fragmenting a multigluon string based upon the Area Law. It can be described as an iterative stochastic process along the directrix curve, which fulfils the Area Law at every step. We have discussed a few different approaches for passing a gluon corner, cf section 2.5.2, and from among these we have picked a preferred one. In this section we present a few basic results from this preferred solution and we also compare it with JETSET and the other approaches we have discussed.

We start with comparing the distribution of x^2 from our model with the distribution of the proper time of the break-up points derived inside the (1+1)-dimensional model [3].

$$H(\Gamma) = N\Gamma^a exp(-b\Gamma) \tag{2.69}$$

The result is presented in Fig.2.14. As mentioned in the discussion at the end of section 2.5.2, sometimes certain values of z can not be accomodated when we pass the corner according to choice C3. Our Monte Carlo simulation program handles this by starting a new event from the beginning whenever this occurs. One may then expect that this might cause changes in the z-distribution and also in the Γ-distribution that we obtain. This is, however, not the case as can be seen from Fig.2.14 and Fig.2.15. Further these distributions are as they should be according to the Lund Model formulae. The Γ-distribution is completely independent of the mass value used just as in the standard, $1+1$-dimensional Lund Model.

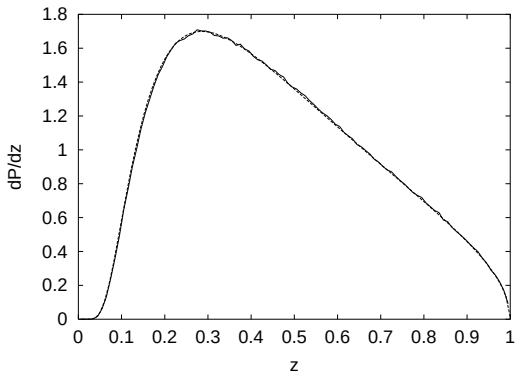

Figure 2.15: z values used in particle production in our method (solid line) compared to the Lund fragmentation function f(z)(dotted line). Though z value generation is according to the distribution f(z), not every value produced is used. This plot shows however, that the rejection of z values in the present method is unbiased.

To examine further effects in connection with our "restart strategy", we define the following measure Δy, of the correlation between two adjacent particles in the production process

$$\Delta y = ln(\frac{z_1}{z_2(1-z_1)}) \tag{2.70}$$

It corresponds to the difference in rapidity between the particles in the $(1+1)$-dimensional model. This distribution would be altered if we rejected particular correlations between successive values of z (e.x. a large value followed by a small value etc) more often than others.

In Fig.2.16 we compare our result with the result one obtains using only the Lund symmetric fragmentation function. There is no noticeable difference between the two curves, suggesting that the restart procedure (involving possible rejection of some z values) is effectively insensitive to such correlations between adjacent values.

In Fig.2.17 we show the distribution of our "local bending" parameter, $k^2_{\perp 2}$, defined in Eq.(2.43). This figure illustrates that the modifications of the directrix that we make when we apply our method are of the order of the hadronic mass scale. For values of $k^2_{\perp 2} > m^2$ there is a fall off faster than a gaussian.

In the left-hand side plot of Fig.2.18 we summarize the rapidity distributions obtained using the different approaches for passing a gluon corner, C2

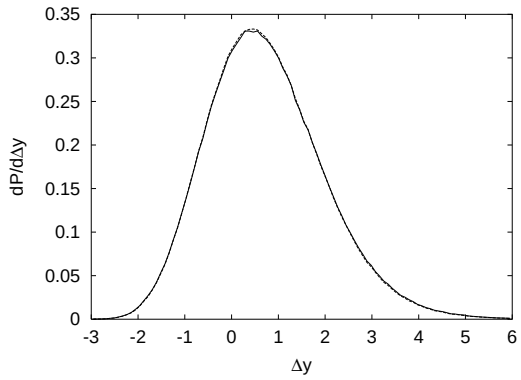

Figure 2.16: The Δy distribution, defined in Eq.(2.70), from our method (solid line) compared with the distribution obtained using only the Lund symmetric fragmentation function (dashed line).

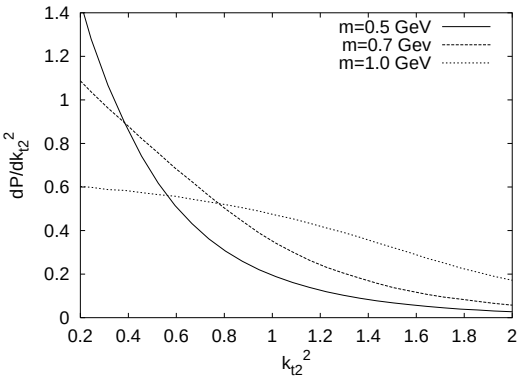

Figure 2.17: Plot of $\frac{dP}{d(k^2_{\perp 2})}$ vs $k^2_{\perp 2}$ measured in $(GeV)^2$. Modifications of the directrix are on the scale of hadronic mass.

and C3 described in section 2.5.2, and compare them to a curve produced using PYTHIA in one simple situation: a perturbative string state consisting of a quark, an antiquark and a single gluon. We conclude that modifying the directrix leads to the production of too many particles over a large range of rapidity if the modifications are not "smooth". In the right-hand side of Fig.2.18 we show a few rapidity distributions obtained from using our preferred method for different energies of the gluon. In Fig.(2.19) we show an example of in-

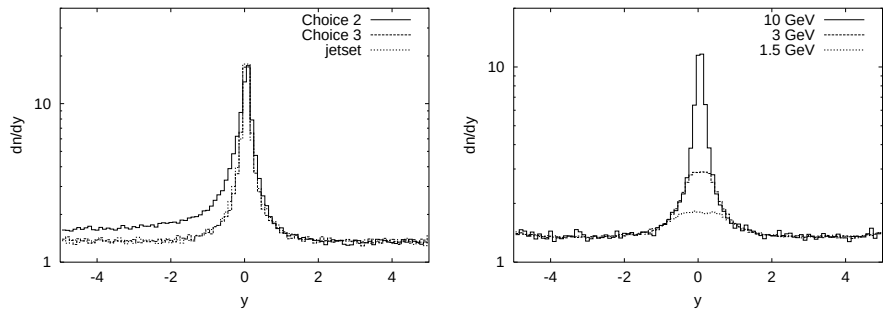

Figure 2.18: The figure to the left shows rapidity distributions for different choices for the vector k. The figure to the right shows rapidity distributions for a 3 jet event, obtained with the preferred method (C3), for different gluon energies. Note that the y axis is plotted on a log scale here.

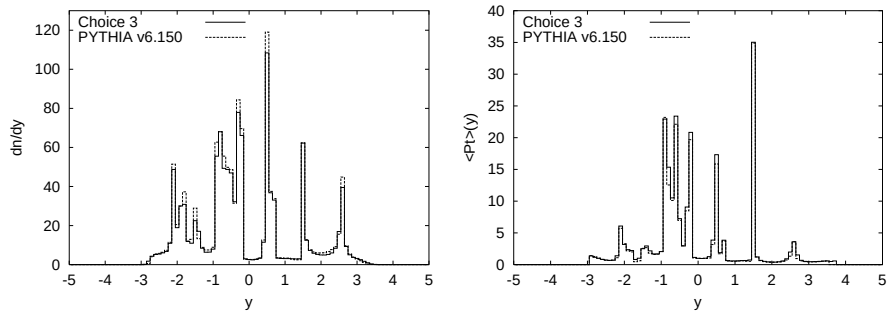

Figure 2.19: The rapidity distribution (left) and mean $|p_\perp^{hadrons}|$ (GeV) as a function of rapidity (right), for a string state of λ measure 70 (which is above the average λ for the energy and $p_\perp^{cut}$ used for this plot: $\sqrt{s}$ = 2000 GeV , $p_\perp^{cut} = 2GeV$) generated by ARIADNE, fragmented using our method (solid curve) and PYTHIA (dashed curve).

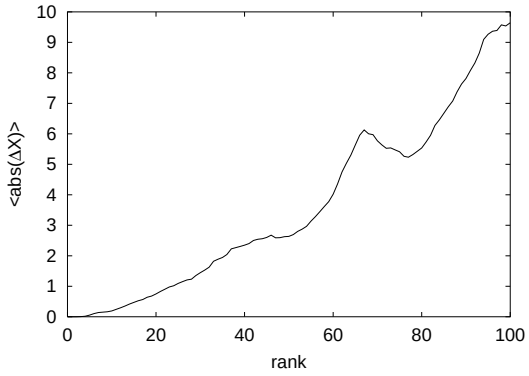

Figure 2.20: Comparison of JETSET and our method on an event to event basis: We plot here the average of the absolute value of the difference (GeV) between the hadronic curves for the same partonic event used in Fig.(2.19), obtained from the two programs as a function of rank, where for every event the particles of a certain rank were produced using exactly the same value of z in the two alternative procedures.

clusive rapidity distributions obtained by JETSET/PYTHIA and our method. For the comparison, we have used an arbitrarily chosen partonic event taken from ARIADNE. A close examination will show that in general there is a small multiplicity difference in the gluon jets. We have traced that to the fact that the two to three particles with the largest energy-momenta in the jets are faster according to our method compared to JETSET. It is impossible to compare to experimental data because firstly in this case we have only made use of a single partonic event. And secondly, at present we have not introduced the "fragmentation transverse momenta". Nevertheless we conclude that the inclusive distributions are very similar.

But we are definitely not dealing with the same particles on an event to event basis. To show this, we compare the two procedures on an exclusive, event to event basis in Fig.2.20. For this plot we devised a procedure to use exactly the same values of z for particle production in both programs. Since both our procedure, and PYTHIA might need to reject some sequences from time to time, we took only those events where no such rejection was required by either program. We have plotted the distribution of the absolute value of the difference of the two hadronic curves, $\sqrt{|\sum_{j=1}^{n}(p_{C3})_j - \sum_{j=1}^{n}(p_{PYTHIA})_j|^2}$,

as a function of rank. The curve clearly shows that the hadronic curves obtained from the two programs are different. The absolute value prevents cancellation of the differences which would occur in an average over a large number of events, as we find from the comparison of the inclusive distributions.

2.7 Concluding Remarks

We have presented a precise method to implement the Lund Area Law (Eq. (2.1)) to fragment a multigluon string state. The final state hadrons are produced in an iterative stochastic process. The energy-momentum vectors $\{p_j\}$ can be laid out in rank order as a curve, the X-curve, with a vertex vector at every point connecting to the directrix curve. The directrix corresponds to the parton energy momentum vectors laid out in colour order. It describes on the one hand the orbit of a (massless) q-particle connected to a string and on the other hand the whole string surface.

It is possible to describe the whole process by analytical means, in particular in terms of a transfer matrix formalism similar to the one used for the $(1+1)$-dimensional model in [5]. This time it is necessary to make use of a $(1+3)$-dimensional framework. We will investigate this problem in the future.

In this paper, we have neglected the possibility of introducing transverse fluctuations in the hadronisation process. Such fluctuations are introduced on the basis of tunnelling arguments in the $(1+1)$-dimensional model. We feel that they are necessary for a consistent quantum mechanical treatment (there is no way to localise the string surface area better than what is allowed by Heisenberg's indeterminacy relations). We will examine the effects of such transverse fluctuations on our results in the future.

The directrix curve is in general given by a perturbative cascade (although in some cases precise matrix elements are also available). This means that the partonic states we are fragmenting, are resolved only down to some cutoff, usually in virtuality or in terms of the smallest allowed partonic excitations. String dynamics is infrared stable in the sense that minor modifications of the directrix only have a local influence, due to the minimal nature of the string world surface. We have made use of this freedom in the fragmentation process and in this way the partonic states will be defined down to the hadronic mass-scale. We will investigate the properties of the soft gluons thus introduced into the partonic state, in the future.

We have shown that the fragmentation process, with step size equal to the hadronic mass can be defined also in the limit of a vanishing mass in terms of a differential process. The corresponding solution, the $\mathcal{P}$-curve, is stretched in between two curves, the original directrix, $\mathcal{A}$, and another curve, the $\mathcal{L}$-curve, also with a light-like tangent. The correspondence to the vertex vectors for the fragmentation process are connectors to the $\mathcal{P}$-curve reaching out to the

$\mathcal{A}$ and the $\mathcal{L}$-curves. The area in between the $\mathcal{P}$-curve and the directrix $\mathcal{A}$ corresponds to a generalised rapidity variable in the same way as the average hyperbola defines rapidity for the $(1 + 1)$-dimensional model. There is an interesting relationship to the group of rotations in a $(1 + 4)$-dimensional space which we will investigate further in the future.

We have also shown that there is a duality (with properties similar to the Parton-Hadron Duality introduced by the St. Petersburg group [10]) between hadronic X-curve, defined by our process and the original directrix. We note, however, that the hadrons produced in our process always stem from the energy-momenta of two or more partons. The vertex vectors x_j contain the "memory" of the earlier partons. It is nevertheless possible to reconstruct the directrix from the X-curve, although the relationship contains a large number of degrees of freedom (the number of degrees of freedom increases further if we introduce transverse momentum fluctuations in the fragmentation process). We will investigate these properties in the future.

The process we have defined has also been implemented into a Monte Carlo simulation program. Due to the way it is constructed it is fairly direct to include also the multi-particle production features of the original JETSET, i.e. to include probabilities for different $(q\bar{q})$-flavors, different kinds of mesons, the decay of resonances etc. This is necessary for a comparison with experimental data.

2.8 Acknowledgements

We would like to thank G. Gustafson for extensive discussions and T. Sjöstrand and L. Lönnblad for a lot of help both with the material and in particular with the way the Monte Carlo programs JETSET and ARIADNE work.

References

[1] B. Andersson, G. Gustafson and B. Söderberg, Z. Phys. **C20**, 317 (1983).

[2] B. Andersson, G. Gustafson and B. Söderberg, Nucl. Phys. **B264**, 29 (1986).

[3] B. Andersson, The Lund Model, (Cambridge University Press 1998).

[4] T. Sjöstrand, Computer Physics Commun. **82**, 74 (1994).

[5] B. Andersson and F. Söderberg, Eur. Phys. J. **C16**, 303 (2000).

[6] T. Sjöstrand, Nucl. Phys. **B248**, 469 (1984).

[7] Ya.I. Azimov et al., Phys. Lett.**B165**, 147 (1985). Yu.L. Dokshitzer, V.A. Khoze and S.I.Troyan, in A.H. Mueller ed., Perturbative QCD, p.241, World Scientific.

[8] G. Gustafson and U.Pettersson, Nucl. Phys. **B306**, 746 (1988).

[9] L. Lönnblad, Ariadne v 4.10, Computer Physics Commun. **71** (1992) 15.

[10] Yu.L. Dokshitzer and S.I.Troyan, Proceedings of the XIX Winter School of the LNPI, **1**, 144 (1984). Ya.I. Azimov, Yu.L. Dokshitzer, V.A. Khoze and S.I. Troyan, Z. Phys. **C27**, 6 (1985).

The λ-Measure and the Generalised Dipoles in the Lund Model

Paper III

LU TP 02-13
July 2002

The λ-Measure and the Generalised Dipoles in the Lund Model

Bo Andersson
Sandipan Mohanty[1]
Fredrik Söderberg[2]
Department of Theoretical Physics, Lund University,
Sölvegatan 14A, S-223 62 Lund, Sweden

Abstract We demonstrate that the multiple gluon emission phase space in the dipole cascade model has a strong linear correlation with the number of gluons emitted. The number of gluons per unit available phase space at a certain resolution scale is found to be remarkably independent of the cms energy and global event properties like thrust, and even changes in the ordering variable or resolution scale. We show that the distribution of sizes of gluon-gluon dipoles in a parton cascade has stability properties which are sufficient to account for those of the phase space variable. We observe that certain more abstract entities, defined in the context of hadronisation and related to the gluon emission phase space, share those properties of colour dipoles and name them Generalised Dipoles. We also present an analytical model to qualitatively describe our findings.

[1]sandipan@thep.lu.se
[2]fredrik@thep.lu.se

3.1 Introduction

The phase space for multiple bremsstrahlung emission of photons in QED is entirely given by the properties of the original current. The reason is that the photon-quanta are uncharged and therefore the currents are not changed because of emission of photons (besides the recoil effects from hard emissions).

On the other hand the QCD field quanta, the gluons, are charged. Already the emission of a first QCD gluon in e^+e^--annihilation means that the original $q\overline{q}$ dipole is changed. It so happens that the change is (to a very good approximation) from one dipole to two independent dipoles, one between the quark (q) and the first gluon and the other between the gluon and the anti-quark ($\overline{q}$). The initial dipole is at rest in the total cms whereas the two "new" dipoles move away from each other. The combined phase space for emitting from either one or the other of these dipoles is found to be larger. In rapidity space the increase can be described as an extra region of a size corresponding to the logarithm of the squared transverse momentum of the first emitted gluon.

In the Dipole Cascade Model [1], as implemented in the event generator ARIADNE [2], a second emission leads to three independent dipoles and so on. The ordering variable is an invariantly defined transverse momentum of the emitted gluons. The dipole masses decrease quickly with successive emissions.

HERWIG [3], and PYTHIA [4], subdivide the emerging dipole angular regions into independent cones for each emitting parton. One way to state the coherence conditions is that they do not permit double-counting in the emission process. HERWIG and PYTHIA implement the coherence conditions by means of angular ordering to avoid such overlaps. The ordering variable for HERWIG is just the angle (or the rapidity variable) occurring in the coherence conditions. PYTHIA uses the "virtuality" along the emission lines as an ordering variable and only afterwards introduces an angular ordering condition.

In this paper we will mainly describe the emerging features in terms of the notions of the Dipole Cascade Model (ARIADNE) and only perform a cursory comparison to similar results from PYTHIA. Some of the ideas presented here were also discussed in [20] in their priliminary form. Our aim is to investigate a set of distributions stemming from the perturbative parton cascades. We will show that the cascades result in a local structure, corresponding to sets of independent entities, which we are going to call Generalised Dipoles (GDs). The GDs are linked together along the colour lines of the QCD force field. They have a common distribution in a generalised rapidity range λ, and in the (local) transverse momentum. This structure is independent of the total cms energy, the global event variables like thrust and the number of hard emissions. Further the GDs show a surprisingly small scale dependence, i.e. almost the same distributions occur inside a wide range of the ordering variable.

We will concentrate upon e^+e^--annihilation events, where the gluon cascade is produced through the bremsstrahlung from an originally produced $q\overline{q}$

pair (although we expect that the same structures will emerge also in other dynamical situations). Such a multi-gluon state is conveniently described by means of a four-vector valued function, the directrix $\mathcal{A}_\mu$ [5]. The directrix is obtained by laying out the energy–momentum vectors, k_j, of the emitted partons in colour-order, starting with the q and ending with the $\overline{q}$ (we will neglect the production of "new" q$\overline{q}$-pairs through the gluon splitting process). As we will use massless partons, the directrix is a curve with a tangent that is lightlike everywhere.

As mentioned earlier the phase space available for gluon emission at a certain value of the ordering variable $k_\perp$ depends on the partons present and their colour order. It could, therefore, be regarded as a functional of the directrix $\mathcal{A}_\mu$. In section 3.2, we will discuss a measure of this phase space, to be called ℓ, for multiple gluon emission in perturbative QCD. An infrared stable generalisation of this phase space, involving a "resolution parameter" m_0 leads to the concept of the λ-measure [6].

The λ-measure was introduced many years ago [6], as a generalisation of the rapidity range, to describe the phase space for hadronisation. At the same time [6], a curve similar in appearance to a set of connected hyperbolae along the directrix was introduced, the $\mathcal{X}$-curve. Its length is related to λ in the same way as the "ordinary" rapidity variable measures the length of a hyperbola spanned between two lightlike vectors.

The tangent vector, to be called q_T, at a point on the $\mathcal{X}$-curve that reaches out to a point on the directrix quickly reaches a constant length, $q_T^2 = m_0^2$, just like the constant distance in Minkowski metric between the lightcones and an ordinary hyperbola. The parameter m_0 is a resolution parameter for the properties of the directrix. In the context of hadronisation, it is fixed by the properties of the spectrum of hadrons produced. Thought of as a generalisation of ℓ, the λ-measure has a resolution parameter which can be directly related to the ordering variable in the perturbative cascade. When the tangent vector q_T follows the directrix it will span a surface between the directrix and the $\mathcal{X}$-curve. The λ-measure is also proportional to the area of this surface.

In the dipole model, the available phase space for gluon emission, ℓ, in the Leading Log Approximation (LLA) [7] and in the Modified Leading Log Approximation (MLLA) [7] schemes is a sum of a series of terms , $(\Delta\ell)_j$, one for each pair of consecutive vectors along the directrix [6]. These terms are contributions to the phase space from individual dipoles in the Dipole Cascade Model. We will show that the λ-measure can be similarly subdivided into a number of parts $(\Delta\lambda)_j$, one for each vector along the directrix, and that they are strongly related to the contribution from the dipoles, $(\Delta\ell)_j$. The process of subdividing λ corresponds to a partitioning of the surface mentioned above into "plaquettes"[3] that are enclosed by one "initial" q_T and one "final" q_T vector

[3]In this paper, we will use the word plaquette to denote this area even though one part

together with a hyperbolic segment of the $\mathcal{X}$-curve and the parton energy–momentum vector in between, cf. Fig 3.1 in section 3.2. It is the regularity in the $(\Delta\lambda)$ distribution that will lead to the definition of the GDs. For the surface mentioned above this regularity implies a simple general structure, which shows only a slowly varying dependence on the ordering variable.

The directrix also plays a major role in the description of the state of the massless relativistic string, which is used as a model for the QCD force fields in String Fragmentation [5]. The surface spanned by the string during one period is a minimal surface. This has two consequences. On the one hand the surface is completely determined by its boundary curve. On the other hand the surface is stable against small deformations (the model is infrared stable). In the motion of a massless relativistic string, a wave moves across the string surface bouncing at the endpoints defined by the orbits of the q and the $\overline{q}$. This means that the internal excitations (which in the Lund Model are identified as the gluons) will reach and affect the endpoints in turn, i.e. in the colour order of their emission. The corresponding orbit of the q endpoint is the directrix.

It is interesting to note that the $\mathcal{X}$-curve (or rather a close relative, called the $\mathcal{P}$-curve in [8]) and the λ-measure play a major role in the String Fragmentation process for multigluon string states. In the process that we devised in [8], the final state hadron energy–momenta, laid out in rank order, constitute a curve, the X-curve. The X-curve follows the directrix at a typical stochastically fluctuating distance and the area in between the two curves could be thought of as the area in the Lund Model Area law [8]. It turns out that the average X-curve is just the $\mathcal{P}$ curve with a length given by λ. The generalised dipoles to be defined in this note also play an interesting role in the fragmentation process. Just as they emerge as independent entities from the partonic cascades, they also fragment essentially independently of each other into the final state hadrons, in a fragmentation scheme along the directrix.

The λ-measure has been used in many different contexts in investigations over the years. It was quickly found, that the $\mathcal{X}$-curve shows properties of a fractal character [9] and the multi-fractal dimensions were shown to be identical to the so-called anomalous dimensions of QCD [10].

In section 3.2, we recapitulate some features of the gluon emission phase space ℓ-measure and the λ-measure with the aim of pointing out similarities and differences between the two quantities[4]. We also introduce the quantities $\Delta\lambda$ and present a geometrical interpretation for them. In section 3.3, we describe our findings and define the Generalised Dipoles. In section 3.4, we present a

of the boundary curve is a part of a hyperbola. The plaquettes defined in this paper are not related to the plaquettes used in Lattice QCD.

[4] In the past, like in the references listed in this paper, the gluon emission phase space has often been called the λ-measure. But since both this phase space and the phase space for hadronisation are relevant for this work, we make the distinction here and give them different names.

model to understand the distributions we have obtained. At the same time we will consider some earlier results and the theoretical analysis. Finally, in section 3.5 we make some concluding remarks.

3.2 The λ-Measure and The Perturbative Cascades

3.2.1 The phase space in a dipole cascade and the ℓ-Measure

The probability for the emission of gluons in the Dipole Model can be described in terms of an inclusive density of gluons (cf. [1]):

$$\mathrm{d}n = \alpha_{\mathrm{eff}} dy \frac{dk_\perp^2}{k_\perp^2} \times (\sum\nolimits_p) \tag{3.1}$$

with α_{eff} the effective running coupling and $(\sum_p)$ the polarisation sum, i.e. the coupling between the spin of the emitters and the gluon. The coherence conditions in this case are identical to energy–momentum conservation, i.e. the cms energy of the gluon cannot exceed half the total cms energy

$$k_\perp \cosh(y) \leq \frac{\sqrt{s}}{2} \tag{3.2}$$

A convenient approximation, corresponding to the Leading Log Approximation, is $|y| < \frac{1}{2}\ln(\frac{s}{k_\perp^2})$ so that the total rapidity range is $\Delta y \simeq \ln(\frac{s}{k_\perp^2})$. As we mentioned above the emission of a gluon will change the current. But it is an immense simplification that this change is simply a change from one dipole to two independent dipoles (to a very good approximation) [7, 11]. Thus the density for the emission of two gluons is factorisable, so that we obtain

$$\mathrm{d}n(\mathrm{q}\mathrm{g}_1\mathrm{g}_2\overline{\mathrm{q}}) \simeq \mathrm{d}n(\mathrm{q}\mathrm{g}_1\overline{\mathrm{q}})\,[\mathrm{d}n(\mathrm{q}\mathrm{g}_2\mathrm{g}_1) + \mathrm{d}n(\mathrm{g}_1\mathrm{g}_2\overline{\mathrm{q}})] \tag{3.3}$$

(with a negative correction that formally is of the order of $1/N_c^2$ for a finite number of colours, but reduced further in practice due to kinematics). Eq. (3.3) is valid if the transverse momenta are ordered so that $k_{\perp 1} > k_{\perp 2}$ or else the two gluons are exchanged. While the original $(\mathrm{q}\overline{\mathrm{q}})$ dipole is at rest in the cms the two "new" dipoles move apart. Each of them will decay in

its own restframe with a phase space given by Eq. (3.2) and this means that the combined rapidity region for emitting the second gluon with transverse momentum $k_\perp$ is

$$\begin{aligned}(\Delta\ell)_{01} + (\Delta\ell)_{12} &= \ln\left(\frac{s_{01}}{k_\perp^2}\right) + \ln\left(\frac{s_{12}}{k_\perp^2}\right) \\ &= \ln\left(\frac{s}{k_\perp^2}\right) + \ln\left(\frac{s_{01}s_{12}}{sk_\perp^2}\right)\end{aligned} \tag{3.4}$$

The expression $\frac{s_{01}s_{12}}{s}$ is the conventionally defined invariant squared transverse momentum of the first gluon, $k_{\perp 1}^2$. Similarly, for an emission at $k_\perp^2$ from a system of n gluons, we can write the phase space as:

$$\ell = \sum_{i=0}^{n}(\Delta\ell)_{i,i+1} = \sum_{i=0}^{n}\ln(\frac{s_{i,i+1}}{k_\perp^2}) = \ln\prod_{i=0}^{n}(\frac{s_{i,i+1}}{k_\perp^2}) \tag{3.5}$$

At this point, it is necessary to differ between two definitions of the transverse momentum. The one we have used up to now is the ordering variable $k_\perp$, i.e. the value used for the emission of a gluon and defined by the partitioning of a dipole of mass M into a pair of dipoles with masses (m_1, m_2) so that $k_\perp^2 = m_1^2 m_2^2/M^2$. There is another local variable, to be called k_t, which is defined along the directrix so that we have

$$k_{tj}^2 = \frac{(2k_{j-1}k_j)(2k_jk_{j+1})}{(2k_{j-1}k_j) + (2k_jk_{j+1}) + (2k_{j-1}k_{j+1})} \equiv \frac{s_{j-1,j}s_{j,j+1}}{s_{j-1,j,j+1}} \tag{3.6}$$

in terms of the energy–momentum vectors of the (colour) adjacent gluons.

We note that the two values of $k_\perp$ and k_t coincide for the last emitted gluon. But in general the transverse momentum k_t of a gluon may be much smaller than the $k_\perp$ value at which it was emitted, because of the recoils from subsequent emissions. In fact, in this way k_t can even become smaller than the resolution scale at which the state is being sampled. But the "emission" $k_\perp$ and the concepts of the "first emitted" gluon and the "second emitted" gluon etc are necessities of the strategies used to simulate this quantum mechanical process, and not properties of the final state of partons. When one asks what the probability is for the production of a state with a certain number of partons, where colour connected partons with transverse momenta smaller than a certain value would not be considered as resolved emissions, the only relevant transverse momentum is the k_t, which is calculated using vectors in the final state. Therefore, it is undesirable that this variable is pushed to values smaller than the resolution parameter. We have used two different methods to avoid such situations. The first is to veto such emissions along the cascade[5] and

[5]This feature will be made available in the next version of ARIADNE

the second to change the ensuing directrix vectors so that three neighbouring lightlike vectors are combined into two. All the results of this investigation are independent of the method that is used. Furthermore, such a procedure is essential for the inclusion of the second order matrix element corrections into ARIADNE [12].

3.2.2 The λ-measure, its properties and its connection with the ℓ-measure

When a string without gluonic excitations fragments under the usual Lund Model assumptions, hadrons are formed by breaking of the string field at "vertices" which, on the average, lie on a typical hyperbola parametrised by a squared proper time from the origin, usually called Γ_0 or m_0^2. The rapidity range available along this hyperbola is given by $\ln \frac{s}{m_0^2}$.

In the Lund Model interpretation for a string with a single gluon excitation, there will be two parts of the string; one string piece spanned between the q and the g and one between the g and the $\overline{q}$. Therefore there will be two hyperbolic angular ranges $(\Delta y)_{01}$ and $(\Delta y)_{12}$ for hadron formation. The sum of these ranges is

$$(\Delta y)_{01} + (\Delta y)_{12} = \ln(\frac{s_{01}}{2m_0^2}) + \ln(\frac{s_{12}}{2m_0^2}) = \ln(\frac{s}{m_0^2}) + \ln\left(\frac{s_{01}s_{12}}{4sm_0^2}\right) \qquad (3.7)$$

We draw attention to the factor of 4 in Eq. (3.7), and its absence in Eq. (3.4). In the Lund Model, when the partons move apart stretching a string-like field between them, they lose energy–momentum to the string field. A gluon is attached to two string pieces while a quark or an anti-quark is attached to one. Therefore a gluon will lose energy–momentum twice as quickly as a quark or an anti-quark. Flat string regions will therefore be formed, bounded by the whole of quark or anti-quark momenta, but half of gluon momenta. Since hadrons form from this field, the phase space is calculated by adding up the lengths of typical hyperbolae in each of these flat string regions. For instance, the invariant mass of the region involving the quark and the gluon, for the system in Eq. (3.7), is $(k_{\rm quark} + \frac{1}{2}k_{\rm gluon})^2 = \frac{s_{01}}{2}$, and its contribution to the phase space for hadronisation is $\frac{s_{01}}{2m_0^2}$.

Such a factor was not necessary in Eq. (3.4). A gluon is shared between two dipoles, but both of those dipoles are modified by the emission of a single gluon from either of these dipoles. This is because the gluon in common between them would receive a recoil and that would change the invariant masses of both the dipoles. Formation of a single hadron in string fragmentation does not give recoils to the partons making up the string. Hadron formation occurs from the string, which has a spatial extent. Gluon emission, on the other hand, is a perturbative phenomenon and the new emission is thought to come

directly from one or the other of the two partons making a dipole, or from the dipole as a whole regarded as a unit. Therefore, in the implementation of the dipole cascade model in ARIADNE, the full gluon momentum is used for both the dipoles involving the gluon. There is no problem in conserving energy–momentum because both the dipoles can not emit "simultaneously". As soon as there is an emission from one dipole, the whole system is updated into a new chain of dipoles.

The expression in Eq. (3.7) does not make sense for soft or collinear gluons, as these would give negative contributions to the effective rapidity range. An infrared stable generalisation applicable for arbitrarily many gluons was presented in [6] and its relation to the hadronisation process was discussed in [13]. For a state with a single gluon we replace the expression in Eq. (3.7) with:

$$\ln\left(\frac{s}{m_0^2}+\frac{s_{01}s_{12}}{4m_0^4}\right) \tag{3.8}$$

This is a nicely interpolating expression between the results for a string with and without a gluon. It can be generalised to an arbitrary number of gluons by introducing the following quantities, defined as integrals along the directrix $\mathcal{A}(\xi)$ (with ξ a suitable parameter, here taken to be the energy along the directrix):

$$\begin{aligned} t_j \;=\; & \int_0^{E_{tot}} d\xi_1 \int_0^{\xi_1} d\xi_2 \left[\frac{d\mathcal{A}}{d\xi_1}\cdot\frac{d\mathcal{A}}{d\xi_2}\right] \int_0^{\xi_2} d\xi_3 \int_0^{\xi_3} d\xi_4 \left[\frac{d\mathcal{A}}{d\xi_3}\cdot\frac{d\mathcal{A}}{d\xi_4}\right]\cdots \\ & \cdots \int_0^{\xi_{2j-2}} d\xi_{2j-1} \int_0^{\xi_{2j-1}} d\xi_{2j} \left[\frac{d\mathcal{A}}{d\xi_{2j-1}}\cdot\frac{d\mathcal{A}}{d\xi_{2j}}\right] \end{aligned} \tag{3.9}$$

This corresponds to a $2j$-fold partitioning of the directrix into non-overlapping pieces and then to multiplying the adjacent vector differentials two by two. For a massless relativistic string, a point on the string (parametrised by the energy (σ) between the point and the quark end) at time t will be at $x(\sigma,t)$:

$$x(\sigma,t)=\frac{[\mathcal{A}(t+\sigma)+\mathcal{A}(t-\sigma)]}{2} \tag{3.10}$$

i.e. it is given by one left-moving and one right-moving vector defined by points on the directrix. As the differentials of the directrix are lightlike the quantities $d\mathcal{A}(\xi)\cdot d\mathcal{A}(\xi')$ occurring in the integrals in Eq. (3.9) are surface elements on the string. The integrals in this way correspond to all the possibilities of obtaining j-fold partitionings into non-overlapping areas on the string surface.

We may then define a functional $T\equiv\exp(\lambda)$ as

$$T=1+\sum_{j=1}^{\infty}\frac{t_j}{(m_0^2)^j} \tag{3.11}$$

i.e. as the generating function of the partitioning functionals t_j in Eq. (3.9) with m_0 an energy scale to make it dimensionless. We note that the integrals t_j will vanish if $j > n+1$ where n is the number of gluons emitted. The term involving one power of m_0 is always equal to $\frac{s}{2m_0^2}$ and the last (nonvanishing) term will have the generic form

$$\frac{1}{2}\frac{s_{01}}{2m_0^2}\frac{s_{12}}{4m_0^2}\frac{s_{23}}{4m_0^2}\cdots\frac{s_{n,n+1}}{2m_0^2} \tag{3.12}$$

with $(j, j+1)$ indices of colour-consecutive partons (index 0 for the q, indices 1 .. n for gluons, and $n+1$ for the $\overline{q}$). Besides the addition of 1 and a factor of $1/2$ (both introduced to obtain simple factorisation properties, cf. below) the T functional in Eq. (3.11) coincides with the argument of the logarithm in Eq. (3.8).

It is useful to define a generalisation, $T(\xi)$, by exchanging the upper limit in Eq. (3.9) from E_{tot} to ξ [6]. This functional fulfils

$$T(\xi) = 1 + \int_0^{\xi}\int_0^{\xi_1}\frac{d\mathcal{A}(\xi_1)\cdot d\mathcal{A}(\xi_2)}{m_0^2}T(\xi_2) \tag{3.13}$$

and together with the four-vector valued functional q_T[6]:

$$q_T(\xi) = \frac{1}{T(\xi)}\int_0^{\xi} d\mathcal{A}(\xi')T(\xi') \tag{3.14}$$

we obtain the differential equations

$$\begin{aligned} dT &= \frac{q_T d\mathcal{A}}{m_0^2}T \\ dq_T &= d\mathcal{A} - \frac{q_T d\mathcal{A}}{m_0^2}q_T \\ dq_T^2 &= 2(1-\frac{q_T^2}{m_0^2})q_T d\mathcal{A} \end{aligned} \tag{3.15}$$

They can be integrated to

$$\begin{aligned} T(\xi) &= \exp\left(\int_0^{\xi}\frac{q_T(\xi')d\mathcal{A}(\xi')}{m_0^2}\right) \\ q_T^2(\xi) &= m_0^2[1-T(\xi)^{-2}] \end{aligned} \tag{3.16}$$

Finally, we define a four-vector valued function $\mathcal{X}_\mu = \mathcal{A}_\mu - {q_T}_\mu$[7] so that

$$d\mathcal{X} = \frac{(q_T d\mathcal{A})}{m_0^2}q_T \tag{3.17}$$

[6] Called q in [6]
[7] Called X in [6]

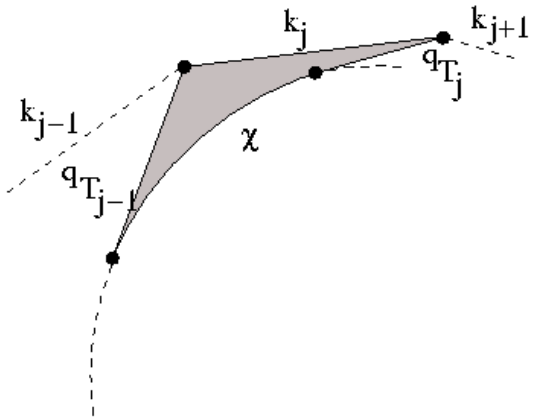

Figure 3.1: A plaquette bordered by q_{Tj}, q_{Tj+1} , k_j and a hyperbolic segment from the $\mathcal{X}$-curve, as described in the text.

i.e. the vector q_T is the tangent to the $\mathcal{X}$-curve reaching out to the directrix. From Eq. (3.16) we conclude that the functional T is the exponential of an area (note that the vector $d\mathcal{A}$ is lightlike, and $q_T d\mathcal{A}$ is an area element between the directrix and the $\mathcal{X}$-curve). This area is proportional to the functional λ as mentioned in the Introduction. We also note that the vector q_T quickly reaches the length m_0. Integrating the differential equations for a directrix built up from a set of lightlike vectors $\{k_j\}$ we obtain the iterative equations [6]:

$$\begin{aligned} T_{j+1} &= (1 + q_{Tj}k_{j+1}/m_0^2)T_j \equiv \frac{T_j}{\gamma_{j+1}} \\ q_{Tj+1} &= \gamma_{j+1}q_{Tj} + \frac{1+\gamma_{j+1}}{2}k_{j+1} \end{aligned} \tag{3.18}$$

The starting values are $T_0 = 1$ and $q_{T0} = k_0$.

The factorisability of the functional T means that its logarithm, λ, can be written as a sum containing one term for each k_j:

$$\lambda \equiv \sum_{j=1}^{n+1} \Delta\lambda_j = \sum_{j=1}^{n+1} \ln\left(1 + q_{Tj-1}k_j/m_0^2\right) \tag{3.19}$$

The $\Delta\lambda_j$ defined in this way is the size of a subarea just as the total λ represents the area spanned between the $\mathcal{X}$ and the directrix curves. In Fig. 3.1 we exhibit such a region bordered by the "initial" q_{Tj-1} and the "final" q_{Tj} together with a hyperbolic segment from the $\mathcal{X}$-curve and the gluon energy–momentum vector k_j from the directrix.

If we define $\gamma_0 \equiv 1$ and the vectors $k_j^{'} \equiv \frac{1}{2}k_j(1+\gamma_j)$, then it is easy to see that the vector q_{Tj} is a weighted sum of the $k_l^{'}$ vectors ($l \leq j$). The weight for any vector $k_m^{'}$ is exponentially suppressed with $\sum_{l=m}^{j-1} \Delta\lambda_{l+1}$.

To see that $\Delta\lambda_j$ as defined in Eq. (3.19) actually has the meaning of a rapidity we go to the rest frame of the vector q_{Tj-1} and assume for simplicity that it has the length m_0. Further assume that the lightlike vector k_j is directed along the 3-axis with the length ω so that $\Delta\lambda_j = \ln(1+\omega/m_0)$. Then it is easy to show that the "next" q_T-vector q_{Tj} will have the lightcone coordinates along the 3-axis equal to $(m_0\exp(\Delta\lambda_j), m_0\exp(-\Delta\lambda_j))$, i.e. the q_T vector has been accelerated from rest to the rapidity $\Delta\lambda_j$ by "the step" k_j along the directrix. The corresponding segment of the $\mathcal{X}$-curve is a part of a hyperbola.

For sufficiently well ordered emissions and a resolution scale much smaller than the smallest transverse momentum present, the last term (Eq. (3.12)) will dominate in Eq. (3.11) and therefore $\lambda(m_0 = \frac{1}{2}k_\perp)$ will be approximately equal to $\ell(k_\perp)$ defined in Eq. (3.5).

From the definition in Eq. (3.19) it is easy to show (cf. the definition of the vectors q_{Tj} in Eq. (3.18)) that the argument in the logarithm of the $\Delta\lambda_j$ is equal to $(1 + s_{j-1,j}/4m_0^2)$ plus terms down by at least a factor of γ. From the definition of the local k_t variables, Eq. (3.6), we may also conclude that

$$k_{tj}^2 < \frac{s_{j-1,j}s_{j,j+1}}{(s_{j-1,j}+s_{j,j+1})} \tag{3.20}$$

and consequently we obtain

$$\begin{aligned} \Delta\lambda_j &> \ln(\frac{s_{j-1,j}}{4m_0^2}) = \ln(\frac{s_{j-1,j}}{k_\perp^2}) \equiv \ell_{j-1,j} \\ \ln(\frac{k_{tj}^2}{k_\perp^2}) &< \min(\ell_{j-1,j}, \ell_{j,j+1}) \end{aligned} \tag{3.21}$$

This implies that there is a minimum positive value of $\Delta\lambda$, if a procedure to exclude or filter out emissions creating gluons with $k_t < k_\perp$ has been used.

3.3 The Properties of the $\Delta\lambda$ Distributions

We will now exhibit a very noticeable regularity of the dipole cascades, cf. Fig. 3.2. In this figure, we show a plot of the average number of gluons as a function of $k_\perp$, $n(k_\perp)$, versus $\ell(k_\perp)$ for e^+e^--events with $\sqrt{s} = 200$ GeV and for a range of values of $k_\perp$ from 4 down to 1 GeV. We have switched off the gluon splitting process so that we end up with one colour connected set of partons. There are several interesting properties of this plot:

- There is a linear correlation between the average gluon multiplicity $\langle n(k_\perp)\rangle$ and the phase space variable $\ell(k_\perp)$ inside a very narrow band. The fact that

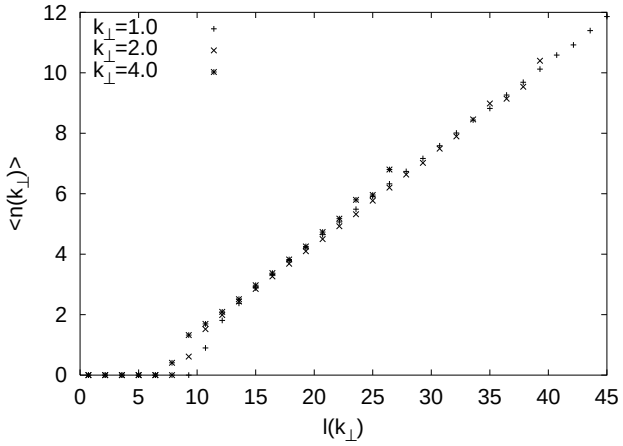

Figure 3.2: The figure shows a plot of $\langle n(k_\perp)\rangle$ versus $\ell(k_\perp)$ for an e^+e^--event with $\sqrt{s} = 200$ GeV from ARIADNE.

the different lines obtained for different values of $k_\perp$ are so close to each other means that the slope of this linear correlation is rather insensitive to changes in the ordering variable in this range. It should be noted that the $\ell(k_\perp)$-distributions are widely varying for these $k_\perp$-values as we show in Fig. 3.3. We have used a running coupling (with $\Lambda_{QCD} = 0.22$ GeV, i.e. the default value in ARIADNE). The region with $\ell(k_\perp) > 20$ is mainly populated by the results from small $k_\perp$-values, $k_\perp < 2$ GeV.

- We find that the linear correlation in Fig. 3.2 is independent of the cms energy (we have used different cms energies ranging from 40 GeV and up to even 2000 GeV, though for small energies there are too few gluons emitted to allow detailed studies), cf. Fig. 3.4. Not only do we find a linear correlation at each value of cms energy (when the number of gluons is more than 2), the slope of the correlation varies rather weakly with respect to energy. This property is also not a function of the total thrust, or the presence of particularly hard emissions (e.g. gluon of $k_\perp > 7$ GeV for $\sqrt{s} = 200$ GeV). There is a minimum value of $\ell \simeq 10$, corresponding to no gluon emission (for $k_\perp = 1$ GeV and $\sqrt{s} = 200$ GeV), and there is a (small) transition region for a few more units, until the number of gluons exceeds two. But after that $dn/d\ell$ is a constant.

- As a consistency check we have used two procedures for sampling the events. It is possible to run the parton cascade in ARIADNE down to a certain value of the ordering variable $k_\perp$, i.e. emit all gluons with larger $k_\perp$'s, sample

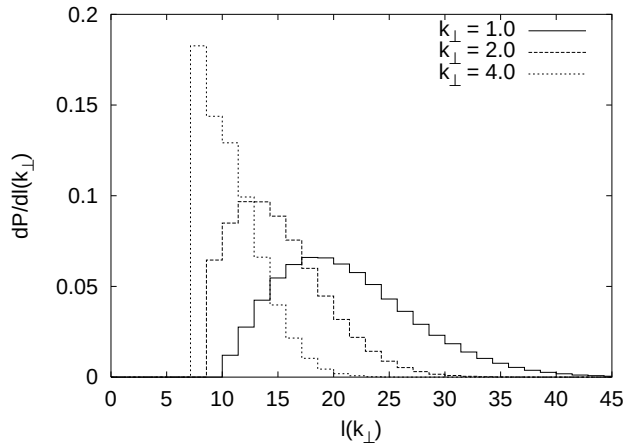

Figure 3.3: The $\ell(k_\perp)$-distribution for different $k_\perp$-values at $\sqrt{s} = 200$ GeV.

the emerging directrix and investigate its properties, e.g. calculate the number of gluons emitted to that point, $n(k_\perp)$, the total length of the $\mathcal{X}$-curve, $\ell(k_\perp)$, the individual $\Delta\lambda(m_0)$'s and the local k_t's. After that we may continue the cascade for the same event down to smaller $k_\perp$-values and do the same exercise. Another possibility is to run the cascade down to a certain value $k_\perp \equiv k_{\perp cut}$ and collect a large sample of events to investigate. After this we can pick a new value of $k_{\perp cut}$ and repeat the process. The result in Fig. 3.2 does not depend upon which of the two methods for sampling the events we use.

We observe the same effect in the parton shower in PYTHIA as in ARIADNE. The ordering variable in PYTHIA is the parton virtuality Q^2, and the variable $\hat{k}_\perp^2 = z(1-z)Q^2$ (where z is the lightcone fraction taken by the emitted parton) is used as the argument for the running coupling. This is a good approximation for the transverse momentum in the case of massless parton kinematics. However, since transverse momentum itself is not the ordering variable in this case, there is no real lower limit to it. Therefore, in order to make the comparisons we filtered the events obtained from PYTHIA and combined partons such that all gluons had k_t above a certain value proportional to Q.

It is then possible to use PYTHIA to obtain an inclusive sample of $n_g(CQ)$ and $\ell(CQ)$. We just note that it is possible to tune the constant C such that, as shown in Fig. 3.5, there is the same $dn/d\ell$ as in ARIADNE. We find that $C \approx 0.5$ It is possible to switch off the coherence conditions in the parton

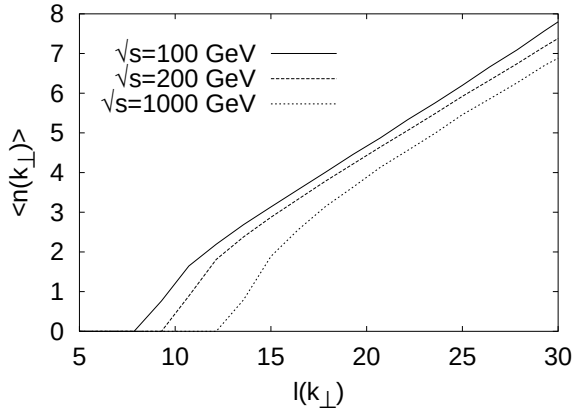

Figure 3.4: The figure shows a plot of $\langle n(k_\perp)\rangle$ versus $\ell(k_\perp)$ ($k_\perp = 1.0$ GeV) for different cms energies from ARIADNE.

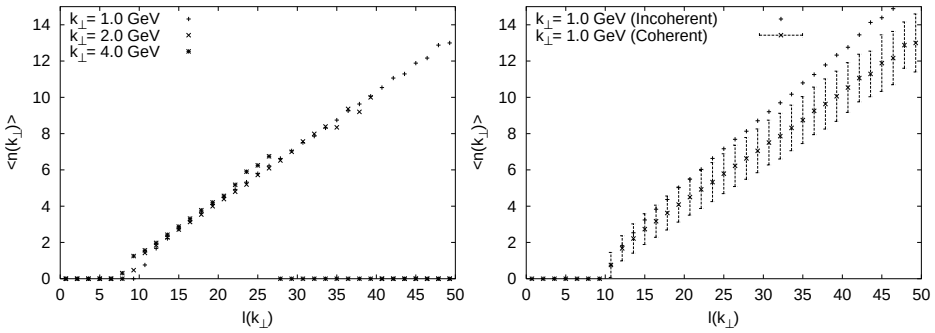

Figure 3.5: The figure to the left shows a plot of $\langle n(k_\perp)\rangle$ versus $\ell(k_\perp)$ for an e^+e^--event with $\sqrt{s} = 200$ GeV from PYTHIA. The figure to the right shows $\langle n(k_\perp)\rangle \pm \sigma$ versus $\ell(k_\perp)$ at $\sqrt{s} = 200$ GeV, $k_\perp = 1.0$ GeV for coherent and incoherent showers in PYTHIA.

shower in PYTHIA, since the strong angular ordering is implemented only after the generation using the ordering variable Q^2. We show the effect of this feature in Fig. 3.5. For the same C we obtain many more partons per unit phase space for an incoherent shower, although they still show a linear correlation to the ℓ-measure.

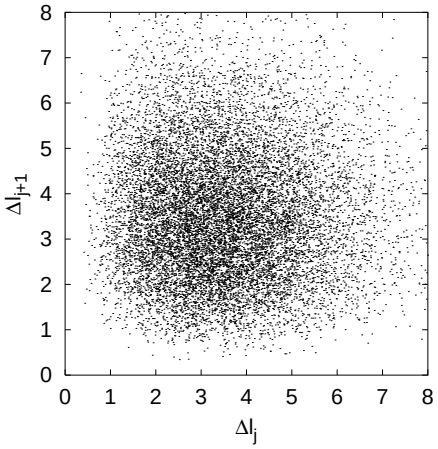

Figure 3.6: Scatter plot of two adjacent $\Delta\ell$ values

The linear relation between $\langle n \rangle$ and ℓ can be understood as follows. If one considers a variable such as ℓ defined as in Eq. (3.5) where the parts $\Delta\ell_j$ are distributed with the averages μ_j and the variances σ_j^2, then ℓ itself will mostly have a gaussian distribution according to the central limit theorem. The average is $\bar{\mu} = \sum \mu_j$ and the variance $\bar{\sigma^2} = \sum \sigma_j^2$. The numbers $\bar{\mu}$ and $\bar{\sigma^2}$ are in general well-defined for large n unless the values of the $\Delta\ell_j$ are correlated. We find that the $\Delta\ell_j$'s indeed show very little correlation, even between adjacent dipoles, cf. Fig 3.6. We also find that the average μ_j shows only a weak dependence upon the total number of gluons in the event, n, for a wide range of n.

We will therefore go over to the investigation of the distribution of the $\Delta\ell_j$ defined in Eq. (3.5). We notice that the first and the last term in Eq. (3.5) are different from the other terms in one important aspect. They are contributions from dipoles involving a quark or an antiquark (with different colour charges than gluons), whereas all the other terms come from purely gluonic dipoles. It turns out that the dipoles at the ends have slightly different distributions than all the rest. However, if the gluon splitting process is switched off, there are only two such dipoles in an event. This means that we can write for the average $\bar{\mu} = 2\langle \mu_{\mathrm{q}} \rangle + (n-1)\langle \mu_{\mathrm{gg}} \rangle$. In Fig. 3.4 we see this effect clearly, because it is only for $n > 2$ that we find a constant slope, i.e. when we have purely gluonic dipoles present. The properties we noted above are about variation of the number of gluons or dipoles with respect to $\ell(k_\perp)$ and the stability of the slope of the correlations, and should correspond to the properties of purely gluonic dipoles. Therefore, from now on we will not include the very first and the very

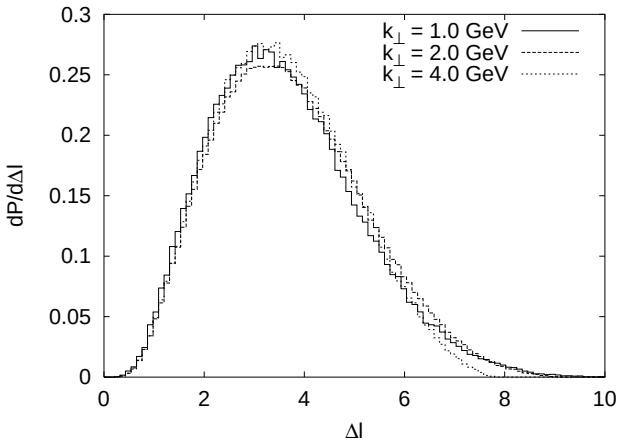

Figure 3.7: The $\frac{dP}{d(\Delta\ell)} \equiv P_\ell(\Delta\ell)$-distribution from ARIADNE.

last $\Delta\ell$-values in the investigations. We have seen that purely gluonic dipoles, irrespective of their position along the directrix, have the same distribution in size. In Fig. 3.7, we show the distribution $\frac{dP}{d(\Delta\ell)} \equiv P_\ell(\Delta\ell)$ from ARIADNE and observe that:

- The distribution P_ℓ has an average μ and a variance σ^2, consistent with the results in Fig. 3.2. We have found that it is independent of the cms energy, of the global event variables like thrust and the total ℓ-value for the event, and also of hard gluon emissions.

- The distribution P_ℓ is rather insensitive to the value of $k_\perp$. In Fig. 3.8, we show the average value of $\Delta\ell$ as a function of $\kappa \equiv \ln(k_\perp^2/\Lambda^2)$ and we find that it changes about 5 %, when the ordering variable goes from 0.8 to 3 GeV.

- There are no noticeable correlations between adjacent $\Delta\ell$'s as we have noted before. In Fig. 3.6, we show the scatter plot beween two adjacent $\Delta\ell$, taken from stochastically chosen pairs in many different events. In Fig. 3.9, we show the values of the average $a(n)$ (defined as $a(n) \equiv \langle\sum_{j=1}^{n} \Delta\ell_j\rangle$), and the standard deviations around it, for chains of n connected $\Delta\ell$. For this figure the statistics was collected from events with a fixed number of gluons.

- In order to further investigate the independence of the $\Delta\ell$ values in an event we have examined events containing a fixed number (N) of gluons. We may

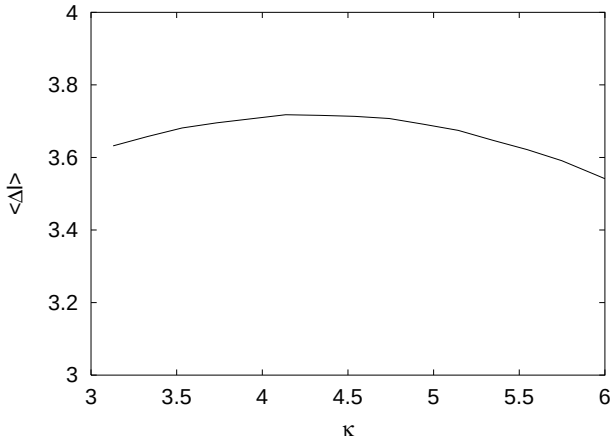

Figure 3.8: The average value of $\Delta\ell$ as a function of $\kappa \equiv \ln(k_\perp^2/\Lambda^2)$. Note that the variation in the average $\Delta\ell$ in the figure is much smaller than the width of the distribution of $\Delta\ell$ as seen in Fig. 3.7.

then ask about the multiplicity distribution, $\hat{P}(N_\Delta)$, of events with N_Δ values of $\Delta\ell \leq \Delta$. We find a binomial distribution with the mean Np and variance $Np(1-p)$ where $p = \int_0^\Delta dx P_\ell(x)$ as expected from uncorrelated dipoles. We have also investigated the average number of $\Delta\ell$-values, which are consecutive and satisfy $\Delta\ell \leq \Delta$. We find a geometric distribution, weighted with the average number of $\Delta\ell$ not fulfilling the condition (which is, once again, expected when we have uncorrelated dipoles). We also find that the distribution $P_{\ell n}$ obtained from the sum of the lengths of n consecutive $\Delta\ell$ is an n-fold convolution of the distribution P_ℓ.

The corresponding results in PYTHIA are very similar to the results in ARIADNE (with the appropriate choice of the constant C as discussed above). To the left in Fig. 3.10 , we show the distributions from PYTHIA and note that PYTHIA is somewhat more concentrated towards small $\Delta\ell$ values and also has a somewhat wider tail so that the average values are the same as in ARIADNE. The "incoherent" option gives a much more narrow distribution centred around smaller values, as expected.

It is also possible to investigate the distributions in terms of the λ-measure defined in Eq. (3.19). In Fig. 3.10 to the right, we show two distributions (one from ARIADNE and one from PYTHIA), to be called $P_\lambda(\Delta\lambda)$ using as before $2m_0 = k_\perp = CQ$ where m_0 is the argument of the λ-measure. Once again we

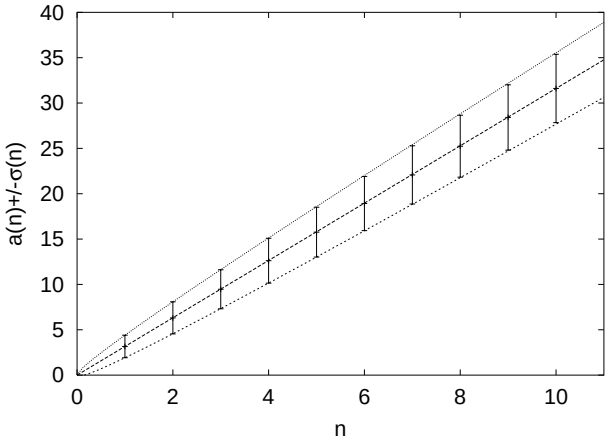

Figure 3.9: The figure shows the average $\Delta\ell$ (and the standard deviations around it) for chains of n connected $\Delta\ell$ called $a(n)$ ($a(n) \equiv \langle \sum_{j=1}^{n} \Delta\ell_j \rangle$). The statistics is collected from events with a fixed number of gluons.

find the same properties as for the distributions $P_\ell(\Delta\ell)$.

We conclude that, inside the whole region relevant to the hadronisation procedure in String Fragmentation, the partonic states are dominated by this structure of independent entities. It is tempting to consider them as a kind of collective variables for the QCD force fields. The $\Delta\ell$ variables represent the local size of the dipoles between adjacent parton energy–momentum vectors, whereas the $\Delta\lambda$ values correspond to a similar although more non-local property depending upon a set of adjacent vectors.

These properties of the distributions of $\Delta\ell$'s are properties of gluonic dipoles, and result from perturbative QCD. In the next section we will make models in the LLA and the MLLA schemes based on simple gain loss considerations on the dipole cascade model, and show that it is possible to understand many qualitative features of these distributions.

The $\Delta\lambda$'s on the other hand are complicated objects, and there is no obvious way to calculate their distributions except by relying on the similarity between the λ-measure and ℓ. But the fact that there are as many $\Delta\lambda$'s as $\Delta\ell$'s, and the $\Delta\lambda$'s have parallels for each of the properties of the $\Delta\ell$'s discussed here, lead us to introduce the notion of Generalised Dipoles (GD) to be the "source" of the contributions to the $\Delta\lambda_j$'s. Whereas a dipole is spanned between two colour connected partons, a GD corresponds to one flat block or "plaquette" in the surface traced between the directrix and the $\mathcal{X}$-curve by the tangent to the $\mathcal{X}$-curve. Regularities in the properties of dipoles which are mirrored in the

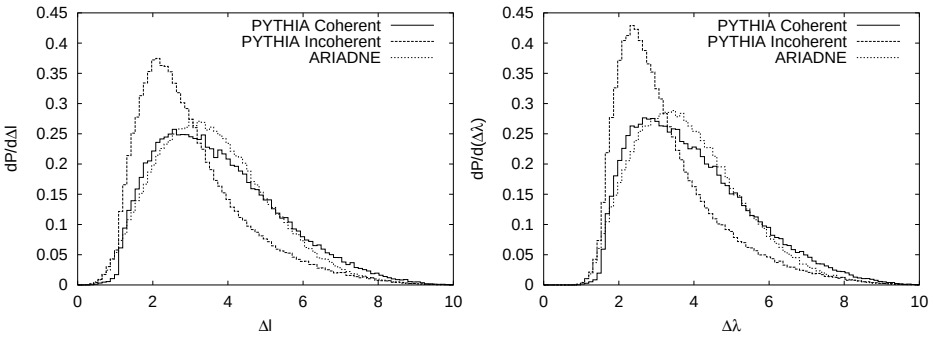

Figure 3.10: The figure to the left shows the $P_\ell(\Delta\ell)$-distribution from PYTHIA compared to the distribution obtained from ARIADNE. The figure to the right shows the corresponding plot for the $P_\lambda(\Delta\lambda)$ distribution.

GD's would be passed on to the hadronised state in a hadronisation scheme based on the λ-measure, such as the one introduced in [8].

3.4 Models to Describe the Dipole Distributions

3.4.1 A Simple Cascade Model

Multiplicity distributions were presented in the parton cascade formalism in [14] and in the dipole cascade formalism in [15] to leading logarithmic order. In this paper we will follow the approach presented in [16].

In order to provide a theoretical framework for our findings in the previous section, we will consider an analytical model for a dipole cascade. We will assume that there is a distribution, $f(\mu,\kappa)d\mu$, that describes the dipoles with size μ at the scale $\kappa \equiv \ln(k_\perp^2/\Lambda^2)$ (where $k_\perp$ is the ordering variable and $\mu \equiv \ln(M_d^2/k_\perp^2)$, in terms of the dipole masses M_d). We will consider the change in f when we make a small change in the scale κ. We note that $\mu+\kappa = ln\frac{M_d^2}{\Lambda^2}$ is independent of κ. If dipoles never decayed, the distribution $f(\mu,\kappa)$ would not change if $\mu+\kappa$ is kept constant as κ varies. Therefore any change in the distribution along the lines $\mu+\kappa = constant$ must purely come from decays.

There are two contributions to this. A dipole of size μ may decay into two smaller dipoles. A dipole of size bigger than μ may decay such that one of the daughter dipoles is of size μ. Gathering these terms together we get a partial integro-differential equation, cf. [16, 17], based upon Eq. 3.1 with $\alpha_{\text{eff}} = \frac{\alpha_0}{\kappa}$

for gluonic dipoles ($\alpha_0 = \frac{6}{11-2N_f/N_c}$):

$$Df \equiv \frac{\partial f}{\partial \kappa} - \frac{\partial f}{\partial \mu} = \frac{\alpha_0}{\kappa}\left[\mu f(\mu,\kappa) - 2\int_\mu d\mu' f(\mu',\kappa)\right] \tag{3.22}$$

The factor of 2 in the contribution from the larger dipoles stems from the fact that we are only considering "central" or purely gluonic dipoles here. When a gluonic dipole decays, there are 2 equivalent ways to obtain a gluonic dipole of size μ.

This integro-differential equation can be made into two coupled differential equations in terms of the first two moments of f, N_1 and N_2

$$\begin{aligned} N_j(\mu,\kappa) &= \int_\mu d\mu_1 (\mu_1)^{j-1} f(\mu_1,\kappa) \\ DN_1 &= -\frac{\alpha_0}{\kappa}(N_2 - 2\mu N_1) \\ DN_2 &= -N_1 + \frac{\alpha_0}{\kappa}\mu^2 N_1 \end{aligned} \tag{3.23}$$

For the normalisation we note that $N_1(0,\kappa)$ is the total number of dipoles available at the scale κ, to be called $\bar{n}$ in this section. $N_2(0,\kappa)$ is their combined length, to be called $\bar{\ell}$. The equations for these quantities can be obtained directly from Eqs. (3.23) in the LLA-scheme:

$$\begin{aligned} \frac{d\bar{n}}{d\kappa} &= -\frac{\alpha_0}{\kappa}\bar{\ell} \\ \frac{d\bar{\ell}}{d\kappa} &= -\bar{n} \end{aligned} \tag{3.24}$$

These equations are solvable in terms of combinations of the modified Bessel functions (cf. the next subsection) as soon as we have defined a "starting value", $\kappa_{max} \equiv L_0$, for the cascade.

In order to solve the coupled equations in Eq. (3.23), we introduce the combination $g(\mu,\kappa) = N_2 - \mu N_1$, which fulfils the equation:

$$Dg = \frac{\alpha_0}{\kappa}(\mu g) \tag{3.25}$$

with the boundary value

$$g(0,x) = \bar{\ell}(x) \tag{3.26}$$

It is related to N_1 through $N_1(\mu,\kappa) = -\frac{\partial}{\partial\mu}g(\mu,\kappa)$.

Including the boundary condition above, we obtain:

$$N_1(\mu,\kappa) = -\frac{\partial}{\partial\mu}\left\{\bar{\ell}(\mu+\kappa)\exp\left[-\int_\kappa^{\mu+\kappa} dy \frac{\alpha_0}{y}(\mu+\kappa-y)\right]\right\} \tag{3.27}$$

This is a derivative of two contributing factors. The first is $\bar{\ell}$ evaluated at $\mu+\kappa \equiv \ln(M_d^2/\Lambda^2)$, i.e. at the largest κ value where the dipole could have been produced. It is multiplied by the probability that the dipole has not decayed until κ. In field theoretical language this second contribution, the Sudakov form factor, corresponds to the sum of all the virtual corrections during the "lifetime" of the dipole. This Sudakov form factor can be easily calculated

$$S(\mu,\kappa) = \exp\left[-\int_\kappa^{\mu+\kappa} dy \frac{\alpha_0}{y}(\mu+\kappa-y)\right] = \frac{\exp(\alpha_0\mu)}{(1+\frac{\mu}{\kappa})^{\alpha_0(\mu+\kappa)}} \quad (3.28)$$

It fulfils

$$\begin{aligned} S(0,\kappa) &= 1 \\ \frac{\partial S}{\partial \mu}(\mu,\kappa) &= -\alpha_0 \ln(1+\frac{\mu}{\kappa}) S \end{aligned} \quad (3.29)$$

The derivative vanishes at $\mu = 0$.

The distribution f is obtained by a partial differentiation of N_1, cf. Eq. (3.23)

$$f(\mu,\kappa) = -\frac{\partial N_1}{\partial \mu} \quad (3.30)$$

so that using Eqs. (3.24), (3.27) and (3.29) we obtain:

$$\begin{aligned} f(\mu,\kappa) = {} & [\bar{\ell}(L_0,\mu+\kappa)\alpha_0 \ln(1+\mu/\kappa)^2 + \\ & 2\bar{n}(L_0,\mu+\kappa)\alpha_0 \ln(1+\mu/\kappa)] S(\mu,\kappa) \end{aligned} \quad (3.31)$$

The result can be understood in a simple and useful way. The logarithmic factors in the parenthesis are equal to

$$\alpha_0 \ln(1+\mu/\kappa) = \int_\kappa^{\mu+\kappa} \frac{\alpha_0 dx}{x} \quad (3.32)$$

i.e. the probability that there will be a dipole breakup somewhere between $\mu+\kappa$, the largest virtuality where a dipole with size μ at κ can be produced, and κ, where it is found. There are two such factors multiplying all interior points in the dipoles at $\mu+\kappa$, counted by $\bar{\ell}(\mu+\kappa)$, and there is one factor multiplying twice the number of dipoles at $\mu+\kappa$ (because if there is already a dipole one can keep either its "left" side or its "right" side and produce the "other" side of the dipole with size μ by a breakup in between). Finally, the Sudakov form factor describes the probability that there is no decay affecting the existence of the dipole at κ.

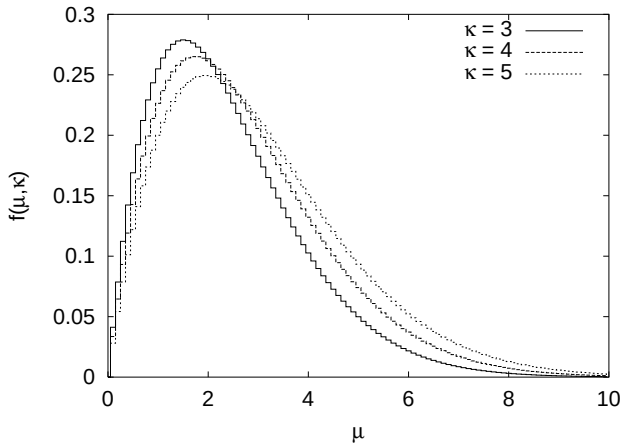

Figure 3.11: The $f_\kappa(\mu)$ function, obtained from Eq. 3.31, normalised to unity.

In the limit when $L_0 \gg (\mu + \kappa)$, and $\mu + \kappa$ is significantly positive, the two functions $\bar{n}$ and $\bar{\ell}$ factorise and we may write in the LLA

$$\begin{aligned} \bar{n}(L_0, x) &\simeq V(L_0)(x)^{-\frac{1}{4}} \exp(-2\sqrt{\alpha_0 x}) \\ \bar{\ell}(L_0, x) &\simeq \sqrt{x/\alpha_0}\bar{n}(L_0, x) \end{aligned} \tag{3.33}$$

In Fig. 3.11, we show the function $f_\kappa(\mu)$, obtained from f in Eq. (3.31) by normalising it to unity, for a set of values of the parameter κ. There is a weak dependence upon the ordering variable κ and for large μ-values it has an essentially exponential falloff with a slope very similar to the ones we find in the distributions $P_\ell(\Delta\ell)$ and $P_\lambda(\Delta\lambda)$ in Section 3.3.

For small values of μ there are quantitative differences. The reason is that the LLA is not sufficient to describe the behaviour of small dipoles. In that case it is necessary to include both the contributions from the $(\sum_p)$ term in the dipole cross section in Eq. (3.1), and also to take into account the recoil contributions which are particularly noticeable for small dipoles. We will consider this question in the next subsection.

3.4.2 The $MLLA$ and Earlier Investigations

In the so-called Modified Leading Log Approximation, subleading effects from the polaristaion sum are included [7, 18]. In general, the assumptions have been that the cms energy $\sqrt{s}$ (or rather its logarithm $L \equiv \ln(s/\Lambda^2)$) is very large and that the main contributions from the cascades will come from well-ordered emissions, i.e. that $k_{\perp j} \gg k_{\perp j+1}$ (at least for adjacent emissions).

Using this approximation, it is possible to write out analytical equations for the expected changes in the average ℓ (to be called $\bar{\ell}(\kappa)$) and the average n (similarly $\bar{n}(\kappa)$) for a given ordering variable $\kappa \equiv \ln(k_\perp^2/\Lambda^2)$ [7, 17, 18]:

$$\begin{aligned} \frac{d\bar{\ell}}{d\kappa} &= -\bar{n} \\ \frac{d\bar{n}}{d\kappa} &= -\alpha_{\text{eff}}\,(\bar{\ell} - \bar{n}\delta) \end{aligned} \tag{3.34}$$

Eqs. (3.34) are simplified versions of the Modified Leading Log Approximation (MLLA) formulae. A more elaborate treatment should include the difference between the quark and antiquark endpoint dipoles with a different effective coupling α and a different correction δ, cf. [18], but these are small corrections if the starting value $L = \ln(s/\Lambda^2)$ is large.

The interpretation is that in a step $d\kappa$, $\bar{\ell}$ changes by $\bar{n}$ contributions from the scale change according to Eq. (3.5), just like the second line in Eq. (3.24). Further, the change in $\bar{n}$ in that step is given by the coupling times the available phase space. This phase space is given by $\bar{\ell}$ to first approximation; but there is a correction from each dipole from the term $\sum_p$ in Eq. (3.1). The polarisation sum $\sum_p \simeq 2$ near the centre of a dipole but decreases in the neighbourhood of the emitters. It has been shown [18] that the suppression of emissions because of this can be approximated by (and this is essentially the MLLA) a constant decrease in the dipole size $\delta = 11/6$ for gluonic dipoles (this number only depends upon the triple gauge boson vertex for 3 colours). In Eqs. (3.34) it is also assumed that the gluon splitting process $g \to q\bar{q}$ is neglected and therefore $\alpha_{\text{eff}} \equiv \alpha_0/\kappa$ with $\alpha_0 = 6/11$ for all dipoles and not only the purely gluonic ones.

The decay of one dipole also affects the two adjacent ones due to recoils. A method to estimate this effect was suggested in [19]. Therefore an extra "loss-term" is added to the first line in Eq. (3.34):

$$\frac{d\bar{\ell}}{d\kappa} = -\bar{n} - C_r \frac{d\bar{n}}{d\kappa} \tag{3.35}$$

with a constant recoil correction estimated to be $C_r \simeq 2$. These equations can

be solved using the following combinations of the modified Bessel functions:

$$\begin{aligned} \mathcal{I}_1(x) &= \sqrt{2}x^{\gamma/2}I_\gamma(2\sqrt{\alpha_0 x}) \\ \mathcal{I}_2(x) &= \sqrt{2\alpha_0}x^{(\gamma-1)/2}I_{\gamma-1}(2\sqrt{\alpha_0 x}) \end{aligned} \tag{3.36}$$

and similarly for $\mathcal{K}_1$ and $\mathcal{K}_2$ in terms of the exponentially falling Bessel function K. Note that they are normalised so that

$$\mathcal{I}_1(x)\mathcal{K}_2(x) + \mathcal{I}_2(x)\mathcal{K}_1(x) = x^{\gamma-1} \tag{3.37}$$

and that there are simple differential relations between them:

$$\begin{aligned} \frac{d\mathcal{I}_1}{dx} &= \mathcal{I}_2(x) \\ \frac{d\mathcal{I}_2}{dx} &= \frac{\alpha_0}{x}\mathcal{I}_1(x) + \frac{(\gamma-1)}{x}\mathcal{I}_2(x) \end{aligned} \tag{3.38}$$

Similar relations hold for the exponentially falling modified Bessel function pair $(\mathcal{K}_1, -\mathcal{K}_2)$.

If we start the cascade at a large value of $L \equiv \ln(s/\Lambda^2) \gg \kappa$ we obtain, with the boundary values $\bar{\ell} = 0$ and $\bar{n} = 1$ at L, the results:

$$\begin{aligned} a &= L^{1-\gamma}\left[C_r\mathcal{K}_2(L) - \mathcal{K}_1(L)\right] \\ b &= L^{1-\gamma}\left[C_r\mathcal{I}_2(L) + \mathcal{I}_1(L)\right] \\ \bar{n} &= b\mathcal{K}_2(\kappa) - a\mathcal{I}_2(\kappa) \\ \bar{\ell} + C_r\bar{n} &= a\mathcal{I}_1(\kappa) + b\mathcal{K}_1(\kappa) \end{aligned} \tag{3.39}$$

using the notations $\gamma = 1 + \alpha_0(\delta + C_r)$.

It is difficult to obtain an anlytically solvable partial integro-differential equation corresponding to Eq. (3.22). The method of moments runs into difficulties because the variation in the $\sum_p$ term in the cross section (Eq. (3.1)) affects the integral contribution, i.e. the gain from the decays of larger dipoles, in such a way that the equations for the first few moments are no longer independent of higher moments. Therefore, we will directly go over to the solution in Eq. (3.31) instead, and modify the ingoing terms according to the MLLA, keeping in mind the interpretation given there.

We assume that each dipole of size μ can decay only in the interior excluding a region $\delta/2$ on each extreme. Then the effective phase space at $(\mu+\kappa)$ in Eq. (3.31) is changed from $\ell(\mu+\kappa)$ into $[\ell(\mu+\kappa) - \delta \cdot n(\mu+\kappa)]$. A dipole of size μ is produced by a breakup first at a point $\kappa = \kappa_1$ and then at $\kappa_2 < \kappa_1$. The region where the "no emission probability" is to be calculated in the Sudakov form factor is changed in the MLLA, first by a loss of $\delta/2$ at κ_1 and then by a

loss of a further $\delta/2$ at κ_2.

$$\begin{aligned} S_{\kappa_1,\kappa_2} &= \exp\left(-\int_{\kappa}^{\kappa_2}\frac{\alpha_0 dz(\mu+\kappa-\delta-z)}{z}\right)\times \\ &\quad \exp\left(-\int_{\kappa_2}^{\kappa_1}\frac{\alpha_0 dz(\mu+\kappa-\delta/2-z)}{z}\right)\times \\ &\quad \exp\left(-\int_{\kappa_1}^{\mu+\kappa}\frac{\alpha_0 dz(\mu+\kappa-z)}{z}\right)= \\ &\quad \left(\frac{\kappa_1\kappa_2}{\kappa^2}\right)^{\frac{\alpha_0\delta}{2}} S(\mu,\kappa) \end{aligned} \tag{3.40}$$

where $S(\mu,\kappa)$ is the Sudakov form factor without the term δ as given in Eq. (3.28). Since this is a function of κ_1 and κ_2 now, we obtain, for the contribution to $f(\mu,\kappa)$ from situations where both gluons involved in a dipole are emitted below $\mu+\kappa$, the result:

$$\begin{aligned} f_1 &\equiv 2(\bar{\ell}-\delta\bar{n})(\mu+\kappa)\int_{\kappa}^{\mu+\kappa}\frac{\alpha_0 d\kappa_1}{\kappa_1}\int_{\kappa}^{\kappa_1}\frac{\alpha_0 d\kappa_2}{\kappa_2}S_{\kappa_1,\kappa_2} \\ &= (\bar{\ell}-\delta\bar{n})(\mu+\kappa)\frac{4\left((1+\mu/\kappa)^{\frac{\alpha_0\delta}{2}}-1\right)^2}{\delta^2}S(\mu,\kappa) \end{aligned} \tag{3.41}$$

The fact that the first break may be either on the "left" or on the "right" side contributes a factor of 2 in the above equation .

In the same way, for the second contribution related to the number of dipoles at $\mu+\kappa$, ie the situations where only one gluon involved in a dipole is produced below the scale $\mu+\kappa$, we obtain,

$$f_2 = \theta(\mu-\delta/2)\bar{n}(\mu+\kappa)\frac{4\left((1+(\mu-\delta/2)/\kappa)^{\frac{\alpha_0\delta}{2}}-1\right)}{\delta}S(\mu-\delta/2,\kappa) \tag{3.42}$$

In this case there can never be a breakup until the dipole size has at least reached $\delta/2$, because one of the end points is already fixed at the virtuality $\mu+\kappa$.

We note for consistency that the result $f_\delta \equiv f_1+f_2$ has the limit f in Eq. (3.31) when δ vanishes. In Fig. 3.12, we show the result of this $MLLA$ version of the dipole size distribution. We have used a fixed value $\delta = 11/6$ but we have allowed the parameters α_0 and C_r vary. The reason for allowing α_0 to vary is that it is feasible to shut off the gluon splitting process in ARIADNE, but the running coupling will always receive contributions from the different number of "active" flavours at different virtualities. From the figure to the left, we conclude that it is in between the distributions from ARIADNE and PYTHIA for the central dipoles when we use $\alpha_0 = 0.70$ (i.e. for three to four active

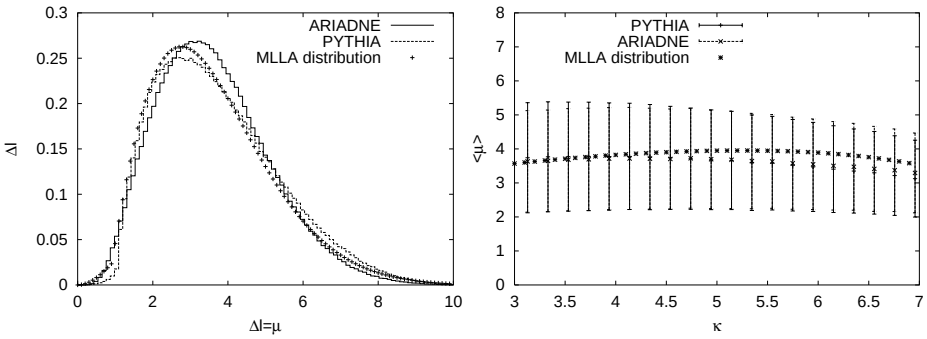

Figure 3.12: The figure to the left shows the distribution $f_\delta(\mu, \kappa)$, obtained from the MLLA approach at $k_\perp$ =1GeV, compared with the $P_\ell(\Delta\ell)$ distribution from ARIADNE and PYTHIA (cf. Fig. 3.10). The figure to the right shows the average value of μ as a function of κ, from the same distribution $f_\delta(\mu, \kappa)$. In the figure to the right, we also compare with the average value of ℓ (cf. Eq. (3.21)) as a function of κ obtained from ARIADNE and PYTHIA, and we also include the standard deviation in the result from PYTHIA and ARIADNE. This result is obtained using $\alpha_0 = 0.7$ and $C_r = 2$ in the MLLA distribution as explained in the text.

flavours), and $C_r = 2$ (according to [19]). This result is rather insensitive to C_r and it can therefore not be used as a test for the claims in [19]. We have also checked the dependence upon the ordering variable. In Fig. 3.12 to the right, we show that f_δ also exhibits a slow change of its average value as a function of the (relevant) ordering variable like the ARIADNE and PYTHIA P_ℓ distributions.

3.5 Concluding Remarks

The number of gluons emitted *above* a certain value of the ordering variable shows an interesting linear correlation (with gaussian fluctuations) with the phase space available at that scale. We have called the phase space variable the ℓ-measure in this paper to distinguish it from the λ-measure, which is an infrared stable generalisation of the ℓ-measure, useful in the context of hadronisation.

Both these quantities are functions of not only the resolution scale ($k_{\perp cut}$ for a dipole cascade, Γ_0 in string fragmentation), but also of the precise geometry of the state under consideration. Therefore they change with every new gluon

emitted in the system.

The resolution parameter relevant for hadronisation is a parameter fixed by the break-up properties of the string and the mass spectrum of the hadrons produced. The λ-measure is constructed in such a way that addition of gluons at transverse momenta much smaller than the scale Γ_0 does not change its value. In that way it is infrared stable.

However, since the resolution parameter for the ℓ-measure is the transverse momentum of the gluon to be emitted, the transverse momenta of all gluons already emitted must be higher in an ordered dipole cascade. Therefore, the only kind of infrared stability relevant for this measure would be the stability, when the ordering variable, which is also the resolution parameter, is small. Technically this is not the case. However, since in this approach we will never compute phase space available at a value of the ordering variable below the Λ_{QCD}, there is an effective infrared stability for the phase space, if all local transverse momenta k_{tj} are required to be above $k_\perp$. It is easily shown that the mass of any dipole with a gluon at one end is greater than the transverse momentum k_t of that gluon, which in turn, will be greater than Λ_{QCD}. Besides, we must remember that it is kinematically not possible for dipoles of mass smaller than $2\Lambda_{QCD}$ to emit gluons above Λ_{QCD}.

The two measures discussed here are quite strongly related. If one keeps only the last (often the dominant) term in the argument of the logarithm in the λ-measure, one gets an expression very similar to the ℓ-measure.

The linear correlation between the ℓ-measure and the number of gluons is a direct consequence of the following facts that we have demonstrated. The ℓ-measure is the sum of a series of terms $\Delta\ell_j$, one for each dipole. A given $\Delta\ell_j$ is the contribution from one particular dipole to the ℓ-measure, and is in some sense the "size" of that dipole. There are two kinds of dipoles. The first kind involves either the quark or the antiquark energy–momentum. The second kind involves only the gluon energy–momenta. These two kinds of dipoles have different distributions in sizes.

It turns out that the size of the dipoles do not show any significant correlations. Therefore the ℓ-measure of a state consisting of a certain number of dipoles, which is just the sum of the corresponding $\Delta\ell_j$'s, is distributed like the sum of several independent random variables, i.e. like a gaussian with a mean that is the sum of the means of the individual independent distributions. This shows up as a linear correlation between the number of partons and the ℓ-measure.

More interesting than the linear relation is the stability of the slope of these lines, which represents the number of gluons per unit phase space, with respect to changes in global event parameters like cms energy or thrust and even with changes in the ordering variable. It seems that parton cascades tend

to form structures at one (relative) size when sizes are measured with the ℓ-measure with a resolution parameter proportional to the ordering variable. As we go down in the ordering variable, the running coupling should increase the number of emissions per unit phase space. However, the phase space variable itself scales appropriately to effectively absorb any increase of emissions per unit phase space.

We have also made another observation in this paper. Just like the ℓ-measure, the λ-measure can be thought of as a sum of terms $\Delta\lambda_j$, one for each vector along the directrix in colour order. Out of the two vectors involved in a particular $\Delta\lambda_j$, only one is a vector along the directrix. The other vector, in a sense a cumulative variable, is a weighted average of the vectors k_i's along the directrix with $i < j$.

It is interesting that all the properties of the ℓ-measure we have discussed here are also reflected in the λ-measure. There is a similar linear correlation to the number of gluons, similar lack of correlation among adjacent terms and similar stability with respect to change of global event variables and the ordering variable. Partitioning the λ-measure into a series of $\Delta\lambda_j$'s corresponds to partitioning the surface spanned between the directrix and the $\mathcal{X}$-curve into a series of "plaquettes" or flat regions along the directrix. Each plaquette is spanned between a parton energy momentum vector k_j, a vector q_{Tj-1} (weighted average of k_i's along the directrix with $i < j$), another vector q_{Tj} and a hyperbolic section of the $\mathcal{X}$-curve. The size of the plaquette $\Delta\lambda_j$ is the length of the section of the $\mathcal{X}$-curve, and is determined by k_j and q_{Tj-1}. Since these plaquettes share so many properties with dipoles, we will call them "Generalised Dipoles".

We note in passing that the possibility of partitioning the contributions to the λ-measure as contributions from connected flat regions has an interesting consequence for the fragmentation of a string according to the Lund model area law. When formulated as a process along the directrix [8, 21], string fragmentation is closely related to the λ-measure and the $\mathcal{X}$-curve. Particle production in this scheme can be thought of as partitioning the plaquettes mentioned here into smaller plaquettes, one for each hadron. Since the hadron energy–momenta will mostly come from these flat regions in the string, particles stemming from one GD will have energy–momenta aligned in a plane in Minkowski space, up to transverse momentum fluctuations. We have found such chains of particles and examined their properties. These chains, which we will call "coherence chains" are important for the study of Bose Einstein correlations in the Lund Model for multigluon systems, which we will elaborate on in a forthcoming publication.

We have also presented here an analytical model for the observations we have made about dipoles, in the LLA and MLLA schemes. There are limitations to this approach, since complications such as the polarisation sum make it very difficult to obtain differential equations which can be solved analytically.

Nevertheless, our analysis based on simple gain-loss considerations broadly reproduces the qualitative features of the observations.

Acknowledgements

We would like to thank G. Gustafson, T. Sjöstrand and L. Lönnblad for helpful discussions. This work was completed by S. Mohanty and F. Söderberg, about two months after the untimely death of our collaborator Bo Andersson.

References

[1] G. Gustafson, U. Pettersson *Nucl. Phys.* **B306** (1988) 746.

[2] L. Lönnblad, *Computer Phys. Commun.* **71** (1992) 15.

[3] G. Corcella, I.G. Knowles, G. Marchesini, S. Moretti, K. Odagiri, P. Richardson, M.H. Seymour and B.R. Webber *J. High Energy Phys.* **0101** (2001) 010.

[4] T. Sjöstrand, P. Edén, C. Friberg, L. Lönnblad, G. Miu, S. Mrenna and E. Norrbin, *Computer Phys. Commun.* **135** (2001) 238.

[5] X. Artru, *Phys. Rept.* **97** (1983) 147.

[6] B. Andersson, G. Gustafson and B. Söderberg, *Z. Phys.* **C20** (1983) 317.

[7] Yu.L. Dokshitzer, V.A. Khoze, A.H. Mueller and S.I. Troyan, Basics of Perturbative QCD (Edition Frontières 1991).

[8] B. Andersson, S. Mohanty and F. Söderberg, *Eur. Phys. J.* **C21** (2001) 631.

[9] B. Andersson, G. Gustafson, P. Dahlqvist, *Nucl. Phys.* **B328** (1989) 76.

[10] G. Gustafson and A. Nilsson, *Z. Phys.* **C52** (1991) 553.

[11] Ya.I. Azimov et al. *Phys. Lett.* **B165** (1985) 147.

[12] L. Lönnblad, hep-ph/0112284.

[13] B. Andersson, P. Dahlqvist and G. Gustafson, *Z. Phys.* **C44** (1989) 455; *Z. Phys.* **C44** (1989) 461.

[14] Yu.L. Dokshitzer, V.S. Fadin, V.A. Khoze, *Z. Phys.* **C15** (1982) 325; A. Bassetto, M. Ciafaloni, G. Marchesini, A.H. Mueller, *Nucl. Phys.* **B207** (1982) 189.

[15] B. Andersson, P. Dahlqvist and G. Gustafson, *Phys. Lett.* **B214** (1988) 604.

[16] B. Andersson , *Nucl. Phys.* **B360** (1991) 109.

[17] B. Andersson, The Lund Model, (Cambridge University Press 1998).

[18] G. Gustafson, *Nucl. Phys.* **B392** (1993) 251; G. Gustafson, M. Olsson, *Nucl. Phys.* **B406** (1993) 293.

[19] P. Edén, G. Gustafson, *J. High Energy Phys.* **09** (1998) 015.

[20] B. Andersson, Closing talk for the XXXI International Symposium on Multiparticle Dynamics, Datong, China, Sep 2001.

[21] B. Andersson, *Acta Phys. Polonica B* **32** (2001) 3993.

Coherence Chains and Bose-Einstein Correlations in the Lund Model

Paper IV

LU TP 03-08
March 2003

Coherence Chains and Bose-Einstein Correlations in the Lund Model

Sandipan Mohanty[1]
Fredrik Söderberg[2]
Department of Theoretical Physics, Lund University.
Sölvegatan 14A, S-223 62 Lund, Sweden.

Abstract We extend an interference based approach for the analysis of Bose-Einstein Correlations in the Lund model to incorporate an approximate treatment of the correlations for general multigluon states.

[1]sandipan@thep.lu.se
[2]fredrik@thep.lu.se

4.1 Introduction

The fragmentation process in which the coloured partons are transformed into colourless hadrons is not understood from first principles, and therefore we have to rely on models for a description. The Lund string fragmentation model [1, 2, 3] is one such model, in which the dynamics of colour connected partons is modelled by proposing a string-like force field between a quark and an antiquark with the emitted gluons as internal excitations along the string field. The probability for the formation of a set of hadrons from a given set of partons is given by what is known as the area law. The model can be formulated as a stochastic iterative process, and is therefore well suited for a Monte Carlo implementation. One such implementation is the well-known PYTHIA event generator [4].

For a state without gluons, the surface spanned by the string in space-time will be a (1+1)-dimensional plane. In general, for a multigluon string the surface will be a curved (1+1)-dimensional surface embedded in (1+3) dimensions. Calculating the energy-momenta of the hadrons according to the area law is rather difficult in this case. PYTHIA handles multigluon states according to the method presented in [5]. It has been found that this procedure fulfils the area law in an average sense but not on an event to event basis.

We have presented a paper [6] where we introduced a model for fragmenting a multigluon state, which fulfils the area law at every single step, at the price of small fluctuations introduced into the string state during hadronisation. The ideas presented in [6] have been developed and implemented in a Monte Carlo fragmentation program called ALFS [7]. In particular the effect of limited phase space for small cms energies have been introduced "effectively" through an energy dependent fragmentation function which differs for small invariant masses from the standard Lund model formula used in PYTHIA.

In the first part of this paper (section 4.4), we will make use of ALFS to study a set of properties of the hadronic state that are noticeable already in the analysis of the perturbative QCD parton cascades as we presented them in [8]. We learned that the multigluon states obtained from the parton cascades can be subdivided into a set of independent entities, that we called Generalised Dipoles (GDs) in [8]. The GDs are linked together along the colour field and they have certain properties which are independent of the total energy and global event variables such as thrust. Moreover, the sizes of the GDs relative to the cut-off scale (used to define the end of the partonic cascades) is remarkably stable against changes in the cut-off scale. In the first part of this paper, we will show that it is possible to define a set of corresponding quantities from the fragmentation process which we will call Coherence Chains (CC). In the second part of the paper we will use the idea of Coherence Chains to formulate a model for Bose-Einstein correlations for general multigluon states.

The CCs are defined by the property that, up to small transverse momen-

tum fluctuations, the particle energy-momenta all belong to a plane, just as the particles stemming from the fragmentation of a simple string state without any interior gluonic excitations. In other words, we will show that the fragmentation of a multigluon state in our model resembles the linked fragmentation of many planar string regions.

In order to study the qualitative properties of CCs we will assume one common mass for all kinds of hadrons. In the applications in the second part of the paper, we will naturally include the full mass spectrum and the decay of resonances.

We will show that the hadron multiplicity distributions from the Coherence Chains, for a maximum allowed transverse momentum, are independent of the total energy and of global event variables such as thrust. We find that the only difference between the events is the occurrence of a different number of CCs. The number of Coherence Chains in an event depends upon the so-called λ-measure that was introduced in [9, 10] to describe the phase space available for hadron formation in multigluon states. The larger the energy and/or the gluonic activity, the larger is the available range of the λ-measure and the number of CCs.

In the second part of this paper, we will use the CCs to introduce a model for Bose-Einstein correlations in multigluon events. This model is a generalisation of the investigation in [11, 12], in which the Bose-Einstein effect for string states without gluons were studied. The Lund model is based on semi-classical approximations and classical probability concepts. This ignores possible interference effects due to the underlying quantum mechanical processes. In [11, 12] an amplitude was introduced that reproduces the area law and also gives rise to interference effects when there are identical bosons in the final state. The origin of the interference effect is the fact that identical hadronic states can be obtained with the hadrons ordered in different ways along the string. We will call these different "configurations" and they will give separate contributions to the production amplitude for this hadron state. The resulting interference effect was introduced in the Monte Carlo by an event weight.

It turns out that symmetrisation of the final state emerging out of the fragmentation of a string with gluonic excitations is much more complicated than for systems without gluons. We will make use of the proposed form for the matrix element in [11, 12] in our approach, and we will also use the concept of an event weight.

In this case, there are severe constraints which limit the alternative configurations of identical particles in the final state, allowed by the string fragmentation model. Configurations which correspond to the exchange of two particles produced in two different planar regions of the string, are either impossible or highly suppressed. This Bose-Einstein correlation model will only take into account exchange of particles in the same planar region.

As we will show in the first part of the paper, an event can be subdivided into a set of Coherence Chains, where all momenta of the particles are nearly aligned in a plane, and this partitioning of the event is insensitive to very soft gluons. The Coherence Chains therefore describe the string regions over which interference effects between identical particles would be considered.

We will develop this scheme in the second part of this paper and show that the CCs stemming from the Generalised Dipoles in coherent perturbative cascades are sufficiently large so that the ensuing distributions show an enhancement for the probability for small momentum differences between identical bosons. We will be satisfied with a study of the hadronisation properties of events stemming from e^+e^--annihilation and the ensuing bremsstrahlung, defined by the perturbative QCD cascades.

In subsection 4.2, we will briefly describe the features of the fragmentation of the multigluon states according to [6, 7] and in subsection 4.3 the properties of the Generalised Dipoles according to [8]. In section 4.4, we will define the Coherence Chains and exhibit their properties. In section 4.6, we introduce our BEC model based upon the Coherence Chains and study the correlations arising among the identical pions. We end with a set of concluding remarks in section 4.7.

PART I: Introduction to Coherence Chains

4.2 The Lund Area Law Applied to Multigluon States

In the Lund string model a colour flux tube is assumed to stretch between the partons at the end of the parton cascades. This colour field is approximated by a massless relativistic string with a constant energy-density [1, 2, 3].

When a quark and an antiquark move apart, they are assumed to stretch a string-like field between them. Consequently, they will lose energy to the string. After a given time, they lose all their energy and are pulled back towards each other. The ensuing motion is periodic.

If the energy stored in the string is large enough, formation of $q\bar{q}$-pairs along the string becomes possible and the string will break into smaller string pieces. A q from one such break-up point ("vertex") together with a $\bar{q}$ from an adjacent vertex along the string field form a hadron (on mass shell) composed of the pair and the field in between. Transverse momentum is generated at these string break-up vertices as described in [13]. The energy-momentum contained in the string piece between the two adjacent vertices and the transverse momenta carried by the quark and the antiquark add to make the energy-momentum of the particle formed.

Therefore, the hadronisation process can be modelled by a break-up of the original string into smaller string pieces, each describing a hadron with a given energy-momentum. The probability for the production of a set of n hadrons with energy-momenta $\{p_\alpha\}$ with total energy-momentum P_{tot} is given by the area law [1, 2, 3]:

$$dP_n(\{p_\alpha\}; P_{tot}) \propto \tag{4.1}$$
$$\propto N_n \prod_{\alpha=0}^{n-1} d^4p_\alpha \delta(p_\alpha^2 - m_\alpha^2) \delta(\sum_{\alpha'=0}^{n-1} p_{\alpha'} - P_{\rm tot}) \exp(-bA) \exp(-\frac{1}{2\sigma^2} \sum_{\beta=0}^{n} k_{\perp\beta}^2)$$

Here A is the area spanned by the string before it decays, and $k_{\perp\alpha}$ are the transverse momenta generated at the vertices where the string breaks. (We assume that transverse momentum is conserved at any breakup. A model where transverse momentum is only conserved within a finite range in rapidity was discussed in [18].) In order to describe the break-up of a string with internal gluonic excitations, it will be useful to consider string motion in a little more detail.

The surface spanned by a string (which does not break) during one period is a minimal surface which means that the surface is completely determined by its boundary curve. This boundary curve, a four-vector valued curve $\mathcal{A}$, is usually called the directrix. The position of an arbitrary point $X(t, \sigma)$ on the surface of the string (open string; parametrised by time t and the energy σ between the quark end point and the point X) is related to the directrix $\mathcal{A}(t)$ in the following way.

$$X(t, \sigma) = \frac{1}{2} [\mathcal{A}(t + \sigma) + \mathcal{A}(t - \sigma)] \tag{4.2}$$

The function $\mathcal{A}(t)$ has the following periodicity and symmetry properties for a string which starts at a single point at time $t = 0$:

$$\begin{aligned} \mathcal{A}(t + 2E) &= \mathcal{A}(t) + 2P_{\rm tot} \\ \mathcal{A}(-t) &= -\mathcal{A}(t) \end{aligned} \tag{4.3}$$

We see from Eq.(4.2) and Eq.(4.3) that the string surface is described by a left moving and a right moving wave, which bounce at the endpoints. The directrix of a string stretched between a certain set of partons is obtained by laying out the energy-momenta of the quark, the gluons and the antiquark in colour order.

The minimal area nature of the string world surface also means that properties of hadrons created during string fragmentation are stable against small perturbations on the boundary, i.e. that the model is infrared stable.

We have recently derived a process for fragmenting a multigluon string state into final state hadrons in accordance with the Lund model area law [6]. As

the directrix completely determines the string state we have chosen to present the fragmentation of a multigluon string state as a process along the directrix.

In the case of a flat string, the Lund fragmentation process typically results in a state like the one drawn in Fig.4.1 to the left. This figure shows the vertices where new $q\bar{q}$-pairs are produced and the corresponding vertex vectors $\{x_\alpha\}$. The momenta of the produced hadrons, $\{p_\alpha\}$, are also shown in this figure. This process can be formulated in terms of the directrix in a way which can be generalised to strings spanned by gluons.

In [6], we defined an iterative process along the directrix to describe string fragmentation. We defined (abstract) dynamical variables called "vertex vectors" x_α. These variables would correspond to true space-time locations for production of quark antiquark pairs if the string had no gluonic excitations. Each particle energy-momentum vector p_α is constructed as a linear combination of a vertex vector x_α and a certain section of the directrix k_α. The same pair of vectors x_α and k_α also determines the next vertex vector $x_{\alpha+1}$.

$$\begin{aligned} p_\alpha &= z_\alpha x_\alpha + \frac{1}{2}\left(1 - \frac{z_\alpha^2 x_\alpha^2}{m_\alpha^2}\right) k_\alpha \\ x_{\alpha+1} &= (1-z_\alpha) x_\alpha + \frac{1}{2}\left(1 + \frac{z_\alpha^2 x_\alpha^2}{m_\alpha^2}\right) k_\alpha \end{aligned} \tag{4.4}$$

Since with this construction, $x_\alpha + k_\alpha = p_\alpha + x_{\alpha+1}$, we associate a "plaquette" bounded by these four vectors with the particle indexed α, cf. Fig.4.1 to the right. Each of the vectors x_α is shared between two plaquettes, and hence production of a set of hadrons from a given string or directrix means construction of a set of connected plaquettes along the directrix in this model. The initial value x_0, for the series of vertex vectors, is taken to be the first segment of the directrix. The numbers z_α are related to the area of the plaquettes, and are required to be distributed according to the following distribution, in order that the construction of plaquettes would be weighted according to the area law:

$$f(z)dz = N\frac{dz}{z}(1-z)^a \exp\left(-\frac{bm^2}{z}\right) \tag{4.5}$$

After the selection of z_α and hence a properly distributed area for the plaquette, the size of k_α is chosen so that the plaquette does indeed have that area.

The distribution in Eq.(4.5) is called the Lund symmetric fragmentation function. It can be derived from the area law in Eq.(4.1) in the limit of large center of mass energies. The effective fragmentation function, which is used in ALFS, is however energy dependent, and reduces to the above in the limit of large energies [7].

There is a one-to-one correspondence between the areas of the plaquettes constructed in this way and certain areas which can be associated with the

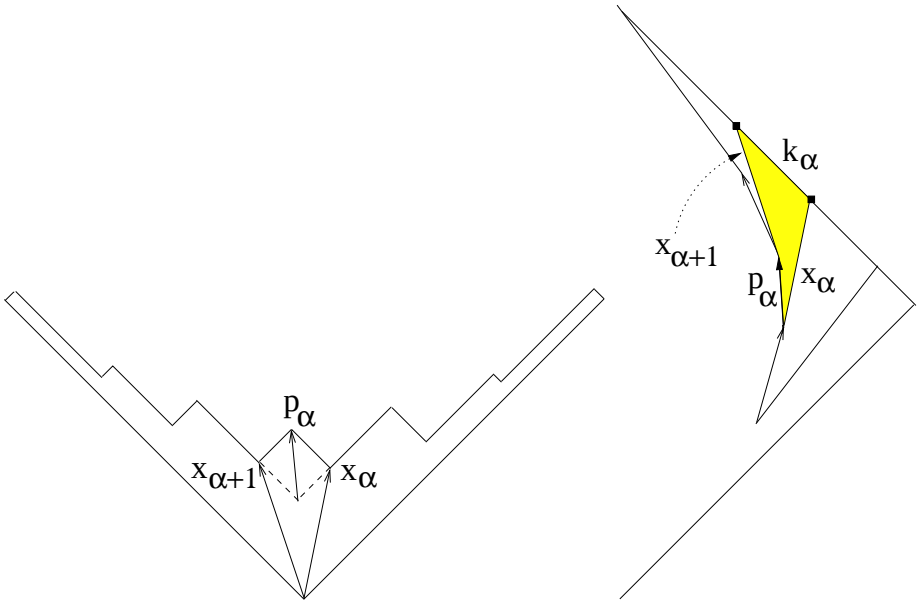

Figure 4.1: The figure to the left shows a typical Lund string break-up for a string state without gluons. The figure to the right shows the corresponding plaquette bordered by x_α, $x_{\alpha+1}$, p_α and a segment from the directrix k_α, as described in the text.

production of individual hadrons in the string fragmentation model without gluonic excitations. Therefore, the sum of the areas of the plaquettes which is also the area between the directrix and the "hadronic curve"[3], i.e. the curve obtained by placing the hadron energy-momenta one after the other in rank order, could be used as the area in the Lund model area law. Therefore, the area law on the whole event can be implemented by weighting the construction of each plaquette according to its area, which amounts to choosing the variables "z_α" in Eq.(4.4) according to the Lund symmetric fragmentation function and selecting k_α's of the appropriate sizes.

In connection with the plaquette building process in Eq.(4.4) one observes that the vertex vectors contain a memory of the earlier partonic energy-momenta in the iteration process, and hence along the directrix.

The gluon corners pose a problem because the generated z_α value implies a value of the area of the plaquette which does not fit in the space between the hadronic curve and the directrix around the gluon corner. In [6], we solved

[3]The hadronic curve was called the X-curve in [6]

this problem by modifying the directrix locally around the gluon corners. We found that the required distortions of the directrix only have small and local implications on the string state because the string surface is a minimal surface.

The model described above is implemented in the Monte Carlo simulation program ALFS [7] and we will make use of this program in the investigations of the Coherence Chains in section (4.4). We will come back to the hadronisation process in subsection 4.4, but before that we will discuss some relevant properties of the parton cascades in the following subsection.

4.3 The Generalised Dipoles

The Generalised Dipoles were introduced in [8]. In this subsection, we will recapitulate the things we learned in this paper since there is a close resemblance between the Generalised Dipoles and the Coherence Chains defined later in this paper.

Two different phase space measures were discussed in [8], the λ-measure and the ℓ-measure. They are both strongly related to the Generalised Dipoles, but they were originally introduced for different purposes.

1. The quantity we called the ℓ-measure in [8] was introduced in [15]. In the dipole model, the available phase space for gluon emission, ℓ, in the Leading Log Approximation (LLA) [14] and in the Modified Leading Log Approximation (MLLA) [14] schemes is a sum of a series of terms, $(\Delta\ell)_\alpha$, one for each pair of colour-connected partons, i.e. each pair of consecutive vectors along the directrix [15]. These terms are contributions to the phase space from individual dipoles in the Dipole cascade model [15]. The phase space for the emission of a gluon with transverse momentum $k_\perp^2$, from a system of n_g gluons can be expressed as:

$$\ell \;=\; \sum_{\alpha=0}^{n_g} (\Delta\ell)_{\alpha,\alpha+1} = \sum_{\alpha=0}^{n_g} \ln\left(\frac{s_{\alpha,\alpha+1}}{k_\perp^2}\right) = \ln\prod_{\alpha=0}^{n_g}\left(\frac{s_{\alpha,\alpha+1}}{k_\perp^2}\right), \qquad (4.6)$$

   i.e. as a sum over the contributions from the partonic dipoles. $s_{\alpha,\alpha+1}$ is defined as $(\mathcal{A}_\alpha + \mathcal{A}_{\alpha+1})^2$.

2. The λ-measure was introduced in [9] as a generalised rapidity range for measuring the hadronic phase space. In [8] we noted that it can be subdivided into a set of parts called $\Delta\lambda$, which have certain interesting properties. Every $\Delta\lambda$ contribution is built up from one parton energy-momentum vector, $\mathcal{A}_{\alpha+1}$, and from one more abstract vector, $q_{T\alpha}$[4], according to the recursive

[4] The vector q_T was called q in the original paper [9]

formula below:

$$\lambda \equiv \sum_{\alpha=0}^{n_g} \Delta\lambda_\alpha = \sum_{\alpha=0}^{n_g} \ln\left(1 + \frac{q_{T\alpha}\mathcal{A}_{\alpha+1}}{m_0^2}\right) \tag{4.7}$$

$$\begin{aligned} q_{T\alpha+1} &= \gamma_{\alpha+1} q_{T\alpha} + \frac{1+\gamma_{\alpha+1}}{2}\mathcal{A}_{\alpha+1} \\ \gamma_{\alpha+1} &\equiv \frac{1}{1 + q_{T\alpha}\mathcal{A}_{\alpha+1}/m_0^2} \\ q_{T0} &= \mathcal{A}_q \end{aligned} \tag{4.8}$$

The λ-measure is infrared stable and it is insensitive to gluons with $k_\perp$ small compared to m_0. However, if the scale m_0 is smaller than the smallest $k_\perp$, then there is a close similarity between λ and ℓ. Thus we found in [8] that $\lambda(m_0 = \frac{1}{2}k_\perp) \approx \ell(k_\perp)$. We note that the $\Delta\ell$'s are contributions from the dipoles to the total measure while the $\Delta\lambda$'s are more abstract quantities.

In [8], we found that the $\Delta\ell$ and the $\Delta\lambda$ distributions have very interesting properties.

- The distribution $\frac{dP}{d(\Delta\ell)} \equiv P_\ell(\Delta\ell)$ is independent of the cms energy and of global event variables such as thrust and the total ℓ value. It is also independent of presence of particularly hard gluon emissions in the event.
- The distribution $P_\ell(\Delta\ell)$ is rather insensitive to the value of $k_\perp$.
- There are no correlations between adjacent $\Delta\ell$'s
- All the properties of the ℓ-measure are also reflected in the λ-measure. There are as many $\Delta\lambda$'s as $\Delta\ell$'s in an event. Therefore, just as $\Delta\ell$ measures the size of colour dipoles, we introduced the concept of Generalised Dipoles as the abstract entities whose size would be represented by $\Delta\lambda$.

It is possible to give a geometrical picture of the Generalised Dipoles. In the Lund string fragmentation model, for a string with no gluonic excitations, the hadrons are produced along a hyperbola [1, 2, 3] on the average. For a string with gluonic excitations, the hadrons are produced along a set of connected hyperbolae, called the χ-curve[5] in [8], along the directrix [9, 10]. The λ-measure is related to the length of the χ-curve and it is also proportional to the area spanned between the χ-curve and the directrix [9]. Subdividing the λ-measure according to Eq.(4.7) means that we subdivide this area into smaller "plaquettes" very similar to the ones that we defined in subsection 4.2. These

[5] The χ-curve was called the x-curve in the original paper [9]

plaquettes are bordered by q_{T_α} and $q_{T\alpha+1}$, a hyperbolic segment of the χ-curve and a parton energy-momentum vector from the directrix.

These properties of the GDs will have important implications for the fragmentation products of the string as we will see in the next section.

4.4 The Coherence Chains

In this section, we will define and examine the Coherence Chains (CC). For simplicity, we will use a single hadron mass in this study. The idea is to look for "planar" regions in the space of the final state particle energy-momenta.

4.4.1 The Definition of a Coherence Chain

Let us consider a final state, obtained from our fragmentation model, described by means of an X-curve containing the hadron energy-momenta $\{p_\alpha\}$ laid out in rank-order. By a "planar region" we will mean a rank-connected subset of hadron energy-momenta denoted $p_\ell, p_{\ell+1}, \ldots, p_{\ell+n-1}$ which can be written as a linear combination of an "initial" vertex vector x_ℓ and the sum of the corresponding directrix pieces $\{k_j\}$ together with a small transverse component $\delta(\ell,n)$, which satisfies $\delta \cdot x_\ell = \delta \cdot K = 0$:

$$\begin{aligned} K(\ell,n) &= \textstyle\sum_{j=\ell}^{\ell+n-1} k_j \\ P(\ell,n) \equiv \textstyle\sum_{j=\ell}^{\ell+n-1} p_j &= u(\ell,n)x_\ell + v(\ell,n)K(\ell,n) + \delta(\ell,n) \end{aligned} \tag{4.9}$$

Due to the facts that $P(\ell,n), K(\ell,n)$ and x_ℓ are time-like or light-like vectors the remainder $\delta(\ell,n)$ must be space-like (or vanishing). We define the set of rank-connected hadrons as a Coherence Chain of length n and size δ^2 ($\delta^2 > 0$) if:

$$\begin{aligned} -\left[\delta(\ell,n)\right]^2 &\leq \delta^2 \\ -\left[\delta(\ell,n+1)\right]^2 &> \delta^2 \end{aligned} \tag{4.10}$$

It is easy to find an iterative procedure to find the $CC(n,\delta^2)$ from the fragmentation products. We start on a hadron energy-momentum vector and the corresponding vertex vector (for this situation the first condition in Eq.(4.10) is trivially satisfied according to Eq.(4.4)). We then add the energy-momentum vector of the next hadron in rank order and check the resulting $\delta(\ell,n)^2$-value and continue until the first relation in Eq.(4.10) fails. After that we start on the next hadron and repeat the procedure to obtain the next chain.

Especially for small values of δ^2, the event will contain a set of hadrons which cannot be connected to any of their neighbours in rank. We will call them "solitaires". They can be thought of as $CC(1,\delta^2)$, but we will exclude them in

the following investigation of the Coherence Chains, because they contain just one hadron each, and the concept of a "chain" is better formulated with more than one element. For a given value of δ^2, the procedure above will subdivide each fragmentation event into a set of $CC(n, \delta^2)$ with different values of n and we will now consider the properties of these objects.

4.4.2 The Properties of the Coherence Chains

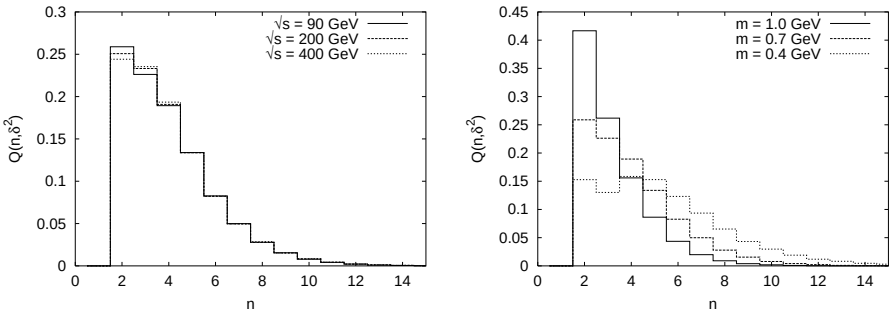

Figure 4.2: The figure to the left shows the $Q(n, \delta^2)$ distribution for different $\sqrt{s}$ values. A single hadron mass of $m = 0.7$ GeV has been used for this result. The figure to the right shows the $Q(n, \delta^2)$ distribution for different values of the common mass at $\sqrt{s} = 90$ GeV. Both the plots are obtained using $\delta^2 = 0.10$ GeV^2.

A Coherence Chain has a length (multiplicity) given by n and a (transverse) size given by δ^2. We will first keep δ^2 fixed and examine the dependence of the multiplicity on different event variables, and after that we will study the dependence upon δ^2.

We consider multigluon events, obtained e.g. from the ARIADNE Monte Carlo implementation of the Dipole Cascade Model [16], and hadronise the strings using ALFS. After hadronisation we trace all the Coherence Chains in the final states. From an inclusive sample of such events, we determine the distribution $Q(n, \delta^2)$, of the hadron multiplicity n inside Coherence Chains. The resulting distributions are shown in Fig.4.2 and we note the following properties.

- The distribution $Q(n, \delta^2)$ is almost independent of the energy of the event. The distribution Q does, however, depend upon the hadron mass value used. Besides these two properties, we have also found that the distribution is insensitive to the presence of gluons with particularly high transverse momenta

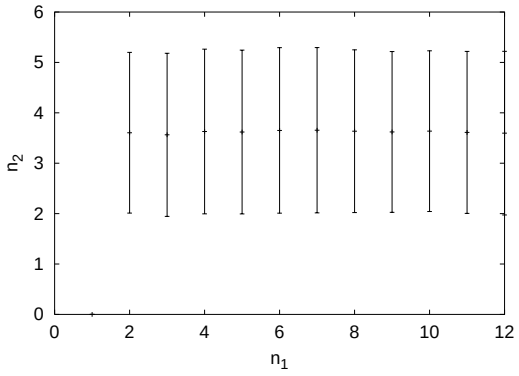

Figure 4.3: The figure shows $\langle n2 \rangle$ versus $n1$ for $\sqrt{s} = 90$ GeV, $m = 0.7$ GeV and $\delta^2 = 0.10$ GeV^2. The error-bars indicate the standard deviation.

in the events. Moreover, it is independent of global event variables such as thrust, sphericity etc.

- The multiplicities (n_1, n_2) of two adjacent Coherence Chains are independent of each other. Fig.4.3 shows $\langle n_2 \rangle$ for different values of n_1. As a further check of the independence, we have examined the distribution of $CC(n, \delta^2)$ with $n \leq r$ in the individual events. If we chose events with a chain multiplicity N we find a binomial distribution with the mean value Np using $p = \sum_1^r Q(j, \delta^2)$ and a variance $Np(1-p)$ (which is expected if there is no correlation).

The distribution in the number, N, of Coherence Chains in a single event, to be called $Q_{CC}(N, \delta^2)$ has the following properties.

- The energy dependence of the distribution is shown in Fig.4.4. At high energies more CCs tend to form.

- In Fig.4.4, we show the distribution $Q_{CC}(N, \delta^2)$ for different values of the hadron mass. We find that the distribution is almost independent of the hadron mass.

- The distribution depends upon the total λ measure for the event but for a given value of λ_{tot} it is independent of the energy, the global event variables and of the number of "hard" gluon emissions.

These properties are analogous to those found in connection with the Generalised Dipoles in [8], as described in subsection 4.3. In the next subsection, we will investigate the connection between these two concepts.

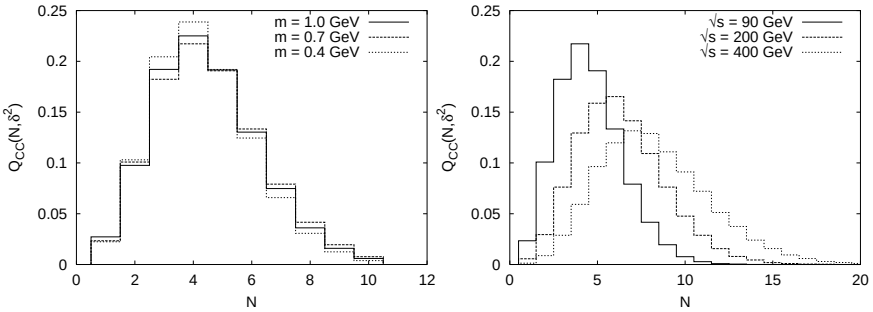

Figure 4.4: The figure to the left shows the $Q_{CC}(N, \delta^2)$ distribution at $\delta^2 = 0.10$ GeV^2 and $\sqrt{s} = 90$ GeV for different (common) mass values. The figure to the right shows the $Q_{CC}(N, \delta^2)$ distribution for different values of $\sqrt{s}$ obtained using a single hadron mass of 0.7 GeV.

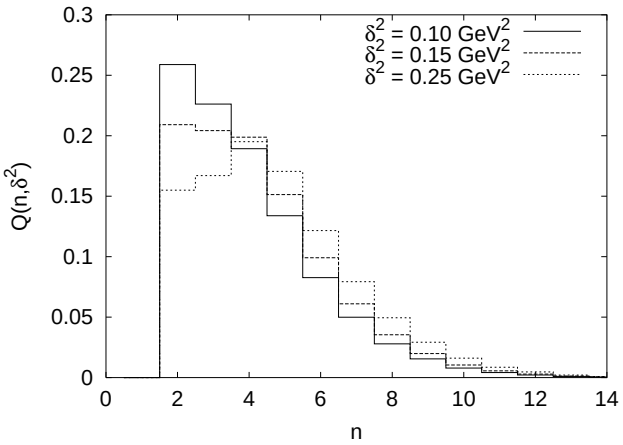

Figure 4.5: The figure shows the distribution $Q(n, \delta^2)$ for different values of δ^2. $\sqrt{s} = 90$ GeV and $m = 0.7$ GeV.

4.4.3 The Correlation Between the Coherence Chains and the Generalised Dipoles

We will see in the next section that the CCs play an important role in connection with Bose-Einstein correlations in multigluon events. In our model for the Bose-Einstein correlations, they roughly describe how far coherent interference effects extend among the final state hadrons. String fragmentation, as noted

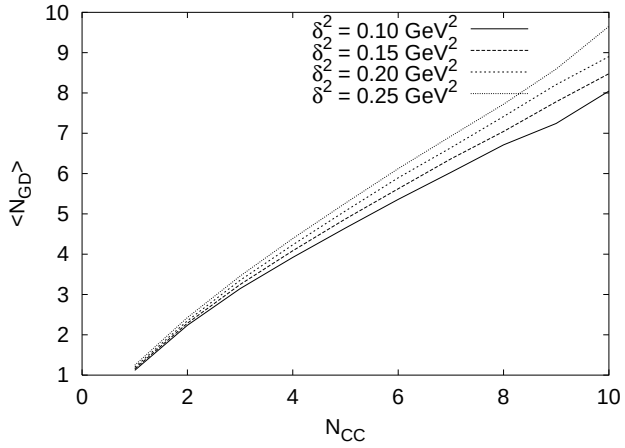

Figure 4.6: The figure shows the average number of Generalised Dipoles ($\langle N_{GD} \rangle$) vs the number of Coherence Chains (N_{CC}) in an event for different values of δ^2. The result is obtained using $m = 0.7$ GeV and $\sqrt{s} = 90$ GeV.

earlier, is infrared stable, i.e. many properties of the final state of hadrons are stable against introduction of very soft gluons. The process of hadronisation resolves the partonic state on the scale of hadron masses. Similarly, the parameter δ^2, since it affects which particles are included in a chain, could be interpreted as a resolution parameter relevant for Bose-Einstein correlations, and an optimal value for it could be fixed from experimental data. In Fig.4.5, we show how the $Q(n, \delta^2)$ distribution varies with δ^2. When δ^2 is larger, we see that longer Coherence Chains tend to form. In Fig.4.6 we show the average number of Generalised Dipoles present in an event as a function of the number of Coherence Chains detected for different values of δ^2. This shows that for larger values of δ^2, there are more dipoles for every Coherence Chain, but the number of dipoles per chain is always close to 1.

Every partonic state is composed out of a set of Generalised Dipoles that define planar regions by means of the (initial) q_T-vector $q_{T\alpha}$ and the corresponding directrix vector $\mathcal{A}_{\alpha+1}$. In principle such a region would decay just as a flat string, i.e. there will be a set of hadrons produced inside that plane, which would be subsequently grouped into a Coherence Chain.

However, the introduction of fragmentation transverse momenta in the process will diffuse the relationship between the Coherence Chains and the Generalised Dipoles. Also, in the string fragmentation model in ALFS, there is a special procedure to create plaquettes around gluon corners. Since it is nor-

mally not possible to fit a planar plaquette weighted with its area in the region between the X-curve and the directrix around gluon corners, the directrix is slightly modified around these corners. Two plaquettes are created with their k vectors not exactly parallel to the local segments of the directrix. Therefore, the two resulting plaquette planes are not aligned with the rest of the plaquettes formed away from the gluon corners. Since the k vectors in the plaquettes are normally sections of the directrix, the procedure around gluon corners is equivalent to slight local deformations of the original directrix on the scale of hadron masses. Normally, this means that our process for finding Coherence Chains using Eq.(4.10) marks the end of a chain around these corners. If this happens, the two particles around each gluon corner may be labelled as solitaires, or with smaller chances, form a chain of two particles themselves.

For a soft gluon it quite often happens that the deformations are so small that one or both of the particles formed with the corner crossing procedure are incorporated into the Coherence Chain. This in itself introduces fluctuations in the total number of CCs detected. If there are only one or two particles with plaquettes which have their k vectors aligned with a gluon energy-momentum vector, they can be "gobbled up" by a bigger Coherence Chain comprising of neighbouring hadrons.

Thus, it is reasonable that the number of CCs is correlated with the number of GDs, and that the correlation is not strictly one-to-one. Since δ^2 is the maximum allowed transverse momentum for a new particle to be included in a CC, the larger its value, the more likely it is that a Coherence Chain will extend beyond a corner crossing and include hadrons from more than one GDs. The effect would be a reduction of the total number of CCs in the event and an increase of the average number of particles in a CC, and that is precisely what is seen in Fig.4.5 and Fig.4.6.

PART II: The Coherence Chains and Bose-Einstein Correlations

It has been shown that Bose-Einstein correlations (BEC) could be introduced into the Lund model as a coherent interference effect [12]. In this approach, it is construed that the Lund model area law, derived using classical probability concepts, stems from an underlying quantum mechanical amplitude. For the production of a system of hadrons containing several identical bosons, one obtains a set of contributions to the amplitude, corresponding to different ways of permuting the final state momenta among the identical particles. The treatment in [12] was restricted to Bose-Einstein correlations for hadrons formed from a string without gluons. The hadronisation procedure in ALFS and the existence of Coherence Chains allows an extension of the model to multigluon strings. We present here this approach to model BEC.

4.5 The Bose-Einstein Effect: Flat Strings

4.5.1 Notation and Preliminaries

Consider the decay of a string into a set of n hadrons in the Lund model. This requires $n-1$ vertices along the string where $q\bar{q}$ pairs are produced. Each hadron is composed out of a quark from one vertex and an antiquark from a neighbouring vertex. The hadrons, which contain the initial quark or antiquark stretching the string, need only one more break-up along the string for their formation, but we associate two imaginary vertices with the original q and $\bar{q}$, and place them at the turning points of those particles. Thus every hadron can be viewed as if it was produced between two vertices, which gives us $n+1$ vertices in total.

We will use the following convention for numbering particles and vertices. Particle properties such as energy-momenta, can be numbered from 1 to n according to the rank order of the particle; or from 0 to $n-1$ so that p_0 would refer to the energy-momentum of the first rank particle etc. We will use this latter convention of numbering elements in a sequence in this paper. Thus, we have a set of (n) hadrons:

$$\begin{aligned} &\{h_\alpha | \alpha \in [0, n-1]\} \\ &\text{with energy-momenta} \\ &\{p_\alpha | \alpha \in [0, n-1]\} \\ &\text{whose creation is associated with plaquettes} \\ &\{P_\alpha | \alpha \in [0, n-1]\} \\ &\text{formed between vertices} \\ &\{v_\alpha | \alpha \in [0, n]\} \end{aligned} \tag{4.11}$$

Given a rank-ordered set of n hadron energy-momenta, we will show that it is possible to determine the $(n-1)$ intermediate vertices and the n plaquettes involved in the production process. The two imaginary vertices associated with the initial $q\bar{q}$ pair are assumed to be known, and they define the string plane.

We let $(p_{l\alpha}, p_{\perp\alpha})$ denote the longitudinal[6] and transverse components of the hadron energy-momentum vector relative to the plane of the string (or local planar region in a gluonic string). Further, let $k_{\perp\alpha}$[7] denote the transverse momentum generated at the vertex v_α in the string break-up process.

Every plane in Minkowski space, which contains a time like vector, has two light-cone directions. If we identify one of them as the positive and the other

[6] We define the longitudinal component of a general four-vector with respect to a plane in Minkowski space as its component in that plane.

[7] The vector $k_{\perp\alpha}$, defined in connection with transverse momentum generation, is not the transverse component of k_α which is defined in connection with Eq.(4.4).

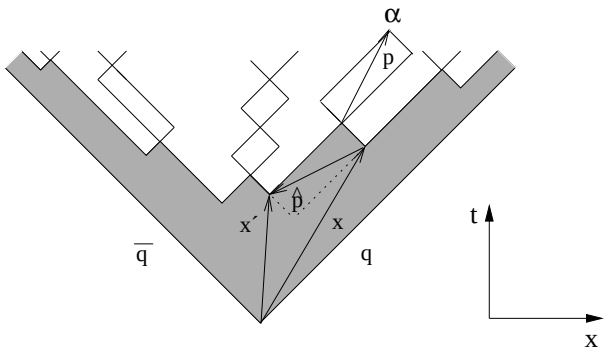

Figure 4.7: The figure shows the fragmentation of a flat string. The longitudinal momentum vector of a hadron $p_\alpha \equiv p$ and its dual vector $\hat{p_\alpha} \equiv \hat{p}$ is shown. The dual vector correspond to the difference between the two vertices involved in the creation of the hadron.

as the negative light-cone direction, the vectors $p_{l\alpha}$ could be specified in terms of the components $(p^+_{l\alpha}, p^-_{l\alpha})$ along the light-cones. We define a dual vector to $p_{l\alpha}$ through its components as $\hat{p}_{l\alpha} = (-p^+_{l\alpha}, p^-_{l\alpha})$. It follows that:

$$\begin{aligned} \hat{p}_\alpha \cdot p_{l\alpha} &= 0 \\ \hat{p}^2_\alpha &= -p^2_{l\alpha} = -(m^2_\alpha + p^2_{\perp\alpha}) = -m^2_{\perp\alpha} \end{aligned} \tag{4.12}$$

One could alternatively define $\hat{p}_\alpha$ in terms of the properties in Eq.(4.12). These would determine the vector up to a sign, since we demand that it is a vector in the string plane like the longitudinal momentum. The sign ambiguity is equivalent to the ambiguity in naming one light-cone direction as positive and the other as negative. An iterative string fragmentation algorithm allows a straight forward identification of one light-cone direction as positive and another as negative. In Fig.4.7, which shows the fragmentation of a flat string, it is easy to see that the dual to the longitudinal momentum vector introduced above would correspond to the difference between the two vertices involved in the formation of the particle.

$$\hat{p}_\alpha = x_{\alpha+1} - x_\alpha \tag{4.13}$$

This relation can then be applied to the "plaquette" associated with the formation of the particle labelled α. Eq.(4.4) and Eq.(4.13) give:

$$\hat{p}_\alpha = k_\alpha - p_{l\alpha} \tag{4.14}$$

This vector satisfies all the defining properties of $\hat{p}_\alpha$ outlined above. Eq.(4.14) then helps identify the negative light-cone direction in the plane of the plaquette with the direction of k. With this background, it is easy to see the following:

Property 1 *Once (i) the string plane (ii) the energy-momentum of a particle, and (iii) the starting vertex (both vertex vector and vertex transverse momentum) for a plaquette are specified, the plaquette is completely determined.*

The vector $\hat{p_\alpha}$ can be constructed from the light-cone components of p_α. We can then find the remaining information for the plaquette, i.e. $x_{\alpha+1}$ from Eq.(4.13), k_α from Eq.(4.14) and $k_{\perp\alpha+1}$ from the following relation:

$$k_{\perp\alpha+1} \quad = \quad k_{\perp\alpha} + p_{\perp\alpha} \tag{4.15}$$

If $\hat{k}$ is a known light like vector, the above can be schematically represented as follows:

$$v_\alpha \oplus p_\alpha \rightarrow (v_{\alpha+1}, k_\alpha) \text{ when } (k_\alpha \cdot \hat{k} = 0) \tag{4.16}$$

Therefore, given a starting vertex vector x_0, a vertex transverse momentum $k_{\perp 0}$ and a set of hadrons with momenta as in Eq.(4.11), it is possible to reconstruct the entire set of plaquettes completely.

$$\begin{aligned} k_{\perp 1} &= k_{\perp 0} + p_{\perp 0} \\ k_{\perp 2} &= k_{\perp 1} + p_{\perp 1} = k_{\perp 0} + p_{\perp 0} + p_{\perp 1} \\ \ldots &= \ldots \\ k_{\perp \alpha} &= k_{\perp 0} + \sum_{\beta=0}^{\alpha-1} p_{\perp\beta} \end{aligned} \tag{4.17}$$

$$\begin{aligned} x_1 &= x_0 + \hat{p}_0 \\ x_2 &= x_1 + \hat{p}_1 = x_0 + \hat{p}_0 + \hat{p}_1 \\ \ldots &= \ldots \\ x_\alpha &= x_0 + \sum_{\beta=0}^{\alpha-1} \hat{p}_\beta \end{aligned} \tag{4.18}$$

For later reference we note the following:

Property 2 *If the plaquettes* $[0, \ldots, n-1]$ *are known to have the property* $k_\alpha \cdot k_\beta = 0$ *for* $\alpha, \beta \in [0, n-1]$*, the vectors* x_n *and* $k_{\perp n}$ *reconstructed like in Eq.(4.17) and Eq.(4.18) are independent of the order of the particles* $[0, .., n-1]$.

The intermediate vertices $[1, \ldots, n-1]$ on the other hand, have different vectors $(x_\alpha, k_{\perp\alpha})$ associated with them. Therefore, the area under these vertices and the Gaussian suppression factor for the transverse momenta in the reconstructed vertices will depend on the order of the particle energy-momenta in the reconstruction process.

4.5.2 The Amplitude

The area law in Eq.(4.1) has a formal resemblance to a quantum mechanical transition probability. It is the product of the final state phase space and a factor which can be interpreted as the square of a matrix element in a quantum mechanical calculation [11, 12]:

$$dP \quad \propto \quad \prod_{\alpha=0}^{n-1} d^4p_\alpha \delta(p_\alpha^2 - m_\alpha^2)\delta(\sum_{\alpha'=0}^{n-1} p_{\alpha'} - P_{tot}) \times |\mathcal{M}|^2 \tag{4.19}$$

An amplitude which would yield the area law was discussed in [12]:

$$\mathcal{M} \quad = \quad \exp\left[(i\frac{1}{2\kappa} - \frac{b}{2})A - \frac{1}{4\sigma^2}\sum k_{\perp\alpha}^2\right] \tag{4.20}$$

Here κ is the string constant (phenomenologically $\kappa \simeq 0.2$ GeV^2), $b \simeq 0.7$ GeV^{-2} and $\sigma \simeq 0.3$ GeV is the size of hadronisation transverse momentum fluctuations. The area is evaluated in energy-momentum space using light cone coordinates. The expression in Eq.(4.20) is motivated by the fact that the action for the (non-breaking) relativistic string is given by κ times the invariant area spanned by the string. Thus $\frac{ib}{2}A$ can be interpreted as an imaginary part of the action, responsible for the break-up of the string. Suppose two hadrons labelled a and b occurring at rank orders (indices) α and β are identical particles. We could reconstruct another set of vertex vectors and transverse momenta by using these particles in interchanged rank orders, in the procedure outlined in subsection 4.5.1. The vertices $[0,\ldots,\alpha]$ and $[\beta+1,\ldots,n]$ will be unaffected by this change, and in fact all the properties of the plaquettes $[0,\ldots,\alpha-1]$ and $[\beta+1,\ldots,n-1]$ will be unaffected by this permutation. However, the vertices $[\alpha+1,\ldots,\beta]$ and the plaquettes $[\alpha,\ldots,\beta]$ may be changed, and therefore the total area of these plaquettes and the transverse momentum suppression factor calculated for these vertices would add up to different values after the exchange.

The exchanged configuration of vertices is a valid alternative way the string could have fragmented to give rise to exactly the same set of hadrons. The amplitude for that alternative process would depend on the area under the reconstructed vertices and the new transverse momentum suppression factor. We illustrate this in Fig.(4.8), where we show that the amplitude of the initial configuration and the exchanged configuration will involve different areas. Since the probability for the formation of the final state is the square of the total amplitude, and there are two possible contributions for the generation of the final hadron state from the same initial parton state, one should add these two contributions and square the sum. This would give rise to an interference term. Since the Monte Carlo implementations of the Lund model are built

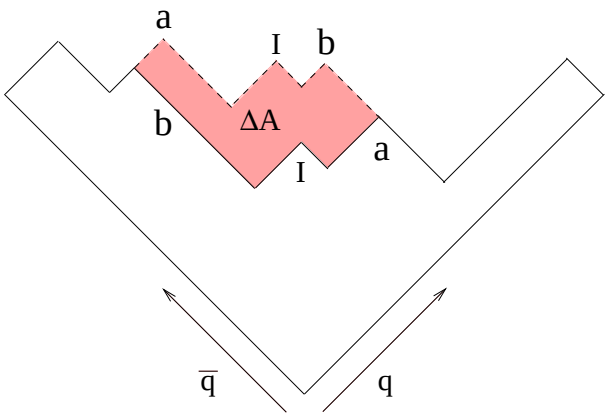

Figure 4.8: The figure shows the decay of a string state with the identical bosons a and b produced with the intermediate state I in between them. The string state drawn with dashed lines is another production possibility (configuration), since the bosons a and b are identical. Each configuration will contribute to the amplitude, and the interference term can be parametrised by the area difference between the two configurations, ΔA, as described in the text.

upon classical probability concepts they will only take into account the squared amplitudes of individual configurations. The effect of the interference term could be introduced as an event weight which would associate a total probability of $|(\mathcal{M}_1 + \mathcal{M}_2)|^2$ with the direct and exchanged configurations together, rather than just $(|\mathcal{M}_1|^2 + |\mathcal{M}_2|^2)$.

The alternative or exchanged configuration of vertices giving rise to the same set of final state hadrons is an allowed set of vertices, and it will occur during a Monte Carlo simulation naturally according to its own probability. The total probability for the hadronic state has to be split between these two configurations. If there are several alternative configurations, the total amplitude is to be calculated by summing over all possible permutations of identical particles, and the squared amplitude is to be split between all those permuted configurations. There is no unique prescription for the weight that should be associated with any one of these configurations as long as the correct total probability is assigned to the ensemble of configurations which can be obtained by a permutation of identical particles in a generated event. One form of event weight was suggested and used in [12]:

$$w_P \quad = \quad 1 + \sum_{P' \neq P} \frac{2Re(\mathcal{M}_P \mathcal{M}^*_{P'})}{|\mathcal{M}_P|^2 + |\mathcal{M}_{P'}|^2} \tag{4.21}$$

For reasons which will be elaborated upon in section 4.6.3, we deemed this choice of event weight unsuitable for our purposes, and instead chose the following event weight:

$$w_P = \frac{|\sum_{P'} \mathcal{M}_{P'}|^2}{\sum_{P'} |\mathcal{M}_{P'}|^2} \tag{4.22}$$

We note that unlike the weight in Eq.(4.21), the above weight partitions the total probability for the production of a certain set of hadrons into individual configurations of identical bosons in such a way that each configuration is reweighted by the same factor. We also note that the weight in Eq.(4.22) is manifestly positive definite. We discuss this choice and its implications further in section 4.6.3. In the next section, we present our method to calculate this weight for a given event.

4.5.3 Calculation of the Event Weight

The calculation of the event weight in Eq.(4.22) involves an estimation of the amplitude contributions corresponding to all possible rearrangements of the identical particles in the event. If $\mathcal{M}_0$ is the amplitude term corresponding to a generated event, and $\mathcal{M}_1$ is the amplitude term of another configuration of identical bosons in the generated event, we have

$$\mathcal{M}_1 = \mathcal{M}_0 \exp\left[(i\frac{1}{2\kappa} - \frac{b}{2})\Delta A - \frac{1}{4\sigma^2}\Delta \sum k_{\perp\alpha}^2\right] \tag{4.23}$$

where $\Delta f \equiv f(configuration\ 1) - f(configuration\ 0)$. We note that the dependence on the transverse momenta rely on the assumption that $k_\perp$ must be exactly conserved in every break-up. This could however be modified if $k_\perp$ is only conserved within a finite rapidity range [18].

The amplitudes $\mathcal{M}_{P'}$ can all be expressed in terms of the amplitude of the generated event, the area differences and the difference of summed up squared transverse momenta. We observe that the amplitude of the original event will cancel between the numerator and the denominator in Eq.(4.22). Thus

$$w_p = \frac{|1 + \sum_{P' \neq P} S \cdot \exp\left((i\frac{1}{2\kappa} - \frac{b}{2})\Delta A - \frac{1}{4\sigma^2}\Delta \sum k_{\perp\alpha}^2\right)|^2}{1 + \sum_{P' \neq P} |S \cdot \exp\left((-\frac{b}{2})\Delta A - \frac{1}{4\sigma^2}\Delta \sum k_{\perp\alpha}^2\right)|^2} \tag{4.24}$$

In Eq.(4.24) we have also included a factor S in front of all the amplitudes. This factor depends on the spin of the particles being exchanged. If the particles being symmetrised are spin 1 particles, they should be treated as indistinguishable states only if they are in the same spin state. Since we do not keep track of the spin of the particles in this analysis, we consider them as identical with

a probability of $\frac{1}{3}$. When two fermions are exchanged in an alternative configuration, the amplitudes should be added with an additional negative sign, and this can be included through this spin factor. When multiple particles appear at exchanged ranks in an alternative configuration, the spin factor is calculated appropriately, i.e. it receives a contribution of -1 for an odd permutation of identical fermions, 1 for an even permutation of the same, 1 for any permutation of scalar bosons and vector bosons which are regarded as being in the same spin state.

For the lowest non-trivial order of permutations, in which only one pair of identical particles are exchanged in ranks the terms ΔA and $\Delta \sum k_{\perp\alpha}^2$ can be shown to be:

$$\begin{aligned} \Delta A &= -2(p_{l\beta} - p_{l\alpha}) \cdot \left[x_\beta - x_{\alpha+1} + \frac{1}{2}(\hat{p}_\alpha + \hat{p}_\beta) \right] \qquad (4.25) \\ \Delta \sum_{\alpha'=\alpha}^{\beta+1} k_{\perp\alpha'}^2 &= \Delta \sum_{\alpha'=\alpha+1}^{\beta} k_{\perp\alpha'}^2 \\ &= (\beta - \alpha)(p_\beta - p_\alpha)^2 + 2(p_\beta - p_\alpha) \cdot \left(\sum_{\alpha'=\alpha+1}^{\beta} k_{\perp\alpha'} \right) \end{aligned}$$

where identical particles with indices α and β ($\alpha < \beta$) are exchanged to form the exchanged configuration of vertices.

For a general permutation, ΔA and $\Delta \sum k_{\perp\alpha}^2$ can be expressed according to the following formulae. Given that $\{e_0, e_1, e_2, \ldots, e_{n-1}\}$ is a permutation of $\{0, 1, 2, \ldots, n-1\}$:

$$\begin{aligned} \Delta A &= \frac{1}{2} \sum_{\alpha,\beta=0}^{n-1} (\epsilon_{e_\alpha e_\beta} - \epsilon_{\alpha\beta}) k_\alpha \hat{p}_\beta \qquad (4.26) \\ \Delta \sum_{\alpha=0}^{n} k_{\perp\alpha}^2 &= \sum_{\alpha,\beta=0}^{n-1} [\max(\alpha, \beta) - \max(e_\alpha, e_\beta)] p_{\perp\alpha} p_{\perp\beta} \end{aligned}$$

where $\epsilon_{\alpha\beta}$ is defined as:

$$\epsilon_{\alpha\beta} = \begin{cases} +1, & \alpha > \beta; \\ 0, & \alpha = \beta; \\ -1, & \alpha < \beta \end{cases} \qquad (4.27)$$

4.6 The Bose-Einstein Effect: Gluonic Strings

We will proceed to extend the BE model described above to multigluon states, but we will first state some of the problems one must encounter in doing so.

The reason why the process in the previous subsection could be consistently formulated for a flat string, is that it is possible to find another set of vertex locations which would produce the same set of hadrons. In the presence of gluons, the situation is far more complicated. If the identical particles being exchanged happen to be separated by one or more gluon corners, one can not find an alternative set of vertices which would lead to the same set of final state particles from the same partonic configuration.

The vectors constituting the plaquettes generated during string fragmentation in ALFS have many geometrical relations between them. If we try to interchange only the momentum of two particles while keeping the plaquette planes in their original locations, we would need to project the particle momentum to longitudinal and transverse components relative to its new plaquette. It is then impossible to arrange that the recalculated vertex transverse momenta are orthogonal to the two plaquettes they are connected to, for all vertices. Also, if the particles are exchanged across a hard gluon corner, the new location for a momentum might be unnatural, i.e. large transverse momenta might be required relative to the new location of the particle, and large transverse momenta are suppressed because of their Gaussian distribution. If the vectors k are exchanged along with the momenta, the relocated plaquettes cease to be planar. In all such methods we considered, we found that once we exchange two particles created out of plaquettes with k vectors which are not parallel, the reconstructed configurations violate some basic geometrical relations obeyed by plaquettes in ALFS, which rules them out as possible outcomes of fragmentation events. Even if we choose to be lenient about some geometrical relations as long as total energy-momentum conservation is satisfied, the rearrangements result in extremely unlikely values for the vertex transverse momenta.

It may be possible to find another set of k vectors for the two plaquettes involved in the exchange and all the plaquettes between them which would preserve all geometrical relations after the exchange; but such a procedure is not consistent with the idea that one could treat the parton showers and hadronisation separately, which is at the heart of most simulation methods. At this moment we would be satisfied with finding approximations which would still stick to the established parton shower techniques, while at the same time trying to incorporate interference effects at the hadronisation stage on these multigluon states.

4.6.1 The Factorisation of the Event Weight

As an approximation, we will completely ignore all possible interference effects between different partonic states leading to the same set of hadrons. In such a case, the amplitude for a process in which two identical bosons are exchanged across a gluon corner must be zero, since, as noted above, it is impossible to reconstruct an alternative set of vertices leading to the same particle momenta without altering the partonic state. One would then consider exchanges of identical particles only inside flat regions or GDs in the string.

The amplitude in Eq.(4.20) can be looked upon as the product of factors corresponding to the creation of individual particles:

$$\begin{aligned} \mathcal{M} &= \prod_{\alpha'=0}^{n-1} \mathcal{M}(v_{\alpha'}, \delta A_{\alpha'}, v_{\alpha'+1}) \\ &= \prod_{\alpha'=0}^{n-1} \exp\left[(i\frac{1}{2\kappa} - \frac{b}{2})\delta A_{\alpha'} - \frac{1}{8\sigma^2}(k_{\perp\alpha'}^2 + k_{\perp\alpha'+1}^2) \right] \end{aligned} \tag{4.28}$$

One could link each of the $\mathcal{M}(v_{\alpha'}, \delta A_{\alpha'}, v_{\alpha'+1})$ to the production of one particle or with what is schematically represented in Eq.(4.16). In ALFS, this factorisation of the amplitude to a set of factors, one for each particle, is valid even for gluonic strings. This is because there is a unique planar area associated with the creation of each particle: the area of a plaquette. The sum of the areas of the plaquettes is the area in the area law. In other words, the fragmentation procedure in ALFS divides the area in the area law into a set of planar areas, one for each particle.

In order to analyse the change in the amplitude when identical particles with indices between α and β are permuted arbitrarily, we will rewrite Eq.(4.28) in the following way:

$$\begin{aligned} \mathcal{M} &= \left(\prod_{\alpha'=0}^{\alpha-1} \mathcal{M}(v_{\alpha'}, \delta A_{\alpha'}, v_{\alpha'+1}) \right) \cdot \\ &\quad \cdot \left(\prod_{\alpha'=\alpha}^{\beta} \mathcal{M}(v_{\alpha'}, \delta A_{\alpha'}, v_{\alpha'+1}) \right) \cdot \left(\prod_{\alpha'=\beta+1}^{n-1} \mathcal{M}(v_{\alpha'}, \delta A_{\alpha'}, v_{\alpha'+1}) \right) \end{aligned} \tag{4.29}$$

If v_α and $v_{\beta+1}$ remain unchanged under the permutations, it is clear that contributions from the first and the third parentheses would be unchanged. But Property 2 guarantees that v_α and $v_{\beta+1}$ remain unchanged under the permutations, if the plaquettes α through to β have their k vectors parallel, or if these plaquettes are parts of the same plane in Minkowski space.

Using the shorthand $\mathcal{M}_\alpha \equiv \mathcal{M}(v_\alpha, \delta A_\alpha, v_{\alpha+1})$, we can now write, for an arbitrary gluonic string, which has fragmented into a group of hadrons like in Eq.(4.11)

$$\begin{aligned} \mathcal{M} &= \left(\prod_{\alpha=0}^{\beta_1} \mathcal{M}_\alpha\right) \cdot \left(\prod_{\alpha=\beta_1+1}^{\beta_2} \mathcal{M}_\alpha\right) \cdot \left(\cdots\right) \cdots \left(\prod_{\alpha=\beta_r+1}^{n-1} \mathcal{M}_\alpha\right) \\ &= \left(\mathcal{M}^A\right) \cdot \left(\mathcal{M}^B\right) \cdots \end{aligned} \tag{4.30}$$

where the connected plaquettes collected into each of the parentheses above are assumed to have their k vectors parallel. In the second line of the equation, the superscripts "A", "B", etc represent these collections of plaquettes which are created with their k vectors parallel. We will call them "coherence regions" for the moment. To calculate the amplitude of an alternative configuration of vertices leading to the same set of particles, in which two particles in group A (for example) occur at interchanged orders, we need to calculate the altered amplitude contribution from group A, and multiply that to the amplitudes from group B,C,... which are not affected by the exchange. One can therefore evaluate permutations inside each coherence region independently.

The total amplitude is obtained by summing over the amplitudes of all allowed permutations of identical particles. If $\pi_i(A)$ represents a particular permutation of identical particles in coherence region A,

$$\begin{aligned} \mathcal{M} &= \sum_{i,j,k\ldots} \left(\mathcal{M}^{\pi_i(A)}\right) \cdot \left(\mathcal{M}^{\pi_j(B)}\right) \cdot \left(\mathcal{M}^{\pi_k(C)}\right) \cdots \\ &= \left(\sum_i \mathcal{M}^{\pi_i(A)}\right) \cdot \left(\sum_j \mathcal{M}^{\pi_j(B)}\right) \cdot \left(\sum_k \mathcal{M}^{\pi_k(C)}\right) \cdots \\ &= \mathcal{M}^A_{tot} \cdot \mathcal{M}^B_{tot} \cdot \mathcal{M}^C_{tot} \cdots \end{aligned} \tag{4.31}$$

Along with the result,

$$\sum_{i,j,k\ldots} |\left(\mathcal{M}^{\pi_i(A)}\right) \cdot \left(\mathcal{M}^{\pi_j(B)}\right) \cdot \left(\mathcal{M}^{\pi_k(C)}\right) \cdots|^2 = \tag{4.32}$$

$$\left(\sum_i |\mathcal{M}^{\pi_i(A)}|^2\right) \cdot \left(\sum_j |\mathcal{M}^{\pi_j(B)}|^2\right) \cdot \left(\sum_k |\mathcal{M}^{\pi_k(C)}|^2\right) \cdots$$

we obtain a generalisation of the weight in Eq.(4.22) for multigluon strings:

$$w = w^A \cdot w^B \cdot w^C \cdot .. \tag{4.33}$$

Thus we have shown that if we associate an amplitude of zero for the exchange of bosons across gluon corners, the Bose-Einstein event weight factorises into a product of individual weights for coherence regions. The weights

for coherence regions can be evaluated independently by permuting particles inside the region and finding a weight as in the case of a flat string, using Eqs.(4.22,...,4.25). In the approximation we have considered up to this point, the hadrons emerging out of the hadronisation process with plaquette planes aligned with one GD in the partonic state will be grouped into one coherence region.

4.6.2 A BEC Model Based on Coherence Chains

The GDs used in the above are, strictly speaking, functions of the cut-off scale used in the parton shower. In [8] we noted that these GDs have interesting scaling properties, in that they seem to have nearly the same distribution in sizes relative to the cut-off scale, for a wide range of the value of the cut-off scale. But compared to a fixed scale, the smaller the cut-off, the larger the number of gluons, and hence the smaller the GDs, even though there might be more of them. This makes it unsatisfactory to not consider exchanged amplitudes across gluon corners. Smaller the cut-off, less the chance that two identical bosons would be found in one GD. In fact, one can imagine making the cutoff scale, and hence the GDs, so small that in the whole event there wont be any instances of two identical particles left in the same GD. Since the cut-off scale is tuned from other considerations, it seems like an artificial limitation of this particular approximation.

However, as the cut-off scale is lowered, the system also exhibits softer and softer gluons. If one such state is interchanged for another, the system does not look radically different either at the partonic or the hadronic level. One could argue that the amplitudes to produce those "slightly different" partonic states should be very similar, and at least some properties of the emerging system of hadrons would be insensitive to any small differences they might have.

This is where the concept of Coherence Chains helps. Defined on the hadronic state, they are answers to the question: "Could this set of hadrons be treated as if they came from one flat region on a string ?". The hadrons might actually come from a region of the string which contains many gluons. But if it can still be regarded as flat, up to a certain scale in transverse momentum, we will assume that they could be identified with our coherence regions in the previous section.

The procedure to calculate the event weight in this approach would therefore be as follows. We first identify all Coherence Chains in an event. The energy-momentum vectors of the particles in every Coherence Chain are projected into longitudinal and transverse components relative to the plane of the Coherence Chain. A set of plaquettes is reconstructed on this plane using the particle energy-momenta and the starting vertex for the Coherence Chain. A weight is calculated for each Coherence Chain, considering permutations of identical

particles inside the Coherence Chain. The weights obtained in all the Coherence Chains are then multiplied to give the total event weight.

Defining a Coherence Chain is tantamount to identifying the amplitudes of all partonic states which could give rise to hadronic states similar to the one used in the construction of the Coherence Chains. Thus, the Coherence Chain approximation of the analysis of BEC is built upon the expectation that the BEC would be insensitive to the small differences in the amplitudes for the formation of different partonic configurations involving very soft gluons. The use of Coherence Chains allows us lower the parton shower cut-off without making BE calculations like in Eq.(4.33) impossible.

4.6.3 A Few Comments About the Event Weight and Our Weighting Procedure

We expect that the weighting only affects the hadronisation process and does not modify the probability for different intermediate partonic states. An event weight gives the relative size of the true probability that should be associated with one particular event compared to the probability with which a Monte Carlo generates it. One could then count "1.3" events for an event which has a weight 1.3 in any statistics one might be interested in. This approach was found unsuitable for our BEC analysis.

The reason was that we found a multiplicity dependence in the weights. This means that events with higher number of particles would be counted more often, and that would change the multiplicity distributions generated in the Monte Carlo. In [12], a simple re-tuning of the Lund model parameters was used to shift the multiplicity distributions back to unweighted positions. This can not be done for multigluon strings, because the multiplicity of the event increases with gluonic activity and multigluon events would therefore end up being weighted higher than events with few or no gluons. The multiplicity distribution would shift more for multi-jet events compared to events with few jets, and an effective re-tuning would have to involve the particular partonic state.

Another way to use a Bose-Einstein event weight is to use it as an internal acceptance probability for the particular hadronisation event, while keeping the partonic configuration unchanged until an event gets accepted. In this method, we always associate one hadronic state with one partonic configuration, thereby keeping the relative normalisations of different kinds of partonic configurations unaffected.

It is desirable that a weight which is to be used as a rejection weight be positive definite. The weight used in [12], i.e. the weight in Eq.(4.21), was not positive definite. Since we needed the weight as a rejection weight, we decided in favour of the manifestly positive definite weight in Eq.(4.22).

Multiplicity distributions will still shift as the events with higher multiplicity have higher weights and have a higher chance of being accepted. But if the shift is larger for events with more jets, compared to events with simpler geometry, jet multiplicities from weighted events, when tuned to match those of the unweighted events for 2-jet systems, would not match up for higher number of jets. Since the unweighted Monte Carlos are known to describe experimental multiplicity distributions quite well, this would be an unhealthy feature of the model.

In this connection, we see the significance of certain stability properties of the Coherence Chains, discussed in section 4.4. We recall that the distribution in the number of particles included inside a CC was relatively insensitive to the global event variables. In an event with many jets, there are probably a large number of Coherence Chains. However, the number of particles inside one Coherence Chain still has the same distribution. This multiplicity will be shifted to higher values by BE weighting. But once we re-tune the program so that the correct multiplicity distribution is obtained for events with simple geometry, i.e. few CCs, the events with a larger number of CCs would automatically stand re-tuned, as they are merely larger collections of CCs of the same kind. Also, since the distribution in size of the Coherence Chains was rather insensitive to the center of mass energy of the event, we expect that it would be possible to re-tune the Lund model parameters in a similarly energy insensitive way.

4.6.4 Resonance Decays

Since a large fraction of all the pions in the final state are produced as decay products of short lived resonances, it is important to consider their influence on the Bose-Einstein weight for an event. The decay of a resonance is normally thought of as a process which is very different from the string breakup. In this investigation, we will adopt the same approach to resonances as in [12]. We will assume that resonances with width larger than a certain cut-off, decay on a time scale short enough for the decay products to directly contribute to interference effects involved in the hadronisation process. We will also choose this cut-off in width at about 0.02 GeV, so that essentially only the decay products of the ρ-resonances and the K^*-resonances are considered during the Bose-Einstein calculations.

Even though resonance decay of the ρ is considered to be isotropic, when the energy momenta of its decay products are projected as longitudinal and transverse components relative to the string plane, they always give reasonable values since the mass of the resonance happens to be about twice the scale for hadronisation transverse momenta for hadrons. Had the hadronisation transverse momentum scale been about one tenth of its phenomenological value (about 0.4 GeV for a hadron), it would have been quite unnatural to regard

the decay products from a ρ decay as if they came directly from the decay of the string.

Once an order has been assigned to the decay products, the plaquette reconstruction process of section 4.5.1 can assign new plaquettes corresponding to the decay products in place of the plaquette corresponding to the resonance. Without going into much detail, we state that sometimes (eg. $\rho \to \pi^+\pi^-$) the rank order of decay products can be deduced from the requirement of consistency with the decay of the original string. However, in many cases it is not possible to assign a unique order from such considerations. For such situations, we have chosen to reconstruct in all possible orders, to find the area law probabilities that would be associated with different orderings and then to select one of them based on the Bayesian probability for that particular ordering.

4.6.5 Higher Order permutations and Computing Time

As pointed out in [12], certain higher order permutations of identical particles might lead to configurations with significant contributions to the amplitude, while many lower order contributions might be negligible. Calculating the contribution of all permutations of identical particles takes an unacceptable amount of time. In [12], Andersson and Ringnér suggested a method to estimate which configurations might make significant contributions and generate only those configurations.

The concept of a "link" between two ranks was introduced from purely practical considerations. Two ranks, α and β, are said to have a link between them if and only if:

- The particles at ranks α and β are identical
- $Q^2 = -(p_\alpha - p_\beta)^2 < Q^2_{\max} \simeq 1\text{GeV}^2$
- $|\hat{P}^2| = |(x_{\alpha+1} - x_\beta)^2| < |\hat{P}^2_{\max}| \simeq 20\text{GeV}^2$ (slightly different from the condition used by Andersson and Ringnér)

Consider a permutation of the indices $\{e_0, e_1, \ldots, e_{n-1}\}$. It turns out, as expected from the expression for the amplitude terms in Eq.(4.23), that normally the contribution of the permutation is either strictly 0 or negligible, if there is no link between the ranks α and e_α. Therefore, only a small error is made in some rare events by considering permutations with the constraint that for all α, there is a link between α and e_α. The advantage in terms of computing time because of the use of this procedure is tremendous, and justifies its use.

We also point out that multijet events will typically have a much larger multiplicity than events with simpler structure. Even though the coherence chains breakup the events into smaller groups over which symmetrisation of

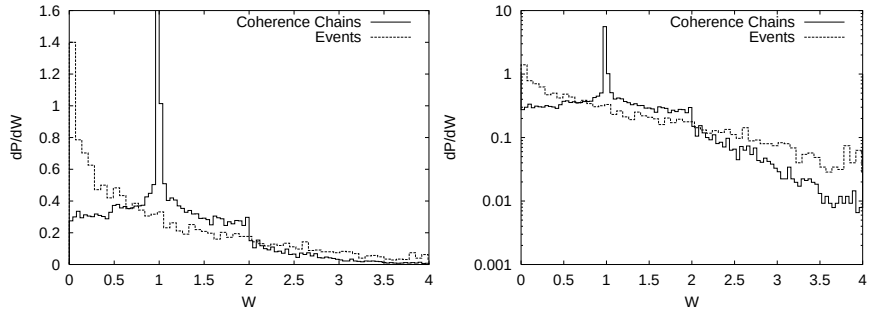

Figure 4.9: The figure to the left shows the weight distribution for an inclusive sample of events and the corresponding weight distribution for the Coherence Chains. We have used $\delta^2 = 0.10$ GeV^2 and $\sqrt{s} = 90$ GeV. The figure to the right shows the same result using a log scale instead. Note that the weight distribution for CCs extends beyond the range of the y-axis in the left-hand plot.

the amplitude is carried out, going through all permutations may still be prohibitively computation intensive. A coherence chain with 6 π^+s and 6 π^-s, for instance, will involve about 500.000 possible configurations. Though such chains are not the most common, they are not forbidden. Events with many identical particles in one chain will therefore slow down the simulation considerably, without affecting the end results, unless the above constraint is used to select the appropriate permutations.

4.6.6 Results

In this subsection, we will present a study of the distributions obtained from a Monte Carlo implementing the BE model described earlier.

The weight distribution for an inclusive sample of events at a center of mass energy of 90 GeV is shown in Fig.4.9. As pointed out earlier, this weight is the product of as many terms as there are Coherence Chains in the event. In Fig.4.9, we also show the weight distribution for Coherence Chains. As with most properties of Coherence Chains, this weight distribution is rather insensitive to changes in the center of mass energy and thrust of the event.

The "cliff" in the weight distribution for Coherence Chains at a weight value of 2 can be understood as follows. The events in which exactly one alternative permutation of the identical particles exists, have only two terms in the expression for the total amplitude. For this situation, the weight in Eq.(4.22) can not be larger than 2. But if there are more allowed permutations,

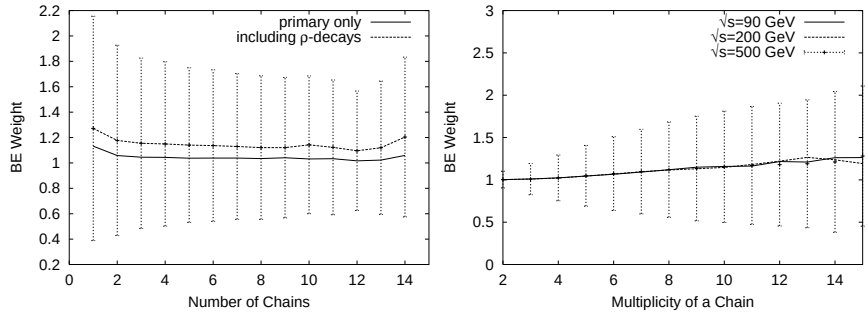

Figure 4.10: The plot to the left shows the mean weight of Coherence Chains vs the total number of chains in the event. The plot to the right shows the mean weight of Coherence Chains vs the number of particles included in the chains. The result was obtained using $\sqrt{s} = 90$ GeV and $\delta^2 = 0.10$ GeV^2.

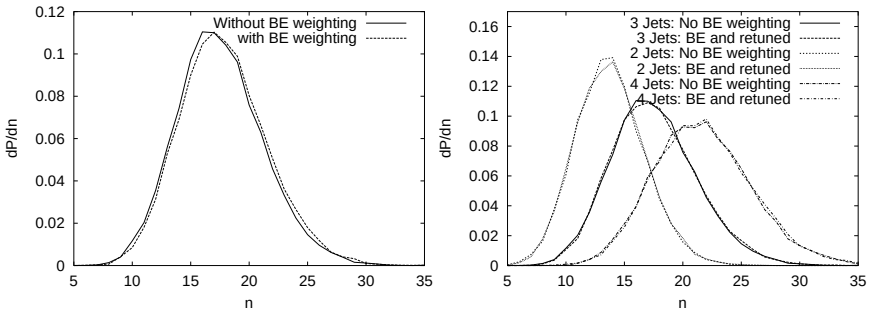

Figure 4.11: The weight shifts the multiplicity distribution, but it can be restored by a simple re-tuning of Lund model parameters as described in the text.

the weights could be either greater or smaller than 2. So, the weight distribution receives contribution from different (but not disjoint) sets of events on either side of 2. We plot the mean weight of Coherence Chains vs the total number of chains in the event in Fig.4.10. It shows that events with more Coherence Chains have the same kind of chains but in greater numbers, and that the weights of individual chains are similar to the weight of chains in other kinds of events. The weight of CCs plotted against the number of particles included in the chains is shown in Fig.4.10. We see that the average weight for events with higher multiplicities is slightly higher than for events with smaller multiplicities.

As discussed earlier, a higher average weight for chains with higher multi-

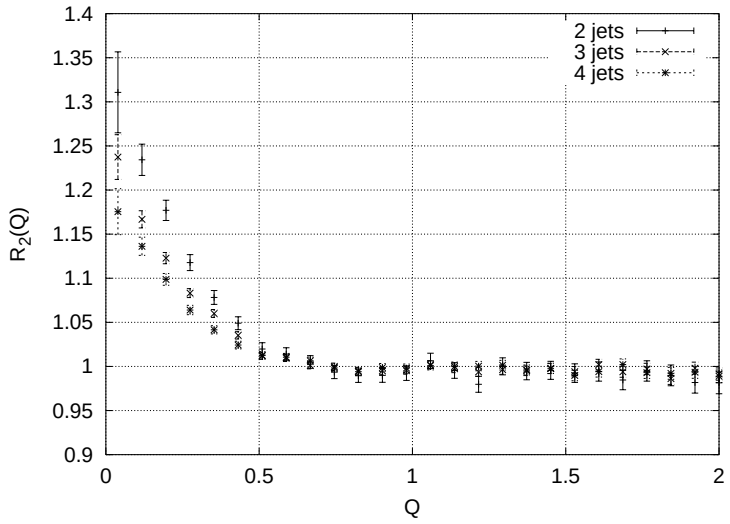

Figure 4.12: The figure shows the two particle correlation function for 2,3 and 4 jet events. $\sqrt{s} = 90$ GeV and $\delta^2 = 0.25$ GeV^2. The sample consists of the particles used in the symmetrisation.

plicity would shift the multiplicity distributions towards higher multiplicities, as is seen in the left-hand plot in Fig.4.11. However, as mentioned earlier, once the multiplicity distribution for one type of events, 3-jet events for instance, is tuned through an adjustment of the Lund model parameters, the multiplicity distribution on Coherence Chains would have been tuned back to their proper values. Since other kinds of events merely have a collection different average number of Coherence Chains, their multiplicity distributions would be automatically re-tuned. We demonstrate this in the right-hand plot in Fig.4.11, which shows multiplicity distributions in 2-jet, 3-jet and 4-jet events. After the application of BE weights, the multiplicity distributions shift to higher values like in the left-hand plot in Fig.4.11. We then re-tuned the Lund model b parameter (cf. Eq.(4.5)), so that the 3-jet multiplicity distribution was restored. With the re-tuned parameter values, we generated multiplicity distributions for 2-jet and 4-jet events with BE weights applied, and found them to be restored as well.

It should be mentioned here that Fig.4.10 shows a slight increase of the average weight for events in which there is only one chain. Either such events have no gluons in them, or only have very soft gluons which were overlooked by the Coherence Chain. Thus, the entire set of hadrons is included in one CC, which ends up with a slightly higher multiplicity than chains in events which

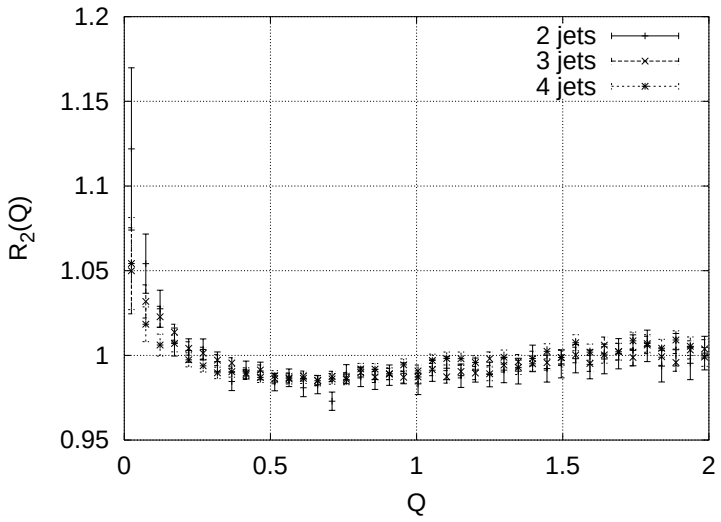

Figure 4.13: The figure shows the two particle correlation function for 2,3 and 4 jet events. $\sqrt{s} = 90$ GeV and $\delta^2 = 0.25$ GeV^2. Including pions from long-lived resonances screens the enhancement-effect shown in Fig.4.12 to a large extent.

have more chains. This would suggest that the tuning of 2-jet events would be special, but we find that tuning of weighted 3-jet multiplicity distribution is sufficient to restore not only multiplicity distributions of events with more jets, but also 2-jet multiplicity distributions.

In Fig.4.12, we show the plot of the two particle correlation function, obtained using our way of calculating the event weight. We separated the event into 2-jet, 3-jet and 4-jet events using the LUCLUS jet clustering algorithm [17]. The Bose-Einstein effect clearly becomes weaker for systems with more jets. This figure shows the correlation function for particles involved in the symmetrisation process. Resonances like η and η' contribute with a rather large fraction of pions to the final state. These pions are not considered in our symmetrisation procedure. Consequently, their distribution is not affected by the weighting procedure and therefore they appear as background. In Fig.4.13, we show the correlation function including the pions from long-lived resonances. We see that the background caused by long-lived resonances screens the enhancement effect shown in Fig.4.12 to a large extent.

4.7 Summary and Conclusions

We have formulated a model for the description of Bose-Einstein correlations (BEC) inside the framework of the Lund string fragmentation model, for general multi-jet events. This is an extension of a similar attempt at modelling BEC for flat $q\overline{q}$ strings, presented earlier [12]. An amplitude is proposed for an underlying quantum mechanical process which would give rise to the Lund model formulae. The total amplitude for a final state with many identical particles is calculated by summing over contributions corresponding to permutations of identical particles in the final state. The effect of the interference terms are introduced into the Monte Carlo through an event weight. One signature of this re-weighting of the events is the enhancement of the probability of formation of identical pions a shade closer in phase space compared to a Monte Carlo without such a re-weighting procedure.

Our treatment of flat $q\overline{q}$ strings is largely similar to that in [12]. However, we use a different partitioning of the total probability among alternative configurations of final state particles, which is manifestly positive definite, in contrast to the weight used in [12]. We reformulated the treatment in the hadronisation scenario in ALFS, and observed that there was a possible generalisation to multigluon strings.

The properties of the hadronisation process in ALFS allow a symmetrisation procedure for fragmentation products of multigluon states; but they impose stringent constraints on possible contributions to the total amplitude from permuted configurations. Effectively, the result of these constraints is that the total amplitude and event weight can be factorised, and written as a product of contributions from local flat regions associated with the string. Consequently the correlation among particles comes out as a local effect in this approach.

The expression "local flat regions" for a string has to be understood in perspective. The multigluon strings considered in string fragmentation normally consist of a finite number of gluons with transverse momenta above a transverse momentum resolution scale. Such a resolution of the state results in a directrix consisting of a few light-like segments, and the resulting string world surface is a collection of planar regions. Choosing a smaller cut-off or resolution scale resolves smaller planar regions. Any choice of the scale is an approximation of the state, but the infrared stability of hadronisation process implies that it is possible to choose a scale such that properties of hadrons would be insensitive to any structure on the string at smaller scales. Moreover, different properties of the final state might be sensitive to structures at different resolution scales. Our approach to the Bose-Einstein correlations favours the use of a different resolution scale, which is defined on the final state of hadrons, and does not introduce a new constraint on the resolution parameter used to define partonic states.

We defined structures called Coherence Chains (CCs) on the set of hadrons

obtained as fragmentation products of multigluon strings, in the fragmentation scheme in ALFS. A CC is roughly a set of rank connected hadrons whose energy-momenta lie in a plane, up to small transverse fluctuations. Certain stability properties of the CCs with respect to global event properties like center of mass energy, thrust, multiplicity of events etc, makes this structure an attractive basis upon which to base our BEC model.

Seen as a collection of coherence chains, the total BE weight for an event factorises into a set of independent contributions, one for each CC. Almost independent of the total energy, event topology, multiplicity, thrust etc, every event exhibits the same kind of coherence chains. The size of coherence chains is of course, determined by the maximum transverse momentum allowed in their definition. Once this scale is set however, events with larger multiplicity, or more complicated jet structure, merely appear as larger collections of CCs, each of which has more or less the same distributions in size. Consequently, BE weights for CCs are independent of the kind of events under consideration.

These properties allowed us to formulate a model for BEC using event weights which did not change the relative normalisations of different partonic configurations, using an event weight which did not average to unity. An average weight higher than 1 for CCs meant a shift of the multiplicity distributions for all kinds of events towards higher multiplicities, but a simple re-tuning of fragmentation related parameters to restore multiplicity distributions for CCs to their pre-weighting values resulted in an effective re-tuning of all kinds of events.

In this model for BEC, the pions in the final state which result from the decay of relatively long lived particles (eg. mesons containing c or b quarks, the pseudo-scalar states η, η') would not have correlations with the rest of the pions in the events. The decay of these resonances is thought of as a process independent of string fragmentation, and the decay products are not available at the time scale of string fragmentation to contribute to the symmetrised amplitude.

Short lived resonances like the ρ-mesons on the other hand decay on a time scale comparable to string decay. It is reasonable to expect that the decay products from such decays would play a role in the total symmetrised amplitude. We have treated these short lived resonances in the same way as in [12], i.e. we treated the resonance decay products as if they were results of string fragmentation, while evaluating the BE weight. A different treatment of short lived resonances would necessarily affect our results.

This model certainly results in an enhancement of the two particle correlation function for small momentum transfers. There is also an unambiguous trend for the correlation strength to go down for more complicated event topologies. However, the overall correlation strength, taking into account the background created by the decay of long lived resonances, appears to be rather

low. We stress that the distributions in this paper should not be compared with those in [12], as they were correlations between "participant" pions on a flat string, whereas we have presented distributions from all pions, from events including parton showers. Naturally the correlation between direct pions is larger, but we believe that it is not possible to identify particular pions in the final state as decay products of particular resonances.

Though re-tuning of model parameters can affect the correlation strength and correlation length to a small extent, the signal remains small in the rather large background from resonance decays. Thus comparison with experimental data indicate that other physical processes contribute to the correlations. However, in particular the dependence of the matrix elements upon the transverse momenta is very uncertain, and in the future we will study if a modification of the $k_\perp$-dependence or some other possible effect may enhance the correlation strength in the model. If this turned out to be the case, the result could eventually lead to an increased understanding of the hadronisation process on a quantum mechanical level.

Acknowledgements

We are grateful towards the late Prof. Bo Andersson for his guidance in the initial stages of this project. We would like to thank G. Gustafson, L. Lönnblad and T. Sjöstrand for many valuable discussions.

References

[1] B. Andersson, G. Gustafson and C. Peterson, *Z. Phys.* **C1** (1979) 105.

[2] B. Andersson, G. Gustafson and B. Söderberg, *Z. Phys.* **C20** (1983) 317.

[3] B. Andersson, The Lund Model, Cambridge University Press, 1998.

[4] T. Sjöstrand, P. Edén, C. Friberg, L. Lönnblad, G. Miu, S. Mrenna and E. Norrbin, *Computer Phys. Commun.* **135** (2001) 238.

[5] T. Sjöstrand, *Nucl. Phys.* **B248** (1984) 469.

[6] B. Andersson, S. Mohanty and F. Söderberg, *Eur. Phys. J.* **C21** (2001) 631.

[7] S. Mohanty, LU TP 03-09 (2003).

[8] B. Andersson, S. Mohanty and F. Söderberg, *Nucl. Phys.* **B21** (2002) 631.

[9] B. Andersson, G. Gustafson and B. Söderberg, *Nucl. Phys.* **B264** (1986) 29.

[10] B. Andersson, P. Dahlqvist and G. Gustafson, *Z. Phys.* **C44** (1989) 455; *Z. Phys.* **C44** (1989) 461.

[11] B. Andersson and W. Hofmann, *Phys. Lett.* **B169** (1986) 364.

[12] B. Andersson and M. Ringnér, *Nucl. Phys.* **B513** (1998) 627.

[13] B. Andersson, G. Gustafson and T. Sjöstrand, *Z. Phys.* **C6** (1980) 235.

[14] Yu.L. Dokshitzer, V.A. Khoze, A.H. Mueller and S.I. Troyan, Basics of Perturbative QCD (Edition Frontières 1991).

[15] G. Gustafson and U. Pettersson, *Nucl. Phys.* **B306** (1988) 746.

[16] L. Lönnblad, *Computer Phys. Commun.* **71** (1992) 15.

[17] T. Sjöstrand, *Computer Phys. Commun.* **28** (1983) 227.

[18] B. Andersson, G. Gustafsson and J. Samuelsson, *Z. Phys.* **C64** (1994) 653.